Adquant;
an image analysis toolbox for the automated, quantitative investigation of cell adhesion

Emma Spanjaard

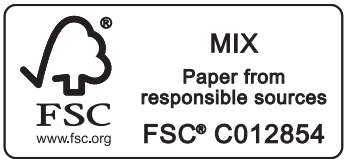

Cover: N. Boehrer & E.Spanjaard
Printing: Gildeprint
- Enschede, The Netherlands

Adquant;
an image analysis toolbox for the automated, quantitative investigation of cell adhesion

Adquant; beeldanalyse software voor geautomatiseerd, kwantitatief onderzoek naar cel adhesie
(met een samenvatting in het Nederlands)

Proefschrift

ter verkrijging van de graad van doctor aan de Universiteit Utrecht op gezag van de rector magnificus, prof. dr. G.J. van der Zwaan, ingevolge het besluit van het college voor promoties in het openbaar te verdedigen op donderdag 11 september
2014 des ochtends te 10.30 uur

door
Emma Spanjaard

geboren op 28 augustus 1983 te Amsterdam

Promotor: Prof. dr. J.L. Bos

Copromotor: Dr. ir. J. de Rooij

Table of contents

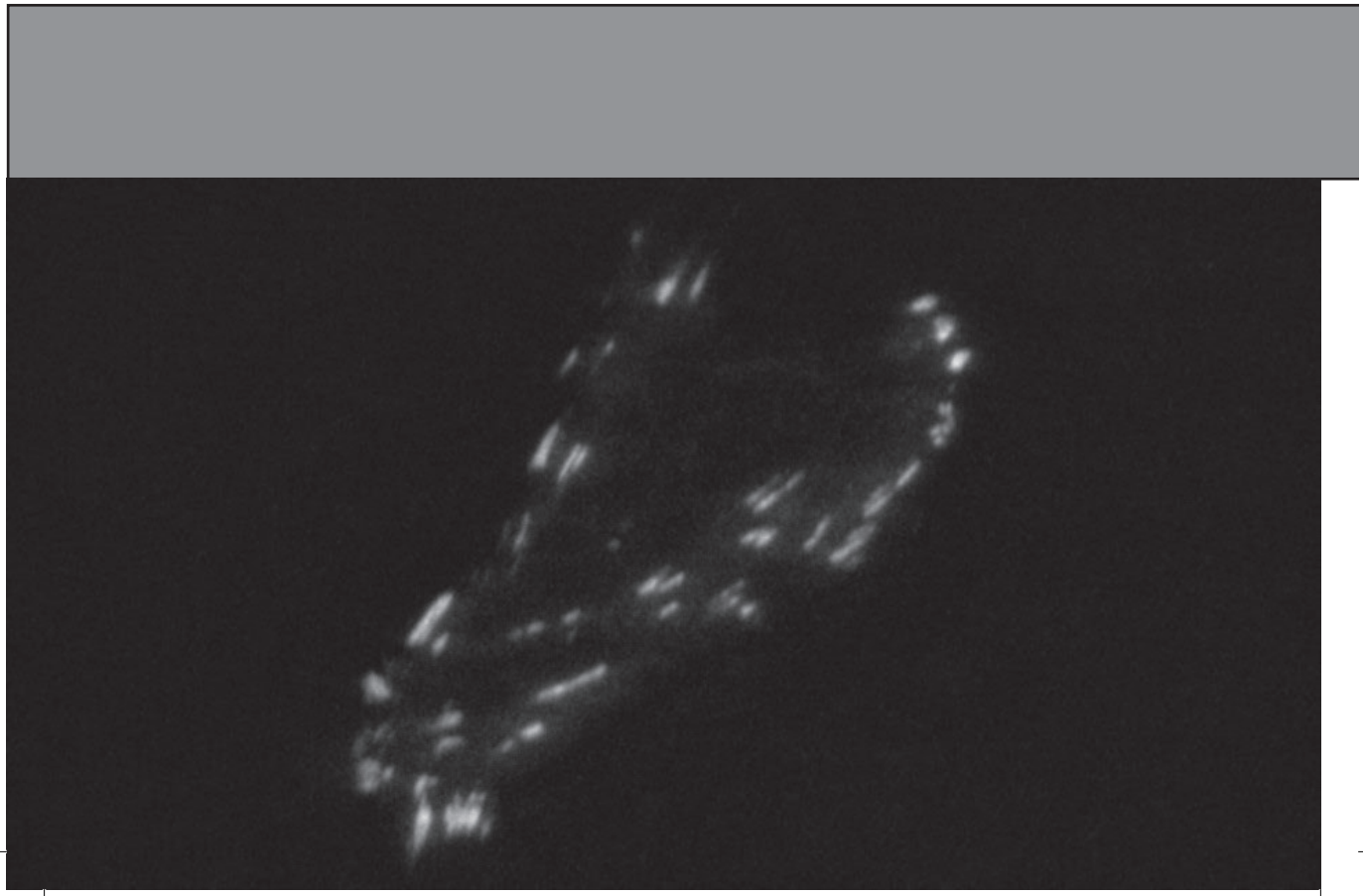

General Introduction 1

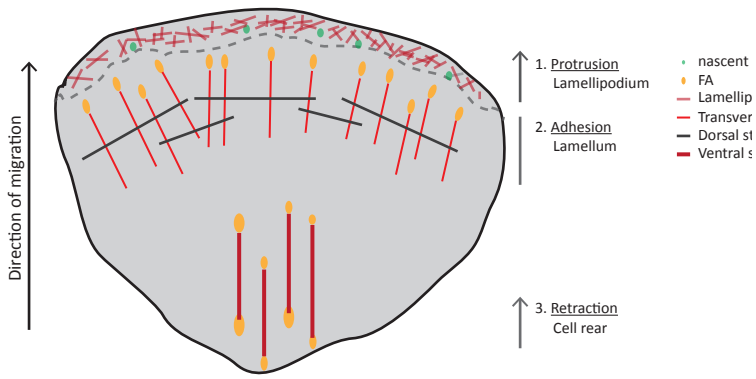

Figure 1: The migratory cell
Schematic representation of a migrating cell with depicted the three stages of the migration cycle (protrusion, adhesion and retraction), their associated cellular regions and the actin structures and adhesions that are found in each region.

Cell migration and adhesion

The migrating cell

Cell migration occurs during the entire life of an organism. At varying stages of embryonic development it is necessary, from gastrulation to the development of the nervous system (reviewed [1]). In the adult organism the inflammatory response requires migration of leukocytes into the infected site and fibroblasts and endothelial cells have to migrate to close a wound. Deregulation of cell migration often leads to aberrant embryonic development and also underlies various diseases, including inflammatory and vascular diseases (reviewed [1]). Cell migration also contributes to cancer metastasis. Cells first invade the tissue surrounding the tumor site, for which migration is necessary. Then they enter the blood circulation from which they extravasate into different organs, again requiring cell migration (reviewed [2]). Cells need to interact dynamically with their environment to migrate, which is far more complex in physiological circumstances compared to the two dimensional cell culture conditions often used in studies of cell migration. However, mechanisms of migration revealed by 2D studies have been found to occur similarly in embryonic development and tumor metastasis [3]. The reductionist approach of 2D cell migration studies is therefore useful and relevant and can provide insights into the mechanisms underlying cell migration in general. Here we will describe the cell migration machinery based on 2D cell migration studies.

The migration cycle consists of three different, but continuous, stages: protrusion, adhesion and retraction. Directional migration requires polarization of the cell, generating a clearly separated cell front and rear. This is largely mediated by distinct actin cytoskeleton dynamics in the front and rear of the cell during migration and will be further discussed below. Upon migratory cues, the leading edge of the cell protrudes. Different forms of protrusion exist, including broad lamellipodia or thin filopodia that can also occur together. Both are driven by actin polymerization [4-6]. Lamellipodia are flat structures of 3-5 µm wide, characterized by a fast inward flow of F-actin (retrograde flow), generated by the polymerization machinery at the cell edge [7], and a criss-cross pattern of actin filaments [8]. In the lamellipodium initial

integrin mediated protein complexes can be formed that bind the extracellular matrix (ECM), called nascent adhesions [9, 10].
Right behind the lamellipodium lays the lamella. Here, bundled actin filaments start to interact with the maturing integrin-based adhesions (now called focal adhesions (FAs)), forming a link from the ECM to the actin cytoskeleton. This stabilizes the protrusion and slows down the retrograde flow of F-actin [11, 12]. Contraction of the cytoskeleton reinforces the FAs in the front of the cell and induces de-adhesion in the back of the cell followed by retraction of the cell rear, allowing the cell to move forward [5] (Figure1). During the entire migration process, signaling from the FAs modulates the organization of the actin cytoskeleton and its dynamics. In turn the actin cytoskeleton, its dynamics and the tension that it generates influence the dynamics of the FAs. This constant, bidirectional signaling, both biochemical and mechanical, between the actin cytoskeleton and the FAs creates a complex, highly connected machinery that mediates cell migration. Here we will describe in some more detail the signaling and force-mediated regulation that underlie the cell migration cycle. Focus will lay on the FAs and the regulation of their continuous formation and disassembly.

Integrin mediated adhesion

The integrins form a large family of transmembrane proteins that mediate cell adhesion via FAs. Integrins respond to signals from outside and inside the cell. They are therefore bidirectional signal transducers. Signal transduction by the integrins mediates not only cell adhesion and migration, but also cell proliferation and growth [13]. Integrins are composed of an α and a β chain that form a heterodimer. Each chain consists of a large extracellular domain, a single transmembrane region and a relatively short cytoplasmic tail. There are 18 α and 8 β chains that by non-covalent dimerization form 24 different integrins. These different integrins exhibit affinity for specific ECM substrates and show differential expression patterns [14]. They can be in an inactive, bent state, or in an upright conformation that is considered to be the active state [15]. Active and inactive integrins are present in equilibrium at the plasma

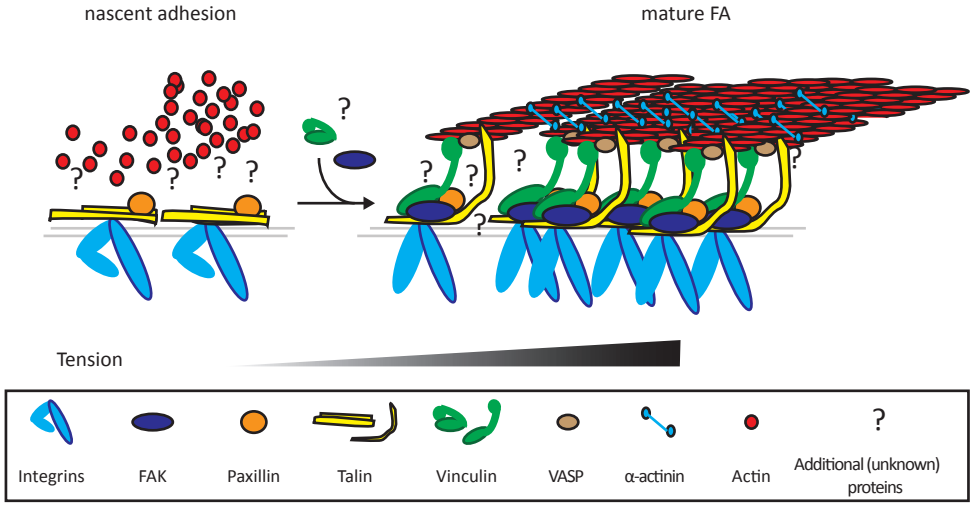

Figure 2: Integrin mediated adhesion the FA

A schematic representation of focal adhesions in their nascent stage (left) and upon maturation (right). Nascent adhesions contain at least integrins, talin and paxillin. Tension induces FA maturation for which FAK and paxillin are important. Localization of vinculin at the FA further stabilizes the adhesion strength and the FA enlarges.

membrane. Integrins can be activated by binding to extracellular ligand, known as 'outside-in' activation, or by the binding of intracellular proteins, known as 'inside-out' activation. Also the clustering of integrins, the avidity, plays an important role [16]. This creates a platform at the intracellular side where signaling and structural focal adhesion proteins can localize and recruit other proteins, eventually forming a link to the actin cytoskeleton.

The 'inside-out' activation of integrins requires protein binding at the intracellular side. The focal adhesion protein talin potentiates this. Although the mechanism of activation by talin has been described in detail for only one specific integrin (αIIb β3), talin is also involved in the activation of other integrins, as shown both in vitro and in vivo [17, 18]. Talin consists of a FERM domain containing head region that is joined by a short linker to a long multi-helical tail region and holds binding sites for many proteins, among which integrins, actin and vinculin. Binding of the head region to the transmembrane domain of the β-integrin chain releases an inhibitory connection between the α and β chains. In addition, an interaction of the talin head region with the phospholipids in the plasmamembrane is required for full integrin activation [19]. Although talin is integral for integrin activation, other proteins are also involved. For example, the kindlins, another group of FA proteins, appear to modulate the talin integrin activation. However, different studies have shown varying effects of kindlins depending on cell- and integrin types. Therefore the exact mechanism underlying its involvement in integrin activation remains to be elucidated [17]. Recruitment of the FA protein vinculin promotes the binding of talin to integrins, thereby stabilizing the FA and maintaining the integrin in the activated state. Although this has been mainly shown in vitro, also in cells such a function has been reported [20-25] (Figure2).

The integrins connecting to the ECM form the basis of FAs. At the intracellular side FAs consist of a large amount of proteins, some of which can link to the actin cytoskeleton (see below) (Figure 2). Thus a connection is formed between the ECM and the cytoskeleton. The strength of the adhesion depends on the mechanical properties of the ECM. This affects the FA proteins, their signaling and the tensional state of the cytoskeleton. But vice versa, the amount of tension exerted by the cytoskeleton on the FA also affects the strength of the FA. This interplay of forces and FA signaling mediates the continuous formation and disassembly of FAs. A balance in this interplay is crucial for cell migration. This is illustrated by the fact that cell migration occurs at an optimum of ligand concentration, where adhesion is not too strong but also not too weak and remains dynamic [26].

The actomyosin machinery in cell migration; organization and dynamics

The first step of the cell migration cycle is the formation of a protrusion, the lamellipodium. This is driven by the polymerization of the actin cytoskeleton at the cell membrane. Elongation of actin filaments occurs at the barbed end of branched actin and is catalyzed by the nucleating Arp2/3 complex. The activity of this complex is regulated by the Rho-GTPases Rac1 and CDC42 via the downstream effectors of the WASP protein family. Capping proteins stop the elongation and new branches can form from here. Further away from the leading edge, close to the lamellum, severing and depolymerization of the actin filament is mediated by the protein cofilin (or ADF) of ADP-bound actin. Subsequently, profilin catalyzes the hydrolysis of the ADP bound actin monomers to ATP-bound, thus recycling them for polymerization again [4, 5]. Protrusion is a constantly occurring process that is balanced by continuous retraction, also in immotile cells. In migrating cells the net retraction is smaller than the net protrusion [27].

The actin cytoskeleton is not an immotile framework but constantly moves towards the

center of the cell, which is called retrograde flow [10, 28]. In the lamellipodium this is a rapid flow caused by the resistance of the cell membrane against which polymerizing actin filaments push. In the lamellum actin filaments are organized in bundles that undergo a slower retrograde flow, mediated by MyosinII activity [5, 7, 10, 11, 26]. The interaction of the FAs with the cytoskeleton may slow down this retrograde flow [12] and potentiates therefore a net forward translocation of the cell.
Although the cytoskeleton architecture differs per cell type, three common types of actin bundles exist, located from the lamella to the rear of the cell: dorsal stress fibers, transverse arcs and ventral stress fibers [29, 30]. Dorsal stress fibers are located at the lamella. They anchor at one side at a focal adhesion from which they elongate. The other side may rest at transverse arcs. Transverse arcs run parallel to the cell membrane and are not anchored. Ventral stress fibers are located further to the rear of the cell and they are anchored on both sides to FAs (Figure1) [5, 29, 31].

The actomyosin machinery in cell migration; contractility and force-generation

To exert traction force on the FAs and retract the rear, very important steps in cell migration, contractility of the cytoskeleton is required, which is mediated by the motor protein MyosinII [32]. MyosinII consists of a head domain, with which it binds to actin and where the motor activity resides. The head domain is linked to a heavy chain via 2 light chains (MLC). MyosinII molecules first dimerize with their heavy chains and then form antiparallel bundles with other MyosinII dimers. Actin filaments are bundled by α-actinin. The antiparallel MyosinII filaments bind to actin with the 4 head domains, at the α-actinin-binding-induced spaces on the actin filaments (Figure 3A) [5, 33]. The motor activity of MyosinII moves antiparallel actin filaments past each other, thus inducing contractility, much like the coordinated contractility observed in the highly specialized cells of skeletal muscles. The activity of MyosinII is mediated by the reversible phosphorylation of the light chains. One of the main regulators of this is the small GTPase RhoA that activates the Rho-associated, coiled coil kinase (ROCK), which primarily leads to inactivation of myosin light chain phosphatase but also phosphorylates MLC directly. Another downstream target of RhoA is myosin light chain kinase (MLCK) that also directly phosphorylates MLC. Other upstream regulators are CDC42 that activates its downstream kinase myotonic dystrophy-related Cdc42-binding kinase (MRCK), leading to activation of MLCK and inhibition of MLC phosphatase and Rac that via its effector Pak can inhibit MLCK and thus reduces MLC phosphorylation (Figure 3B). For some cell types it has been shown that ROCK and MLCK localize respectively more central and more peripheral, suggesting that there is spatial regulation of myosin contractility [33-36]. The combined inhibition of ROCK and MLCK is often used to inhibit cytoskeletal contractility in cell culture.

Focal adhesion structure and function

The focal adhesion architecture

The connection of the integrins to the actin cytoskeleton is indirect and includes over 150 different proteins that participate in the linkage to the actin cytoskeleton and the functioning of the FA. The abundance, interactions and signaling of all proteins are precisely regulated. Because of the complexity of the FA and the growing knowledge about all the interactors, the entity has been named ‘adhesome’ [37, 38]. Recently, high-resolution microscopy has indicated that the FAs are layered structures with a basal layer of adhesion, an intermediate

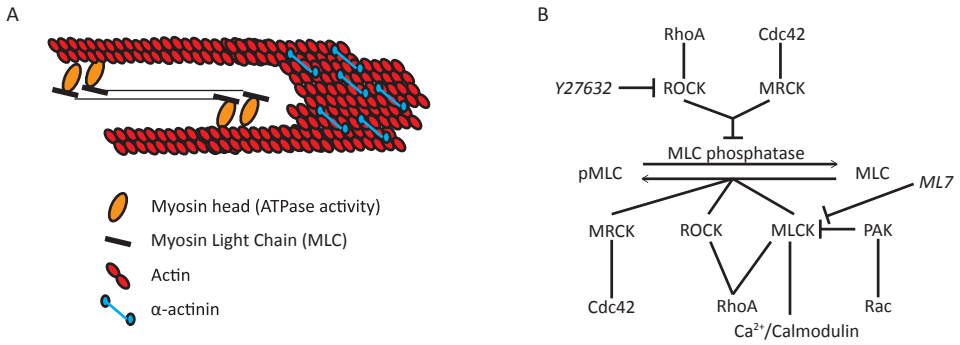

Figure 3: Regulation of myosin contractility

A) A schematic representation of myosin localized at an actin bundle where, by ATP-ase activity of the myosin head, it moves antiparallel actin bundles past each other, inducing contractility. B) Five of the kinases that regulate MLC phosphorylation and thus myosin contractility. ROCK, MRCK and MLCK can increase MLC phosphorylation directly and indirectly via inhibition of MLC phosphatase. PAK inhibits MLCK and thereby reduces MLC phosphorylation. These kinases are regulated by the small GTPases RhoA, Cdc42 and Rac. Pharmacological inhibition of ROCK (by y27632) and MLCK (by ML-7) is sufficient in most cells to inhibit all cytoskeletal contractility and thus release tension from FAs.

layer of signaling and a top layer where actin regulation takes place (Waterman model). Adaptor proteins, kinases and actin binding proteins localize to the different layers [39]. It is beyond the scope of this introduction to discuss all of the different proteins involved in integrin adhesion and we will focus on a small set of core proteins that have different functions in the focal adhesion; talin, vinculin, focal adhesion kinase (FAK) and paxillin (Figure 2).

Following the Waterman model, vinculin and talin reside in the same layer of adhesion potentiation and adhesion strength [39]. Where talin is required for integrin activation, the first connection to the actin cytoskeleton and for adaptor protein recruitment to the focal adhesion [40], vinculin is involved in the stabilization of the link to actin, keeping talin in the activated conformation and strengthening the adhesion [20, 41-44]. The importance of vinculin in cell adhesion and migration is shown by the fact that vinculin null cells have very small FAs and are more motile [45]. Vinculin consists of a head and a tail domain, connected by a small, proline rich linker region. Binding sites for several proteins are located on these domains and vinculin can interact with talin via its head domain and to actin via its tail domain [44]. In solution, both talin and vinculin adopt a highly folded, auto-inhibited conformation and thus the multiple protein binding sites are obscured that are required for their functioning in the focal adhesion. This has led to the hypothesis that in the FA, they are turned into stretched, or activated states that now allow the different interactions to occur. Evidence for unfolding of vinculin in FAs comes from the use of a FRET probe [46]. The activation mechanism of both proteins is not yet fully understood but several scenarios exist. Activation of talin possibly involves PtdIn (4,5)P2 that can release some of the auto-inhibitory interactions, and the proteins RIAM and vinculin that than stabilize the open conformation [17, 47, 48]. The interactions of the vinculin head and tail regions are very strong [49], and for activation of vinculin two models have been proposed. Either multiple interactors bind to vinculin simultaneously to unfold it [49] or binding of either talin or α-actinin is sufficient [44]. Additionally, mechanical signals are hypothesized to play a role in the activation of both proteins. Talin unfolding can be induced by stretching in vitro [21] and the tail region of vinculin (the actin-binding domain) is necessary for its dynamics and function in response to

myosin activity at FAs [41]. However, the exact mechanisms of tension-dependent talin and Vinculin regulation remain to be elucidated.
FAK and paxillin are proteins that are important for signaling of the FAs, and they reside in the signaling layer of the FA [39]. Loss of FAK results in large and stable FAs and reduces cell migration velocity. Similarly, mutants of the adaptor protein paxillin that cannot be phosphorylated by FAK anymore also induce large and stable FAs and reduce cell migration speed [50], indicating that both are involved in the regulation of the disassembly of the FAs. Auto-phosphorylation of the Tyrosin 397 of FAK induces a conformational change that induces binding of the kinase Src. This interaction increases the activity of FAK and induces the ability of other proteins to bind [51, 52]. Paxillin interacts with the FAK-Src complex that in turn phosphorylates paxillin on multiple sites [53]. Phosphorylation of these sites regulates the affinity of paxillin for many other FA proteins and thus regulates their recruitment to the adhesion [54, 55]. Among others, paxillin phosphorylation has been shown to regulate recruitment of vinculin and the recruitment of activators and inactivators of the small GTPases RhoA, Rac1 and CD42 that are needed for the protrusive activity in cell migration [51, 54]. Thus, paxillin and FAK contribute to the complex regulation and signal transduction of focal adhesions and influence cell migration.
Many focal adhesion proteins have actin binding domains and can make the link to the actin cytoskeleton, including talin, vinculin, zyxin, VASP and α-actinin. This connection appears not to be of static nature but instead a certain amount of force on the link induces brief slippage before the focal adhesion and the cytoskeleton engage again. In vitro experiments have shown that a single talin molecule is required for slippage at 2pN force [56]. In cells so far, in addition to talin, vinculin has also been described to act as such a bond [42, 57]. These focal adhesion proteins at the actin cytoskeleton interaction thus function as a clutch that allows a bearable amount of tension on the focal adhesion and regulates resistance against retrograde actin flow [58, 59].

The focal adhesion lifecycle

The continuous formation and disassembly of FAs that is required for cell migration, which will be referred to as FA dynamics, is tightly regulated by a complex, partially still elusive network of both biochemical and mechanical signals. This network mediates the formation of new adhesions at the front of the cell and regulates whether they swiftly turnover or that they mature and grow to bare the force needed for the cell to move forward. The signaling network also regulates disassembly of the FAs at the rear of the cell that is necessary for the release and retraction of the back. FAs in different stages of this complex lifecycle have been given different names, mainly based on morphological properties. For simplicity reasons, we collectively name all stages “FAs” except for the initial stage in which we call them “nascent adhesions”.
The nascent adhesions form in an actin polymerization-dependent manner at the lamellipodium of the cell [9]. As the lamellipodium passes over the nascent adhesions, they may turnover. Otherwise, at the interface of the lamellipodium and the lamella, the nascent adhesions can mature into FAs, which is at least partially a tension-dependent process during which FAs grow and elongate. Key to the decision between turnover and maturation is the FAK-Src phosphorylation pathway. As described above, FAK or Src null cells have large focal adhesions and are less motile. FAK-Src induced phosphorylation of paxillin on tyrosines 31 and 118 mediates focal adhesion turnover, and the FAK-Src substrate p130Cas is thought to have a similar role [50]. Phosphorylation of serine 273 of paxillin by the Rac effector PAK

also induces FA turnover by increased binding of GIT1 and further activation of Rac1 [60, 61]. One proposed mechanism of FA stabilization is that vinculin can compete with FAK for the binding site on paxillin and thereby could diminish these signaling pathways and stabilize the focal adhesion [62]. Maturation of focal adhesions coincides with recruitment of different proteins and a change in the phosphorylation state of FA proteins [63]. FAK signaling at the FA induces activation of RhoA, through ill-defined intermediates, thereby mediating contractility of the cytoskeleton to enhance FA maturation [64]. Mutually exclusive binding of vinculin and RIAM to talin also regulates FA dynamics. The RIAM talin interaction is important for initial integrin activation and adhesion assembly, whereas its replacement by vinculin is needed for adhesion maturation [65].

FA disappearance is a partly myosin-dependent process that is often preceded by FA sliding. This has been shown to happen everywhere immotile cells thereby keeping these cells in a motionless state [66], but in migrating cells it is mainly observed in the rear. Although mediated by contractility of the actin fibers [67], the sliding itself is probably tread milling of the FA proteins: a faster on-rate of protein binding at the side of the focal adhesion oriented to the center than at the peripheral side where the off-rate is higher. Final disassembly of the focal adhesions at the rear is less studied, but several signaling pathways could be involved, including metalloprotease induced cutting of the integrin ECM connection, microtubule-dependent transport of relaxation factors [68, 69] and calpainII induced proteolysis of several FA proteins, like talin, paxillin and FAK [70-72].

Thus, the regulation of the composition and dynamics of the FA is a complex process that is not fully understood. It is nevertheless clear that misregulation of the focal adhesion machinery is involved in many diseases [73]. Mutations or over-activity of proteins like Src, FAK and paxillin are correlated with different tumor types and metastatic potential. Obtaining more knowledge about the regulation and mechanism of FA regulation and functioning can indirectly provide information about the deregulated mechanisms in diseases.

Focal adhesion mechanotransduction: a role for vinculin

Mechanosensing and the translation of the mechanical cues into cellular signals is of great importance for tissue integrity and regulation of the vasculature in which the FAs are involved [74]. They are mechanosensitive entities, since cells that are plated on stiff substrates have larger FAs than cells on softer substrates, indicating that tension induces focal adhesion growth [75]. In addition, upon inhibition of contractility of the actin-cytoskeleton, FAs disappear [5, 76]. FAs translate force signals into cellular responses, but which FA proteins mediate this and how exactly force transduction occurs, remain subject of debate. Several proteins could be involved, of which vinculin is of special interest to this thesis.

Bead pulling experiments have shown that vinculin gets recruited to the adhesion sites formed between the cell and ECM-coated beads and this reinforces the interaction [77]. Similarly, vinculin has been shown to reinforce cell-cell adhesions in bead pulling assays with E-cadherin coated beads [78]. In vitro studies have shown that force mediated stretching of talin induces vinculin binding [21]. This interaction stabilizes talin in its stretched conformation [43] and thereby increases adhesion strength possibly by locking integrins in an activated state [17, 20, 41]. Also tension dependent phosphorylation of paxillin by FAK induces vinculin recruitment and thereby FA maturation [79]. Maintaining vinculin in the focal adhesions also may depend on tension and this is important for the presence of other FA proteins [41]. Recently, vinculin has been shown to play a role in localization and residence of p130CAS to the focal adhesions [80]. P130CAS is an important mechanosensor in focal

adhesions that upon tension induced extension is phosphorylated by Src kinases and activates downstream signaling pathways including the activation of the small GTPase Rap1 [81] (see below). Thus multiple mechanosensing pathways exist in FAs translating mechanical signals into cellular responses and vinculin appears to be central in these processes.

Rap1 signaling in cell adhesion and migration

Originally identified as a suppressor of Ras-induced transformation [82], the small G protein Rap1 is now known to be involved in regulation of many cellular processes, including cell-matrix adhesion and cell-cell adhesion [83-85]. Cell adhesion is positively affected by activation of Rap1 and concomitantly Rap1 activation inhibits cell migration [86]. Rap1 can regulate both integrin affinity and clustering, dependent on integrin types and cell lines [87, 88]. It has been linked to integrin activation via its effector RIAM that plays a role in the regulation of talin [89, 90], thus affecting cell adhesion via integrin regulation. However, that alone does not explain the inhibitory effects of Rap1 on cell migration. It has been suggested that activation of Rap1 affects cell protrusive activity and FA dynamics [86] and thereby inhibits cell migration. The recently found inhibitory effect of Rap1 on RhoA activity via ARHGap29 [91] explains how Rap1 inhibits the actomyosin contractility required for the cell to migrate. By activating the CDC42-MRCK pathway Rap1 can also induce actomyosin contractility [92]. These findings together suggest that Rap1 can modulate the dynamics of the actin cytoskeleton and of FA at multiple levels to regulate cell migration. This underscores that spatiotemporal control of Rap1 activity is essential for proper cell migration.
Rap1 cycles between a GDP-bound inactive state and a GTP-bound active state (Figure 4). This cycle is regulated by a large collection of activating guanine exchange factors (GEFs) and inactivating GTPase activating proteins (GAPs) [93]. These regulators do not only differ in their specificity for the small molecules that activate them, but also are located in specific cellular locations. Thus varying signals can activate distinct pools of Rap1 and induce specific cellular effects [94]. As an example of this specificity, the activator PDZ-GEF is important for Rap-dependent regulation of cell-cell adhesion [84, 95] and the activator C3G plays an important role in Rap-dependent integrin-mediated adhesion. The importance of this signaling pathway for cell adhesion is shown by the fact that C3G deficient cells migrate faster than C3G expressing cells [96, 97]. Another well-studied GEF of Rap1 is Epac that itself is activated by the second messenger cAMP [98]. Epac can be specifically activated in vitro by the cAMP analogue 8-CPT-2'OMe-cAMP (also named 007) [99] and this has

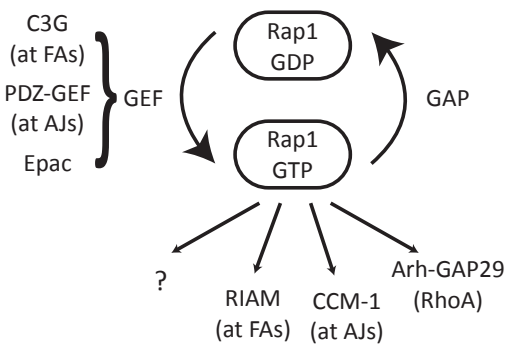

Figure 4: The activation cycle of Rap1
Rap1 cycles between a GDP-bound, inactive state and a GTP-bound active state. GAP proteins induce the hydrolysis of GTP, inactivating Rap1. Several GEFS can activate Rap1, by catalyzing the exchange of GDP for GTP. The ones most relevant to this thesis are depicted here together with their cellular localization. Rap1 has many downstream effects and a number of effectors that specifically bind to its GTP-bound form have been put forward. Relevant effectors here are RIAM, functioning at the FAs, CCM-1, affecting adherens junctions (AJs) and Arh-Gap29 that inhibits RhoA.

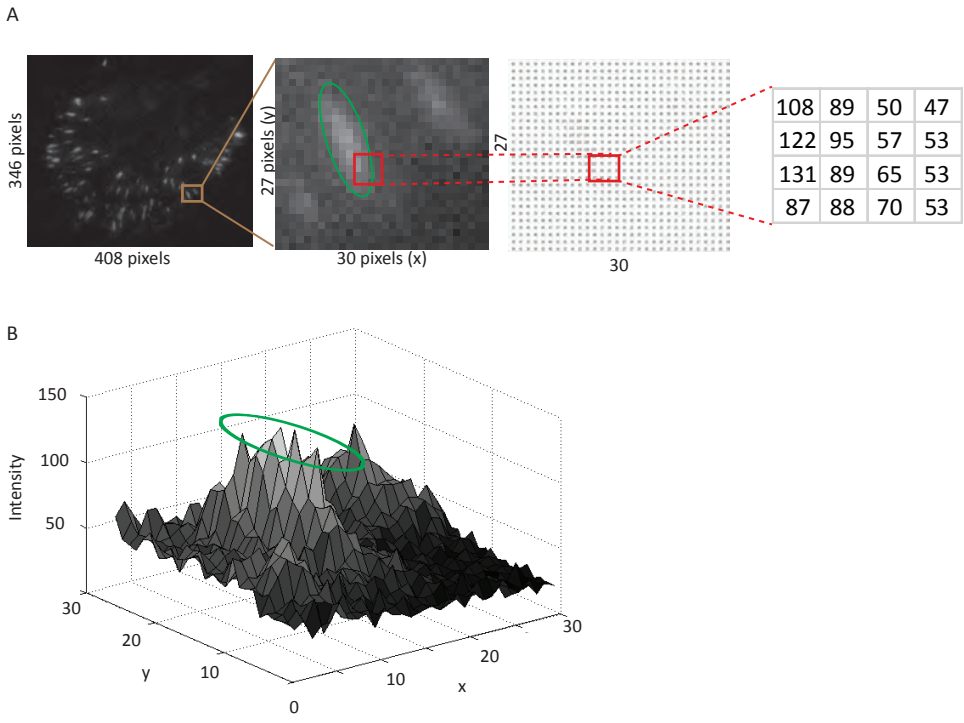

Figure 5: Converting images to numbers for mathematical analysis
A) Part of a fluorescent microscopy image (using TIRF) of a DU145 cell expressing mCherry-Paxillin to label the FAs, measuring 408 pixels in width and 346 in height (left). A close-up of 30 by 27 pixels of 2 FAs (middle) with the numbers representing the intensity value per pixel in a matrix (right). A region on the edge of the FA, in red, on the image and on the corresponding intensity matrix, enlarged to show the pixel intensity values (right). B) A 3D representation of the intensity values of the FA close-up shown in (A middle) with green ellipse depicting the same FA in both images.

turned out to be a useful tool to study mechanisms underlying the cellular effects that Rap1 activation induces.
The effects of Rap1 activation are complex and still subject of debate. A more extensive, systematic description of the effects of Rap1 on cell and FA morphology and behavior by analysis of time-lapse imaging would provide further information. However, analysis of this kind of images requires an automated approach, since analysis by hand would be too much time-consuming and is prone to bias. The development of such analysis tools has been the subject of this thesis project, and the results will be described in the next chapters.

Detection and tracking of (sub) cellular structures (computer vision)

With the advance of automated digital microscopy the amount of imaging data generated by standard microscopy systems has increased to a level at which proper inspection and quantification by individual researchers has become a severely limiting factor. To overcome this, automated image analysis methods are being developed that can measure and quantify the processes of interest. Collectively this methodology is called computer vision. Because

of the use of monochromatic digital cameras, light emitted by fluorophore-labelled proteins, or fluctuations in light intensities (photons per area) due to contrasting methods like phase contrast microscopy, are converted into an X-by-Y matrix of numbers (dependent on the number of pixels on the camera chip) (Figure 5A). High numbers correspond to bright parts of the image and low numbers corresponding to dim parts. This numerical representation forms the basis for the mathematical methods that are developed for automated image analysis. As fluorescent microscopy is generally used to visualize objects (particles) within cells or tissues and measure morphology, movement or dynamic turnover of these objects, particle detection and tracking are the main techniques used in these methods.

A key step in automated detection of objects in (microscopy) images is the separation of an object of interest from its surrounding. This is called image segmentation. Before segmentation of the image, to remove noise and undesired fluctuations in pixel intensities (for instance due to uneven illumination), preprocessing is generally applied. Preprocessing can consist of alignment (in time lapse image series), smoothing or background subtraction or more complex procedures like image deconvolution (in z-stacked image series). For detection of structures, a wide variety of segmentation algorithms exist, many of which have been developed for other purposes than the analysis of biological images. The choice of algorithm or combinations of algorithms is very important for the eventual success of the image analysis method. An image segmentation algorithm that is central to the work in this thesis is the hDome-transformation, developed to detect spots in biological images for a probabilistic tracking method of fast moving particles [100]. It results in an image in which all structures have the same maximum intensity, which is an advantage to subsequently obtain an equal distribution of pixels assigned to an object for the final detection. A second segmentation method that we used to define the boundaries between objects within images is the watershed algorithm [101]. For this method the image is treated as if it was a topographical surface, in which high intensity corresponds to high altitude (Figure 5B). Object separation occurs either at the minima where imaginary water meets that flows from the peaks or there where imaginary water flooding up from the basins (the minima) meets. On images with many small variations in intensity, like microscopy images, this watershed leads to over-segmentation of the image. Therefore often, also in this thesis, a marker-based watershed is applied where extra markers for objects and background are taken along that define top and basin regions in the image.

To obtain temporal information of moving objects, the detected structures need to be linked from frame to frame to create a track (particle tracking). A very common method for creating such a track is nearest neighbor linking in which the object in the subsequent frame that is closest in pixel distance to the object of interest in the current frame is chosen to represent the same object in the subsequent frame of the track. We have used this algorithm in some of our methods. However, for fast moving objects and objects that are very close to each other within an image, like focal adhesions, nearest neighbor tracking is likely to result in erroneous tracks. Therefore, for the tracking of focal adhesions, which are relatively slow moving structures that maintain a distinct size and shape, we used object-overlap as the method of choice for track generation.

During the course of this PhD research, we have developed a set of detection and analysis tools for the specific purpose of studying cellular adhesion that will be made publically available and are described in this thesis.

Scope of this thesis

The goal of this thesis project was to develop imaging analysis tools to analyze the effects of Rap1 on cell migration and FA dynamics. In **chapter 2** we describe the automated analysis of cell spreading induced by Rap1. Here we show that Rap1 can bypass Src signaling to induce cell spreading and the formation of vinculin containing FAs. In **chapter 3** a segmentation and tracking method of FAs in time-lapse microscopy imaging is developed. Analysis of the effects of Rap1 activation on FA dynamics in migrating cells, induced by HGF stimulation, showed effects on some FA features whereas HGF induction itself had no strong effects. This systematic analysis of FA behavior, lead to the surprising conclusion that regulation of cell migration and regulation of FA dynamics are essentially uncoupled processes. The Rap1 affected FA features are very reminiscent of previously described effects of inhibition of RhoA mediated contractility of the actin cytoskeleton. This is in apparent agreement with the identification of the Rho-inactivating protein ArhGAP29 as a downstream effector of Rap1 [91]. In **chapter 4**, using the FA tracking and detection software of the previous chapter, we describe the discovery of a lifetime dependent densification profile that FAs show, which we call compaction. HGF increased the compaction dynamics and the maximum level of compaction reached whereas Rap1 activation had a decreasing effect. This data suggests that compaction is an overall FA feature that is at least partially driven by cytoskeletal force. In **chapter 5** we describe the addition of a dual-color analysis method to the FA detection and tracking software described in the third chapter. This allows the simultaneous study of differently labeled FA proteins. Here, the presence of paxillin and vinculin at the FAs is studied in cells upon inhibition of RhoA-mediated contractility. We show that, although vinculin is described to be a mechanosensitive protein, contrary to paxillin, its release from FAs actually followed paxillin's release. These are rapid effects that occur within seconds upon release of tension. These results question the common notion that vinculin is a key protein in the mechanosensitive regulation of FAs.
In three addenda we describe additionally developed analysis tools: **addendum 1** contains the explanation of an analysis tool to study cell migration, based on the recognition of fluorescently labeled nuclei. In **addendum 2** an analysis tool for the study of cell-cell adhesion dynamics is described. Finally, in **addendum 3**, a method to analyze fluorescent intensity in the cytoplasm versus the nucleus is described, developed for the quantitative analysis of Hippo-pathway activity (by YAP localization).

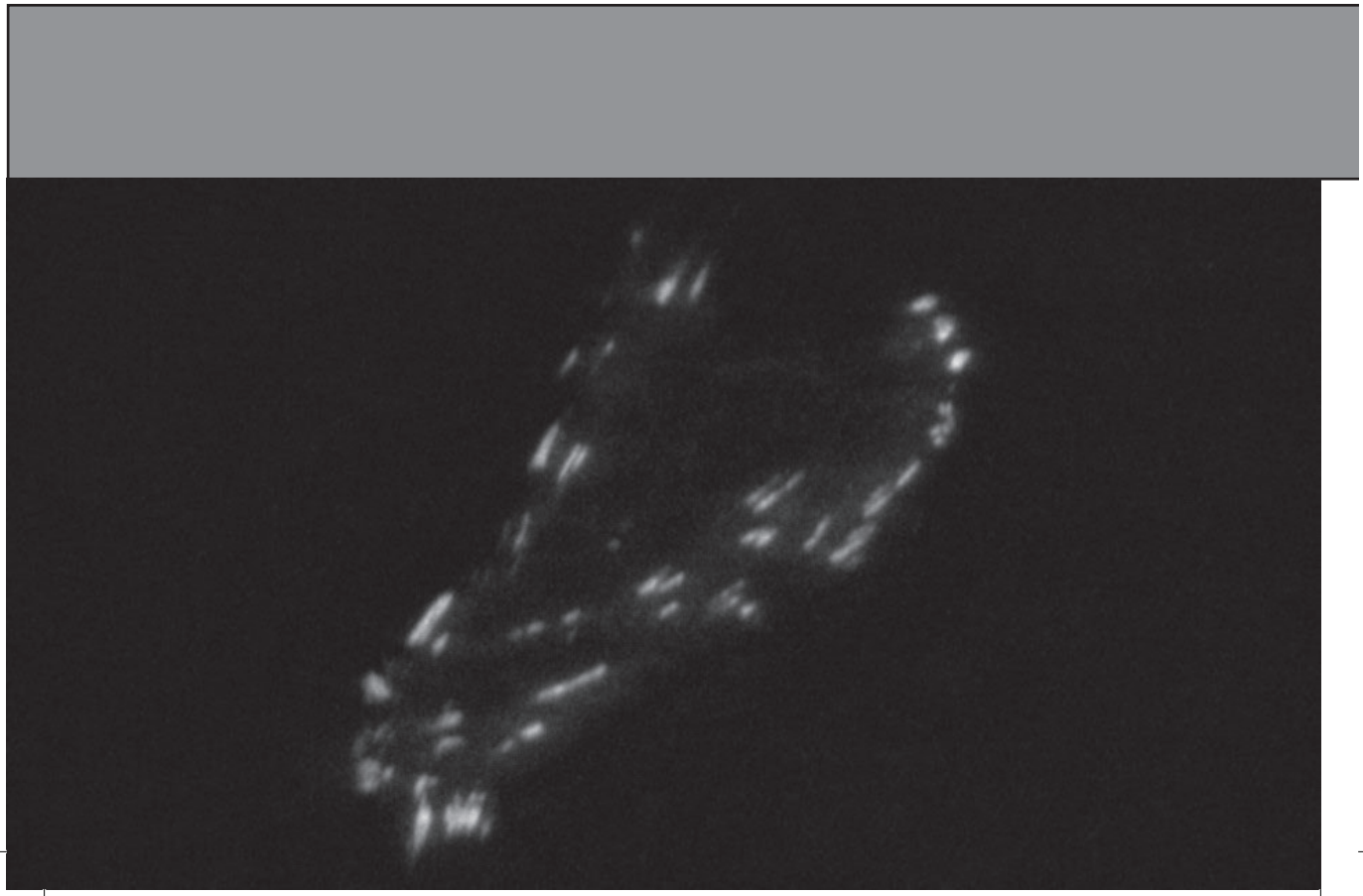

Rap1 can bypass the FAK-Src-Paxillin cascade to induce cell spreading and focal adhesion formation

2

Sarah H. Ross*[1], Emma Spanjaard*[2], Anneke Post[1], Marjolein J. Vliem[1], Hendy Kristyanto[1], Johannes L. Bos[1] and Johan de Rooij[2]

* these authors contributed equally to this work

1 Department of Molecular Cancer Research, Centre for Biomedical Genetics and Cancer Genomics Centre, University Medical Center, Utrecht, The Netherlands.
2 Hubrecht Institute for Developmental Biology and Stem Cell Research, and University Medical Center, Utrecht, The Netherlands

PLoS ONE (2012) Nov 27; 7(11): e50072

Abstract

We developed new image analysis tools to analyze quantitatively the extracellular-matrix-dependent cell spreading process imaged by live-cell epifluorescence microscopy. Using these tools, we investigated cell spreading induced by activation of the small GTPase, Rap1. After replating and initial adhesion, unstimulated cells exhibited extensive protrusion and retraction as their spread area increased, and displayed an angular shape that was remodeled over time. In contrast, activation of endogenous Rap1, via 007-mediated stimulation of Epac1, induced protrusion along the entire cell periphery, resulting in a rounder spread surface, an accelerated spreading rate and an increased spread area compared to control cells. Whereas basal, anisotropic, spreading was completely dependent on Src activity, Rap1-induced spreading was refractory to Src inhibition. Under Src inhibited conditions, the characteristic Src-induced tyrosine phosphorylations of FAK and paxillin did not occur, but Rap1 could induce the formation of actomyosin-connected adhesions, which contained vinculin at levels comparable to that found in unperturbed focal adhesions. From these results, we conclude that Rap1 can induce cell adhesion and stimulate an accelerated rate of cell spreading through mechanisms that bypass the canonical FAK-Src-Paxillin signaling cascade.

Introduction

The interaction between cells and extracellular matrix (ECM) proteins of the interstitial matrix and basement membrane is critical for the structural support of cells, as well as for supplying environmental cues that control the development, maintenance and integrity of tissues [102, 103]. Highlighting the importance of these processes is the vast array of diseases, both developmental and acquired, that derive from defects in extracellular matrix proteins or deregulated cell adhesion [102-106].

Cell adhesion and spreading is under the control of multiple signaling pathways which are derived both from the ECM constituents (outside-in signaling) as well as those originating from inside the cell (inside-out signaling) [5, 51, 107-111]. The integration of these signals controls the attachment and spreading of cells to a surface of ECM proteins, by regulating the assembly of focal adhesions (FAs). These large protein complexes consist of integrins, which facilitate both the attachment of cells and act as signaling receptors for the ECM protein ligand, as well as proteins, such as talin and vinculin, that initiate multiple links between integrins and the actin cytoskeleton [33, 51, 64, 106, 110].

In the canonical model of cell adhesion and spreading, outside-in adhesion signaling is initiated when integrins encounter their ECM ligands, and Src kinase is recruited to adhesion sites by its SH2 domain interacting with the autophosphorylation site of FAK (pY397) [51, 110]. Together, FAK and Src act as a signaling module to induce the phosphorylation of a number of focal adhesion proteins, including multiple sites on FAK itself, paxillin and p130Cas [51, 64, 110] [112]. These phospho-tyrosine residues act as docking sites for other proteins, which regulate the activities of the Rho family GTPases, Rac, Cdc42 and RhoA, to advance cell protrusion and spreading, and promote the link to the actin cytoskeleton [33, 51, 106, 110]. As the ECM-integrin-actin connection is formed, mechanical force develops across adhesions. Vinculin, in particular, is involved in strengthening integrin adhesions in response to force [77, 113-117].

The small GTPase, Rap1, is a known regulator of adhesion processes and can regulate integrins [83, 87, 93, 118-121], the actin cytoskeleton [84, 122-124], membrane protrusion [86] and the inactivation of RhoA [125-128]. Furthermore, Rap1 activity has been linked to the control of talin, through its effector, Riam [89, 90, 129-131], to the inhibition of RhoA, via the effectors, Arap3 [125, 126, 132, 133], RA-RhoGAP/ARHGAP20 [134-136] and indirectly via the effector, Krit [127, 137], as well as to stimulation of Rac1, through regulation of Tiam1 and Vav2 [138]. Activation of Rap1 proteins is spatially and temporally controlled by guanine nucleotide exchange factors (GEFs) which are themselves regulated by different stimuli. The GEF, C3G, acts downstream of Src [96], such that Rap1 may be activated in response to outside-in adhesion signaling [96, 97, 139]. However, Rap proteins can also function in inside-out cell adhesion pathways via GEFs regulated by second messengers, such as the cAMP-regulated Epac proteins and the calcium- and diacylglycerol-regulated CalDAG-GEFs [118, 140-143].

Although implicated in several different aspects of cell-matrix interactions, the functional significance of Rap1 in cell adhesion processes is far less characterised than the roles of the GTPases, Rac1, Cdc42 and RhoA. Previously, we reported that when a suspension of A549-Epac1 cells was applied to an ECM-coated surface, activation of the Rap1 GTPase via Epac1 using the cAMP analogue, 007, promoted focal adhesion formation, increased the spread area of cells and induced a round, rather than angular, cell morphology [144]. In this study, we performed live cell imaging and developed new image analysis tools to enable a quantitative

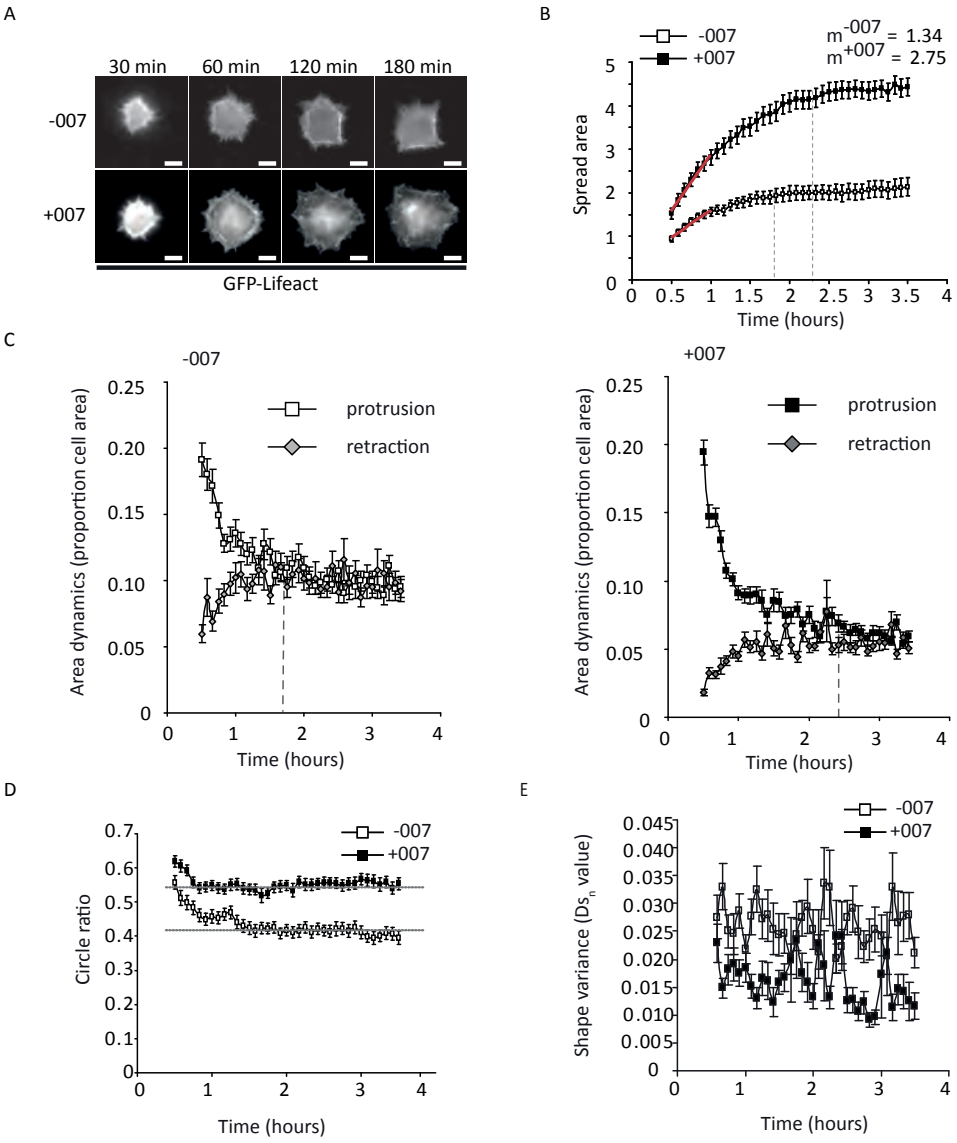

Figure 1: Live-cell imaging of 007-induced adhesion and spreading.

A549-Epac1 cells expressing GFP-Lifeact were trypsinised and allowed to roll for 1 hour before plating out on fibronectin with or without 100 μM 007. Images of cells were captured through the 63× objective every 5 minutes from 30 minutes after plating, with representative images shown in (A). The scale bars represent 10 μm. Altogether, 54 cells without 007 and 41 cells with 007 from 10 separate spreading experiments were quantified. The spread area at each frame was determined in pixels and standardised to the average area of all the first frames of the basal (-007) spreading cells (B). The spreading rate over the first 30 minutes of imaging was calculated using the gradient (m) of the red lines show on each graph and is presented in spread area per hour. Dashed vertical lines indicate the time at which cells approached their maximal area. Area dynamics (C) were determined by measuring the gain or loss of spread area between consecutive frames, and presented as a percentage of the spread area of the second frame. The dashed vertical lines show the time at which the area of protrusion equalled the area of retraction. Cell morphology was analysed by the circle ratio (D), which was calculated by dividing the area of the cell at each time point by the

investigation into how activation of Rap1 can regulate the spreading process. Moreover, we have investigated how Rap1-induced spreading and FA formation relates to the canonical Src-mediated mechanism of cell spreading.

Results

Activation of the Epac1-Rap pathway alters the spreading dynamics and morphology of cells

To investigate how activation of the Epac1-Rap1 signaling pathway led to the large and round cell spreading phenotype in A549-Epac1 cells [144], we performed live-cell imaging and examined the differences in the morphology and in the dynamics of spreading over time in the absence or presence of the Epac1 activator, 007 (Figure 1). Cells were replated onto fibronectin without or with 100 µM 007 and imaged from approximately 30 minutes after their first contact with fibronectin for the next 3 hours (Figure 1A). We then developed custom automated image analysis software in order to quantify and to characterise cell spreading in the presence and absence of 007 (described in Materials and Methods, Supporting Information, Figure S1).

In the presence and absence of 007, cells spread rapidly over the first hour after plating, and in general, cells stimulated with 007 were already more spread than control cells at the commencement of imaging (Figure 1A and 1B). Over the first 30 minutes of imaging, cells with 007 spread at twice the rate of cells without 007 (Figure 1B). After the period of rapid spreading, the cells continued to increase their spread area at a lower rate, until reaching a steady state of total contact with the matrix (Figure 1B). In cells without 007, this maximum spread area was reached after approximately 110 minutes of contact with the ECM, while cells treated with 007 took around 140 minutes to approach their maximal spread area. Therefore, the increase in the spread area of A549-Epac1 cells induced by 007 that we observed after 3 hours of spreading in a fixed time point assay [144], is the result of both a prolonged and a faster rate of cell spreading.

The time-lapse imaging revealed that under basal conditions, cells displayed an anisotropic mode of spreading with unequal protrusion along the cell periphery. Moreover, the spreading was accompanied by remodelling of the spread surface, and cells displaying periods of retraction and protrusion as they increased their coverage of the ECM and as they maintained their maximal spread area (Figure 1A). To analyse the spreading process in further detail, we determined the areas of the spread surface of cells which were gained (protrusions) or lost (retractions) between consecutive imaging frames and related this to the spread area which resulted from these changes (Figure 1C). To initiate spreading, cells in the presence or absence of 007 showed greater protrusion than retraction, consistent with the cells making rapid and persistent spreading contacts with the ECM. Noticeably, cells treated with 007 retracted a smaller proportion of their spread area than basal spreading cells, indicating that retraction was decreased by 007. As cells approached their maximum spread area, protrusion activity decreased (Figure 1C), and an equilibrium between the areas of protrusion and retraction was

area of a circle which encompassed the outer-most tips of the detected cell edges. Changes in the shape of the spread area of cells were calculated by determining the normalised variance ($\Delta\sigma_n$ value) of the distances from the cell centre to each peripheral point of the cell. Then, the change in the variance ($\Delta\sigma_n$ value) between consecutive time points was calculated (E). For all graphs shown, each plotted point is the mean of all cells measured ± the standard error of the mean.

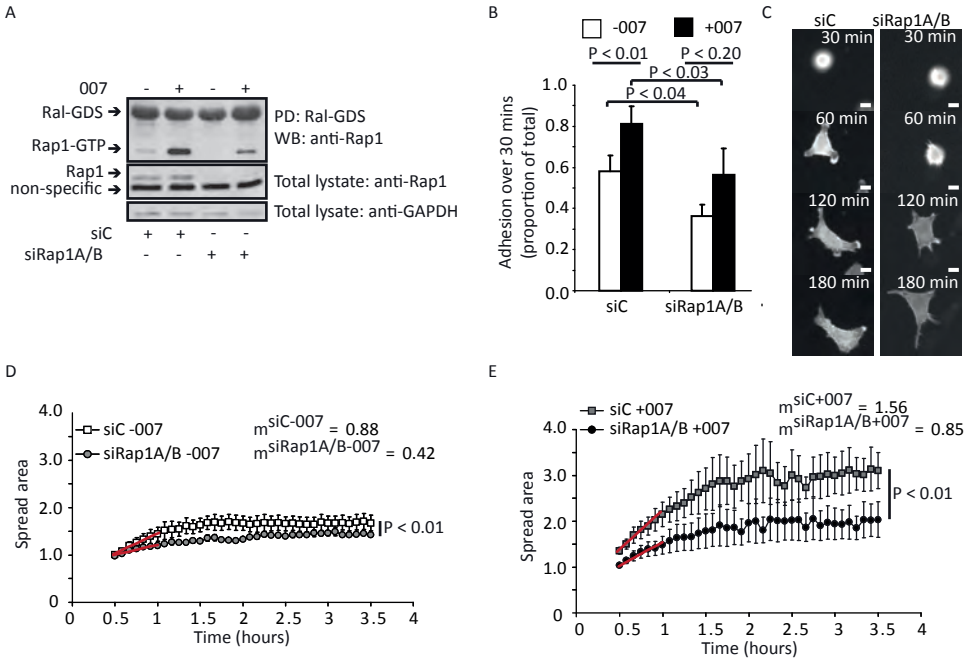

Figure 2: Effects of depleting Rap1A and Rap1B on cell spreading.
A549-Epac cells were transfected with scrambled siRNA (siC) or siRNA against Rap1A and Rap1B together (siRap1A/B) for 48 hours before further analysis. In (A), cells were exposed to mock or 100 μM 007 for 15 minutes. Pull down of Rap1-GTP, by the RalGDS Rap-binding domain, and knockdown of Rap1A/B were detected by western blot. The depletion of Rap1A and Rap1B is representative of the knockdown achieved in cells used for the adhesion and spreading analyses. In (B), siRNA transfected cells were replated with or without 100 μM 007 and cell adhesion after 30 minutes was determined by alkaline phosphatase activity. Adhesion is expressed as a proportion of the total cells added per well and the graph shows the mean adhesion for three experiments ± the standard error of the means. The P value was determined by a paired student's t-test. For spreading analysis, cells treated with siRNA were plated on fibronectin and images were captured every 5 minutes using the 20× objective. Representative time-lapse images are shown in (C). The scale bars represent 10 μm. Cell spreading was quantified for time-lapse movies under basal conditions (D) and in the presence of 100 μM 007 (E). The spread area for each knockdown condition was calculated by standardising all measurements to the average size of siC cells without 007 at the first imaging time point. The graphs show the mean of the spread area for three knockdown experiments ± the standard error of the means. The rate of increase in the spread area of cells over the first 30 minutes of imaging, shown with red lines on the graphs, was determined by calculating the gradient (m) of the lines (calculated as spread area per hour) and is presented alongside the key. The P values were calculated using a two-way ANOVA with replication.

reached. At this point, cells treated with 007 remodelled a smaller proportion of their spread area, compared to basal cells, whilst maintaining their maximum spread area (Figure 1C). These data imply that 007 inhibits cell retraction and stabilises the contacts between cells and their environment.

The round, rather than angular, mode of cell spreading induced by 007 was established by the initiation of more persistent protrusion sites around the entire periphery of the cell than in basal conditions, and, hence, cells exhibited isotropic cell spreading (Figure 1A). To analyse the form of cells over time further, we calculated the circle ratio of the cell at each time point by determining what proportion of a circle, encompassing the outer-most tips of the detected cell edges, was occupied by the area of the cell (Figure 1D). Thus, a higher

circle ratio is indicative of a round cellular shape. Cells spreading without 007 had a lower circle ratio compared to cells spreading with 007, demonstrating that under basal conditions, cells were, indeed, more angular throughout the time course of spreading (Figure 1D). To evaluate cellular form and morphology dynamics further, we devised a method to quantify the changes in shape as the difference of the variance ($\Delta\sigma_n$) of the distance from the cell centre to all points on the cell periphery between consecutive time-lapse frames (Figure 1E). Cells spreading without 007 displayed a higher value of $\Delta\sigma_n$ than 007 treated cells, reflecting the dynamic shape changes of basal spreading cells and the more consistent shape of the 007-stimulated cells as observed in the time-lapse-movies (Figure 1E). This quantitative live-cell imaging shows that 007 promotes a faster rate of cell spreading by promoting protrusion along the entire cell edge, while reducing the retraction activity exhibited by unstimulated cells as they spread.

Rap1A and Rap1B contribute to basal spreading of cells and are responsible for the 007 effects

In order to confirm that the effects of 007 on cell spreading were mediated by Rap1 activity, and to investigate whether the activity of Rap1 was required for basal spreading, we transfected cells with siRNA targeting both Rap1A and Rap1B and investigated the effects on cell spreading. The reduction of Rap1A/B was sufficient to decrease basal and 007-induced Rap1-GTP levels (Figure 2A). As we previously observed with depletion of Rap1A alone [144], depletion of Rap1A/B reduced the adhesion of cells over 30 minutes (Figure 2B). However, depletion of Rap1A/B neither altered the angularity of cells nor prevented the membrane protrusion and retraction activity during spreading (Figure 2C). Quantification of time-lapse movies of Rap1A/B-depleted cells spreading under basal conditions showed that at the commencement of imaging, these cells had approximately the same spread area as control cells transfected with a scrambled, control, siRNA and could initiate spreading (Figure 2C and 2D). However, over the first 30 minutes of spreading, cells depleted of Rap1A/B spread with a rate which was approximately half of the spreading rate observed with control cells, and showed a 20% reduction to the maximal spread area (Figure 2D). Depletion of Rap1A/B significantly decreased the spreading response induced by 007 (Figure 2E). However, compared to basal conditions, a small induction of initial spreading rate and maximum spreading was observed in cells depleted of Rap1A/B in response to 007. This is most likely explained by the incomplete depletion of Rap1 by the siRNAs, and the increase in GTP-loading of this residual Rap1 by 007 (Figure 2A). From these results, we conclude that Rap1A/B is required for 007-induced cell spreading, and controls the basal rate of cell spreading and contributes to the maximum spread area which cells can sustain.

007 bypasses the requirement of Src in cell adhesion, cell spreading and FA formation

Outside-in activation of Src kinases is crucial for stabilising the cell-ECM adhesion and for promoting the membrane protrusion that initiates cell spreading as cells contact an ECM ligand [33, 51, 106, 110]. To determine if 007 promoted isotropic cell spreading via modulation of the Src kinase signaling pathway, we investigated the effects of the Src kinase inhibitor, PP2, on 007-induced cell adhesion and spreading processes. Pre-treatment of cells with PP2 blocked cell adhesion and prevented cell spreading (Figure 3A, 3B and 3C). However, 007 could still induce adhesion in the presence of PP2 significantly, although it was inhibited compared to the level of cell adhesion observed in the presence of 007 alone (Figure 3A). Quantification of cell spreading revealed that 007 and PP2-treated cells spread

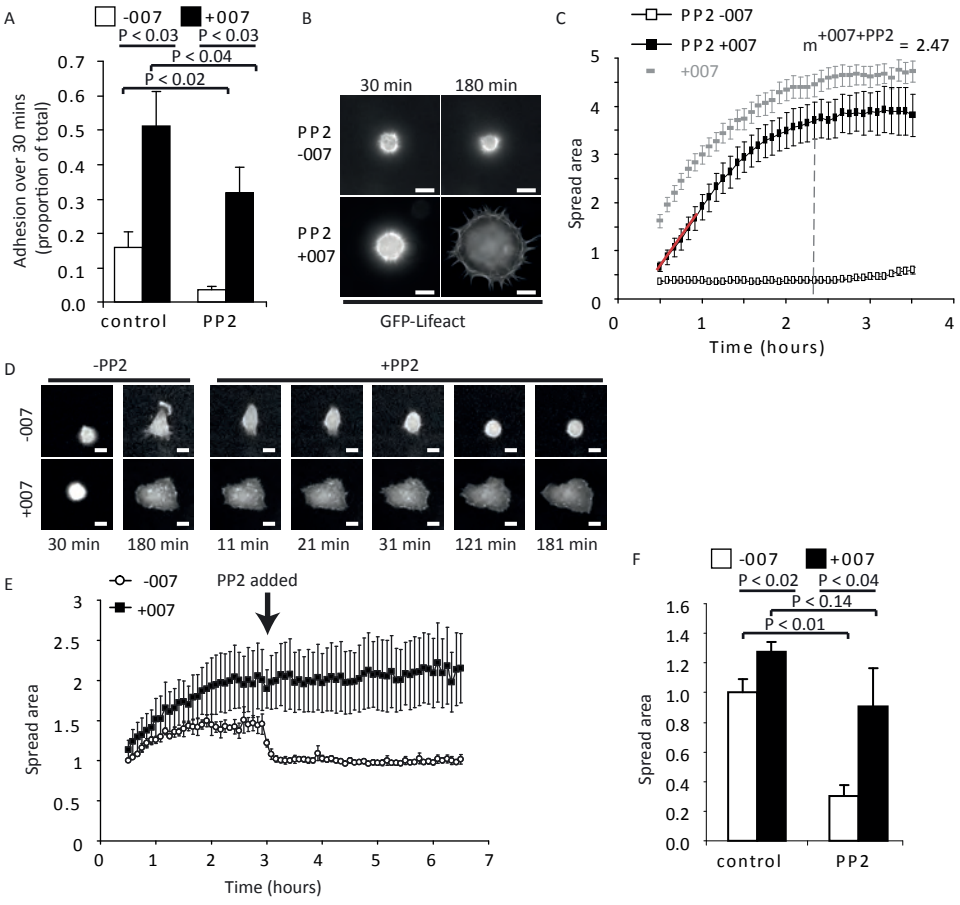

Figure 3: Effects of the Src family kinase inhibitor, PP2, on basal and 007-induced cell spreading.
Cells were trypsinised, rolled for 1 hour without or with 20 μM PP2 pre-treatment and plated on fibronectin with or without 007. Adhesion of A549-Epac1 cells after 30 minutes was determined by alkaline phosphatase activity (A). PP2-treated A549-Epac1-GFP-Lifeact cells were plated on fibronectin and imaged over time using the 63× objective. Shown are representative images (B) and quantification of the mean spread area ± the standard error of the means (C) of 16 cells plated without 007 and 15 cells with 100 μM 007 from three separate spreading experiments. Spread area was standardised to the average area of -007 cells shown in Figure 1B at the first frame of imaging (from assays performed independently, but under comparable experimental conditions). The dashed grey curve shows the spreading kinetics of 007-treated cells from Figure 1B. The vertical line indicates the time that cells reached their maximum spread area. The spreading rate was calculated using the gradient (m), in spread area per hour, of the red line shown on the graph. In (D) and (E), A549-Epac1-GFP-Lifeact-expressing cells captured through the 20× objective spread in the presence or absence of 100 μM 007 for 2.5 hours before 20 μM PP2 was added. For quantification (E), the spread area was standardised to the average area of -007 cells at the first time point of imaging. In (F), human umbilical vein endothelial cells were plated on fibronectin for 1 hour in the presence and absence of 100 μM 007 and 20 μM PP2, before being fixed and stained. At least 30 cells per condition were quantified and standardised to the mean area of cells spreading without 007 or PP2. In (A) and (F), graphs show the mean of 5 and 3 experiments, respectively ± the standard error of the means. P values were calculated by paired student's t-tests.

to approximately 80% of the size of cells stimulated with only 007, and had a spread area which was 1.6 times that of the basal spreading cells (Figure 1B and Figure 3C). Furthermore, in the presence of 007 and PP2, both the initial rate of cell spreading and the point at which the steady state spread area was approached (140 minutes) matched the spreading kinetics of cells treated with 007 alone (Figure 1B and Figure 3C). These data suggest that both Src- and Rap-mediated cell adhesion pathways contribute to the extent of cell adhesion and spreading observed when 007 is added to cells, but that Src activity is not required for 007 to enhance adhesive processes. When PP2 was added after cells were allowed to spread for three hours either in the presence or absence of 007, unstimulated cells retracted, and rounded-up to resemble their pre-spread state (Figure 3D and 3E). However, cells treated with 007 maintained their existing spread area upon PP2 addition (Figure 3D and 3E). To exclude that Src-independent cell spreading is a peculiarity of the A549 cancer cell line, we investigated the spreading of primary human umbilical vein endothelial cells that contain endogenous Epac1. Spreading of these cells was clearly stimulated after 1 hour in the presence of 007 and PP2, although the basal spreading was inhibited by PP2 (Figure 3F). These data demonstrate that 007-induced Rap1 cell signaling can bypass the need for activating Src kinase activity to induce cell adhesion and spreading.

Adhesion and spreading induced by 007 is mediated by the formation of focal adhesions that have a functional link to the actin cytoskeleton

Src activation promotes cells to attach and increase their contact area with their ECM environment by inducing the formation and maturation of integrin-based FAs that are connected to the actin cytoskeleton. These FAs are mechanosensitive, with their size and morphology being altered in response to changes in the contractility of the actomyosin network. Increased actomyosin-induced tension induces larger focal adhesions, and, conversely, a decrease in actomyosin-based tension causes FAs to shrink [51, 67, 79, 145]. We, therefore, investigated if Rap1 could assemble similar integrin-dependent and mechanosensitive adhesion complexes in the absence of the tyrosine phosphorylation steps induced by Src activation.

Firstly, we tested whether the adhesion processes induced by Rap1 were integrin dependent. A549-Epac1 cells were allowed to adhere to fibronectin for 30 minutes in the absence or presence of antibodies which inhibit the function of β1 and β3 integrins in focal adhesions, and the α6 integrin of hemidesmosomes. Both basal and 007-induced adhesion over 30 minutes was inhibited by a mixture of these antibodies, confirming that Rap-induced adhesion requires the activity and function of integrins (Figure 4A). The 007-induced adhesion response was only partially blocked by incubation with the β1-inhibiting antibody alone (data not shown). This is consistent with our previous findings that depletion of the integrin activator, talin, blocked 007-induced spreading in these A549-Epac1 cells [144].

We then investigated the morphology and mechanosensitivity of FAs induced by 007 in cells in which Src was inhibited in order to determine their connection to the actin cytoskeleton. Cells treated with 007 showed FAs around the periphery of the cell, and this was not inhibited by PP2 (Figure 4B). Inhibition of Rock kinases using the inhibitor, Y27632, had no effect on the basal or 007-induced cell spreading response but did decrease the size of adhesions formed under basal conditions or in the presence of 007 or 007+PP2 (Figure 4B). This was also observed with co-depletion Rock I and Rock II (Figure 4C), and indicates that our previous findings that 007-induced cell spreading was inhibited by siRNA depleting only Rock II [144] reflects the differential cellular roles of Rock I and Rock II [146, 147]. Together, these results show that integrin-based, actomyosin-connected and mechanosensitive focal adhesions were

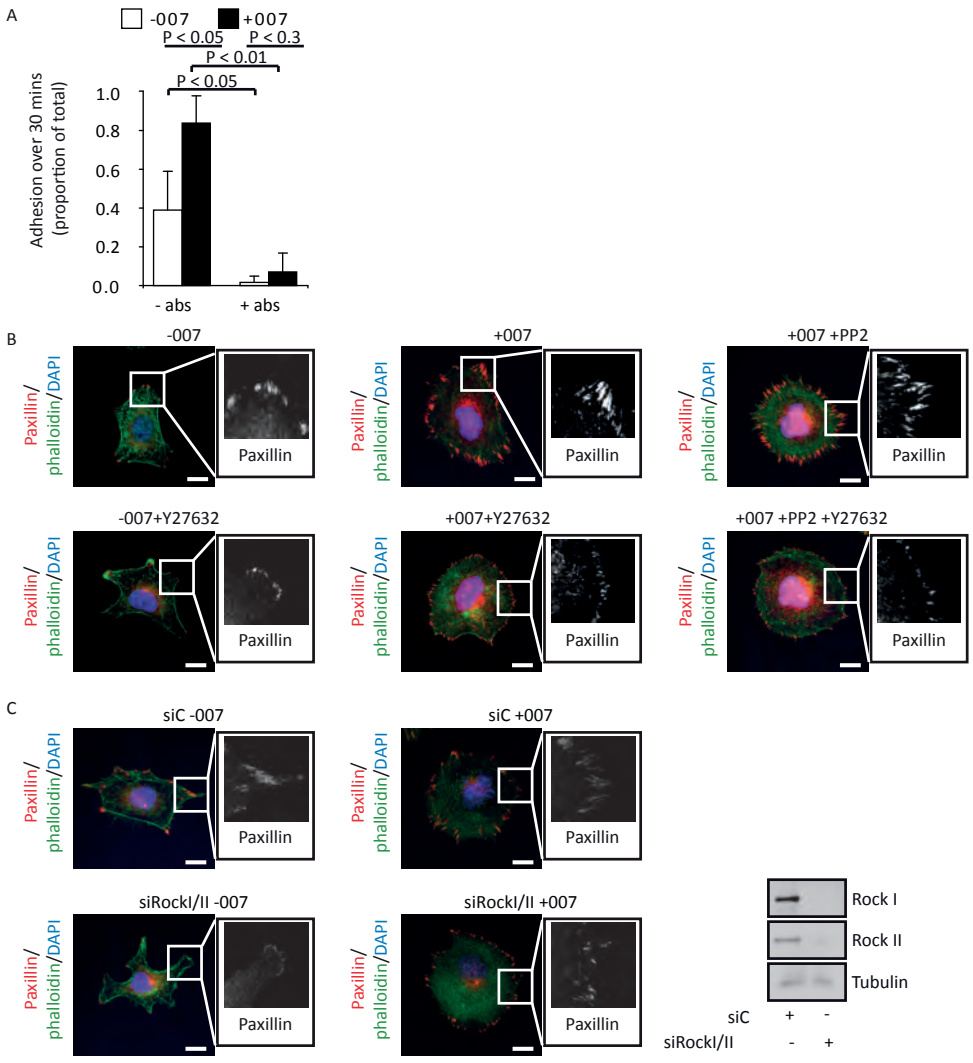

Figure 4: The dependency of 007-induced adhesion and spreading on an integrin-actin link.
A549-Epac1 cells were trypsinised, rolled for 1 hour and plated on fibronectin in the presence or absence of 100 µM 007. The effect of integrin inhibiting antibodies (abs) on cell adhesion was determined by alkaline phosphatase activity (A). The graph shows the mean result of three experiments ± the standard error of the means. The P values were calculated using a paired student's t-test. A549-Epac cells which had spread for 3 hours in the absence or presence of 100 µM 007, with or without 20 µM PP2 or 10 µM Y27632 (B), or cells which had been transfected with scrambled siRNA (siC) or siRNA against Rock I and Rock II together (siRockI/II) for 48 hours and allowed to spread on fibronectin in the presence or absence of 100 µM 007 were fixed and stained with paxillin, to visualise focal adhesions, phalloidin, to detect F-actin, and DAPI. Enlargements of the paxillin staining from within the regions marked on the merged image are shown alongside. All scale bars represent 10 µm. Western blot analysis to confirm the depletion of Rock I and Rock II is shown alongside.

induced by Rap1 activity in the presence of the Src inhibitor, PP2.

007 does not induce tyrosine phosphorylation of FAK and Paxilin

The canonical model of cell adhesion states that adhesion-induced autophosphorylation of FAK pY397 creates a docking site for Src, which then leads to further phosphorylation of FAK on pY576, pY577, pY861 and pY925, as well as the phosphorylation of other adhesion proteins, such as paxillin, which is phosphorylated on pY31 and pY118 [51, 64, 112]. Therefore, we investigated the effect of PP2 and 007 on these phosphorylation events. Pre-treatment of cells with PP2 slightly inhibited the autophosphorylation of FAK (Y397) at the initial stages of adhesion, whilst strongly reducing the Src-regulated phosphorylation of FAK (pY576/577, pY861, pY925) and paxillin (pY118) in cells replated and adhered for 30 minutes or 3 hours (Figure 5A). In cells kept in suspension, PP2 acutely promoted FAK autophosphorylation, possibly through a signaling feedback loop to promote cell survival when Src signals were decreased. Stimulation of cells with 007 did not induce the phosphorylation of these proteins in the presence of PP2 (Figure 5A). Therefore, any increase in phospho-paxillin and phospho-FAK observed in response to 007 in the absence of PP2 (comparing lanes 5 and 6 with lanes 7 and 8, Figure 5A) is likely to be an indirect activation of Src through integrin adhesion processes induced by Rap1. From these results, we conclude that activation of Rap1 did not promote compensatory tyrosine phosphorylation of FAK and paxillin, but rather bypassed the need for Src signaling to induce cell adhesion and spreading.

In the absence of Src signaling 007 still induces the formation of vinculin-containing focal adhesions

Phosphorylation of FAK and paxillin is crucial for the assembly of focal adhesions because of their ability to recruit other proteins to the growing adhesion complexes [51, 106, 110]. Vinculin is an important component of adhesions that contributes to reinforcing the link between actin and integrins when FAs are under tension [77, 113-117]. Previously, the recruitment of vinculin to adhesions has been attributed to Src-driven phosphorylation of paxillin [79]. As 007-induced adhesions in the presence of PP2 are under actomyosin tension, we investigated if vinculin could still be recruited these FAs. We found that adhesions induced by 007 in the presence of PP2 still stained strongly for paxillin, vinculin and FAK pY397 (the auto-phosphorylation site that is upstream of Src recruitment) (Figure 5B). To measure the abundance of proteins specifically localised to FAs, we used quantitative image analysis to measure the fluorescence intensity of FAs relative to the cellular background signal. PP2 reduced the fluorescence intensity levels of paxillin and vinculin in FAs compared to those in FAs of 007-treated cells to about 70% (Figure 5C), showing that FAs were less protein dense in the presence of PP2. However, the reduction in vinculin levels was similar to the reduction in paxillin levels, and the ratio between vinculin and paxillin was not affected by inhibition of Src (Figure 5C). Thus, there was no defect in the ability of vinculin to be recruited to adhesions in the presence of 007 and PP2. Moreover, whereas the ratio of FAK pY397 fluorescence intensity to total paxillin intensity was unaffected by PP2, the ratio of paxillin pY118 to total paxillin fluorescence intensity was significantly inhibited (Figure 5B and 5C). From these data, we conclude that there are multiple mechanisms through which proteins can associate together at sites of adhesions. The current models of FA assembly state that tyrosine phosphorylation of adhesion components by Src is critical for the assembly of integrins, paxillin and other components, such as vinculin, into focal adhesions. Our data demonstrate that Rap1 can induce an alternative FA assembly pathway.

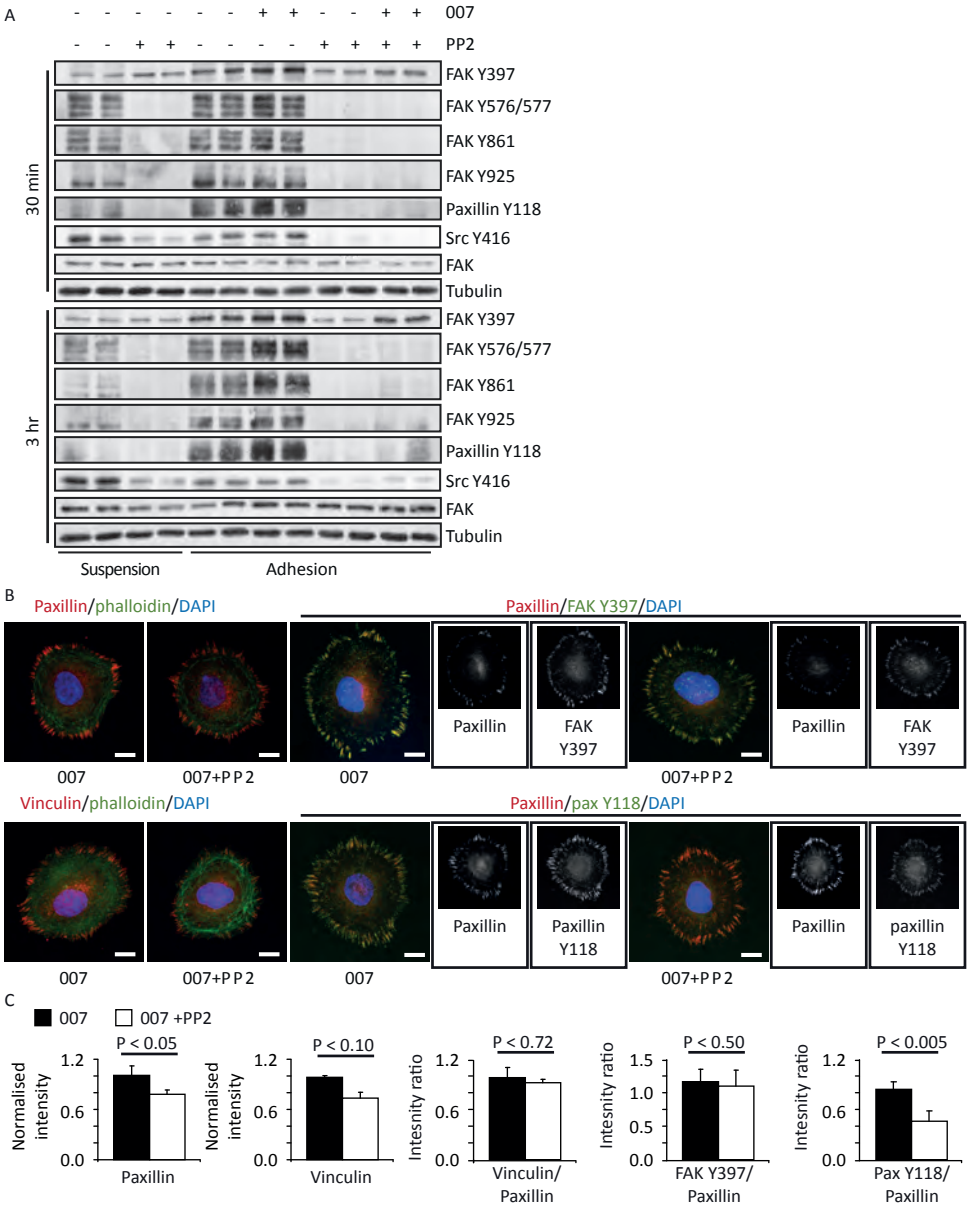

Figure 5: Effect of PP2 on 007-induced focal adhesions.

Cells were trypsinised and allowed to roll for 1.5 hours in the absence or presence of 20µM PP2, before being plated onto fibronectin for 30 minutes or 3 hours with or without 100 µM 007. Cells were then lysed in Laemmli sample buffer and proteins were separated by SDS-PAGE. The levels of phospho-FAK, phospho-Src and phospho-paxillin were determined by western blot (A). A representative of three individual experiments is shown. Rap1-induced focal adhesion composition was investigated by immunofluorescence. Following 3 hours of spreading, cells were fixed and stained for focal adhesions, using anti-paxillin, anti-vinculin, anti-FAK Y397 and anti-paxillin Y118 antibodies, or F-actin, using phalloidin. Representative images are shown in (B), with greyscale images of the single

Auto-phosphorylation of FAK is not required for 007-induced adhesion, spreading and focal adhesion formation

As treatment with the Src inhibitor did not block the kinase activity and autophosphorylation of FAK at pY397, we pre-treated cells with both PP2 and the FAK inhibitor, PF573228, to investigate if FAK signaling to proteins other than Src and paxillin was needed for Rap1-induced FA formation. Combined pre-treatment of cells with PP2 and PF573228 strongly inhibited the adhesion-induced phosphorylation of FAK and paxillin observed after 30 minutes and 3 hours of adhesion, and 007 did not induce either the autophosphorylation of FAK or the phosphorylation of Src substrates substantially (Figure 6A). Pre-treatment with PP2 and PF573228 blocked the basal spreading of cells, but the spreading induced with 007 was significant in both A549-Epac1 cells (Figure 6B and 6D) and in human umbilical vein endothelial cells (Figure 6C). As judged by western blot, after three hours of attachment and spreading, pY397 FAK levels in cells treated with 007 increased to levels approaching those found in cells in suspension in the absence of the inhibitor (Figure 6A). To examine the importance of FAK in 007-induced spreading further, we depleted FAK from cells using shRNA and siRNAs targeting FAK (Supporting Information, Figure S2). FAK levels were depleted most effectively by transfection of stable FAK-knockdown cells with siRNA against FAK (Supporting Information, Figure S2A), and under this condition, FAK staining of FAs was most strongly decreased, although residual staining still remained (Supporting Information, Figure S2B). FAK depletion of cells stimulated the basal spreading of cells, and did not block the 007 spreading response (Supporting Information, Figure S2C). Moreover, treatment of FAK depleted cells with PP2 and PF573228 blocked the basal spreading response, but 007 could still induce significant spreading of the cells (Supporting Information, Figure S2C). Together, these data strongly support the conclusion that FAK levels and activity are not critical for 007-induced spreading.

The A549-Epac1 cells spreading in response to 007 in the presence of PP2 and PF573228 showed a morphology closely resembling that of the cells spreading in the presence of 007 and PP2, but focal adhesions did not stain for FAK pY397 and paxillin pY118 (Figure 6D). Quantification of the fluorescence intensities of these components confirmed that, compared to control cells, the ratio between FAK pY397 and paxillin or paxillin pY118 and paxillin was strongly reduced by PP2 and PF573228 (Figure 6E). Nevertheless, as observed with PP2 treatment alone, we found that the adhesions induced by 007 in the presence of PP2 and PF573228 stained for vinculin (Figure 6D) and that the ratio in the fluorescence intensity of vinculin and paxillin remained the same as in cells treated with 007 alone (Figure 6E). This shows that Rap1 activation can drive recruitment of vinculin to FAs even during combined inhibition of FAK and Src activity.

channel fluorescence from the dual stained focal adhesions shown alongside the merged images. The scale bars in the merged images represent 10 μm. (C) The fluorescent intensity of the focal adhesion staining was determined and standardised to the cellular background. Total paxillin or vinculin levels were normalised to the mean intensity of the 007 condition, and the ratio of vinculin levels to paxillin levels present in each condition was calculated. The levels of phospho-FAK and phospho-paxillin were calculated as a ratio with respect to the co-stained intensity of paxillin. The graphs show the average results for 3 experiments (with 10 cells for each condition) ± the standard error of the means. A paired student's t-test was used to calculate P values.

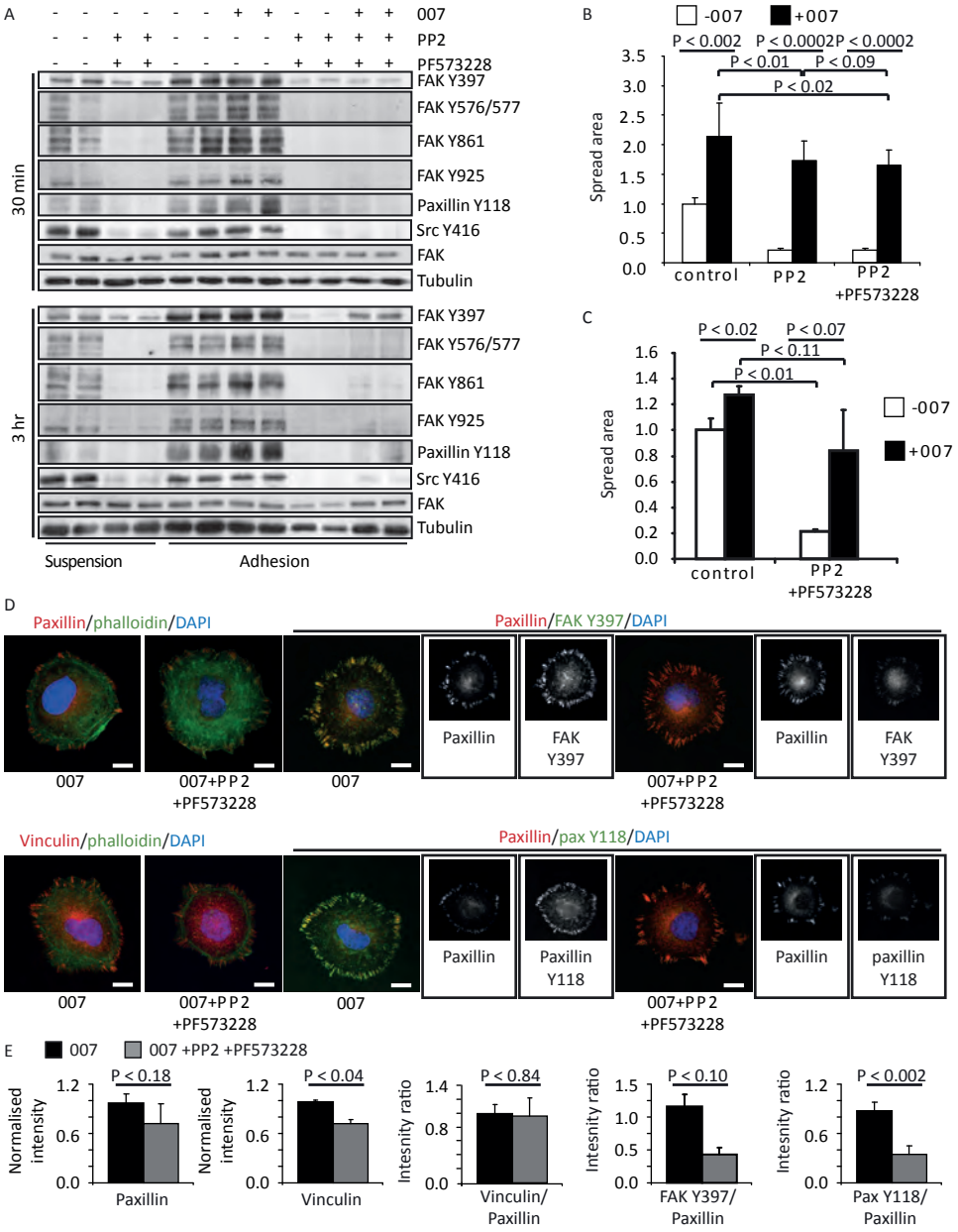

Figure 6: Effect of inhibiting FAK and Src activation on 007-induced cell spreading and focal adhesions.
Cells were trypsinised and allowed to roll for 1.5 hours in the absence or presence of 20μM PP2 and 1μM PF563228 before analysis. In (A), A549-Epac1 cells were plated onto fibronectin for 30 minutes or 3 hours with or without 100 μM 007 and were then lysed in Laemmli sample buffer. Proteins were separated by SDS-PAGE and phospho-FAK, phospho-Src and phospho-paxillin levels were determined by western blot. A representative of 3 individual experiments is shown. To analyse spreading, A549-Epac1 cells were replated and allowed to spread for 3 hours (B) or human umbilical vein endothelial cells were allowed to spread for 1 hour (C) before being fixed and stained. For each experiment, the spread area of at least 30 cells per condition was quantified and standardised to the mean

Discussion

In this study, we developed image analysis tools for the automated and quantitative analysis of cell spreading. For the first time, we have been able to make a detailed analysis of how activation of Rap1 modulates the kinetics and morphology of cells spreading over a fibronectin matrix. We observed that, under basal conditions, A549-Epac1 cells exhibited an anisotropic mode of spreading, where both an increase in cell spread area and a steady state of spread area was accompanied by extensive remodelling of the overall shape of the spread area of cells, mediated through continuous protrusion and retraction of the cell periphery. This anisotropic mode of spreading gave rise to the angular morphology of A549-Epac1 cells observed in fixed samples [144]. Addition of 007, to activate endogenous Rap proteins specifically via the exchange factor Epac1, promoted a faster rate of cell spreading, induced cells to spread isotropically and reduced the remodelling of the spread area which occurred under basal conditions.

A factor that controls whether cells spread isotropically or anisotropically, is the availability of ECM ligand sites to which cells can attach and make protrusions [106]. Lower ECM concentrations promote anisotropic spreading, as cells have to "search" for ligand-dense sites which activate Src sufficiently to induce the formation of stable attachments [106]. Our results show that Rap1 activation can induce isotropic spreading on an ECM substratum that otherwise drives anisotropic spreading. This indicates that Rap1 can promote and stabilise functional adhesion complexes at ligand sites that integrins may be able to attach to, but may not be sufficient to activate Src-driven protrusion. The ability of Rap1 to induce adhesion and spreading in the presence of PP2, even though outside-in signaling and the basal adhesion of A549-Epac1 cells were completely blocked, further supports this conclusion. Through the ability to induce adhesion, spreading and cell morphology changes by mechanisms that do not rely on the canonical ECM-derived signals, Rap1 may influence many stages of tissue development, including stem cell differentiation which is, in part, determined by the constraints induced by the extracellular matrix microenvironment [148-150].

One explanation for the rescue of spreading in the presence of PP2 is that, through the GEF, C3G, Rap1 functions downstream of Src, and, by stimulating Rap1, the next step in the Src pathway is being re-activated [139]. However, our data show that the canonical phosphorylation sites in the FAK-Src-Paxillin module that were blocked by the inhibitors, PP2 and PF573228, were not rescued by Epac1-induced Rap1 activation. These data demonstrate that Rap1 does not regulate the FAK-Src signaling pathway and that the Src pathway is not truly reconstituted by Rap1 activation. Furthermore, as activation of Rap1 via C3G is reported to be mediated, in part, by actomyosin-induced force [97], our findings that

area of cells spreading without 007 or inhibitors. The graphs in (B) and (C) show the mean of 6 or 3 experiments, respectively ± the standard error of the means. Focal adhesion composition after 3 hours of spreading was determined by immunofluorescence using antibodies against paxillin, FAK Y397, paxillin Y118 and vinculin (C). Representative cells are shown, with greyscale images of the single channel fluorescence from the dual stained focal adhesions shown alongside the merged images. The scale bars represent 10 μm. The fluorescent intensity of the focal adhesion staining was determined and standardised to the cellular background (D). Total paxillin or vinculin levels were normalised to the intensity of the 007 condition, and the ratio of vinculin to paxillin present in each condition was calculated. Phospho-FAK and phospho-paxillin levels were calculated as ratios of the fluorescent intensity of the co-stained paxillin. The average results for 3 experiments are shown (with 10 cells for each condition) ± the standard error of the means. P values were calculated using paired student's t-tests.

Epac1-induced Rap1 activation can promote force-dependent FAs indicate that activating Rap1 is not simply reconstituting the Src pathway one-step down. Rather, our results place Rap1 regulation of adhesion and spreading in a parallel, or bypass, pathway from the FAK-Src-signaling module.

We have shown that Rap1 activation creates an ECM-integrin-actomyosin link, and focal adhesions that were responsive to changes in actomyosin contractility, in order to promote adhesion and spreading. It is, therefore, likely that the mechanisms by which Rap1 initiates spreading and FA formation in the presence of PP2 are analogous to the processes by which the FAK-Src module controls adhesion. It is well characterised that the FAK-Src signaling module induces a transient reduction of RhoA activity to promote cell spreading, followed by an induction of actomyosin-induced tension which induces the maturation of FAs [51, 106, 110]. Therefore, as Rap1-initiated spreading in the presence of PP2, our data indicate that Rap1 itself could lower actomyosin-induced tension. Furthermore, as 007-induced focal adhesions were modulated by actomyosin contractility, it suggests that Rap may mediate a temporal and localised regulation of RhoA activity, similar to that which is instigated during Src-mediated spreading [51, 106, 110]. Although Rap1 is implicated in modulating actomyosin tension, it is currently unclear which Rap effectors would regulate RhoA in our cell system, as we previously found that siRNA against Arap3, Krit1, or RA-RhoGAP/ARHGAP20 did not alter Rap-induced cell spreading of A549-Epac1 cells [144].

Our data implicate Rap1 activity as one of the mediators of force-dependent strengthening and maturation of FAs, a process that previously has largely been attributed to the FAK-Src-Paxillin cascade [79]. Indeed, we found that the relative level of vinculin in Rap1-induced FAs was not altered upon the inhibition of the FAK-Src module although paxillin phosphorylation was strongly inhibited. In laser tweezer experiments using fibronectin-coated beads, mechanical force in the absence of Src kinase activity has been demonstrated to recruit vinculin to bead-cell focal complexes [77]. Thus, in Rap1 activated and Src-inhibited cells, we created a similar situation at FAs, and demonstrated that Rap1 activation permitted the recruitment of vinculin to adhesions. As adhesions induced by Rap1 are mechanosensitive, the mechanism by which Rap1 activation recruits vinculin to adhesions may be primarily via stretch-dependent unfolding of Talin [21, 77, 116, 151-153]. This requires further investigation, however, our model system that combines inhibition of Src with active Rap1, will be a valuable tool for the characterisation of FAK-Src independent mechano-regulation of integrin adhesions.

Together, our data demonstrate that activation of Rap1 induces a functional ECM-integrin-actomyosin link that promotes adhesion and spreading, but which does not depend on the activity of the FAK-Src signaling module. Thus, Rap1 induced adhesion and spreading in A549-Epac1 cells shows similarities to Src-induced processes, but we propose that they are driven by parallel pathways. By regulating the ECM-integrin-actin link by distinct molecular mechanisms from the FAK-Src-paxillin cascade, a localised activation of Rap1 in cells within tissues may act to reinforce the contacts between cells and their extracellular environment. Indeed, the regulation of Rap1 activity has recently been implicated as being critical for preserving the attachment of neural stem cells to their niche [154]. Therefore, activation of Rap1 may play a vital and significant role in modulating the physiological interaction between cells and their extracellular matrix environment to contribute to the structural maintenance and integrity of tissues.

Materials and methods

Cell Lines and Culture

The monoclonal Epac1-expressing A549-Epac1 cell line (derived from the A549 carcinoma (ATTC) and previously described in [86, 144] and the derivative cell lines made in this study were cultured in RPMI supplemented with L-glutamine, antibiotics, and 10% FCS (Gibco). Human umbilical vein endothelial cells (Lonza) were cultured using standard procedures [124].

Derivative A549-Epac1 cell lines, stably transfected with GFP-Lifeact or short hairpins, were made by a lentiviral delivery system. Lentiviruses were produced by transfection of 293T cells (ATCC) with SIN-inactivated virus constructs. A549-Epac 1 cells were plated in full medium in a 6-well plate overnight and then transduced with GFP-Lifeact [155] or short hairpin virus supernatants in the presence of 4 µg/ml polybrene for 24 hours before returning the cells to full growth medium. GFP-Lifeact expressing cells were selected by fluorescence-activated cell sorting (FACS) by their GFP expression levels, while cells expressing the short hairpins were selected by adding puromycin to the culture medium at a concentration of 2 µg/ml.

Reagents and Antibodies

8-pCPT-2′-O-Me-cAMP (007) was obtained from BioLog Life Sciences Institute, Bremen. PP2 was from Torcis bioscience and PF573228 and Y27632 were from Sigma-Aldrich.

Antibodies were from BD Biosciences (paxillin, FAK, RockI and RockII), Chemicon (α-tubulin), Sigma-Aldrich (vinculin), Cell Signaling (β-actin, phospho-FAK Y566/567, phospho-FAK Y925, phospho-paxillin Y118, phospho-SrcY416), Invitrogen (phospho-FAK Y397), GeneTex (phospho-FAK Y861) and Millipore (GAPDH). The integrin inhibiting antibodies AIIB2 (anti-β1) and GOH3 (anti-α6) were derived from the hybridoma cell lines (antibody-containing tissue culture supernatant was a gift from A. Sonnenberg, The Netherlands Cancer Institute, Amsterdam). The Pelicluster CD61 antibody (anti-β3) was from Sanquin.

Control and FAK-targeting short hairpin lentiviral MISSION vectors from the TRC1 library were obtained from Sigma-Aldrich. siRNAs were obtained from Dharmacon, and ON-targetplus SMARTpool siRNA oligos were used to deplete Rap1A, Rap1B, RockI, RockII and FAK.

Fibronectin was purified from human plasma as described previously [156].

DNA Constructs

The pRRL LifeAct-pEGF construct for the production of GFP-Lifeact lentiviruses was a gift from O. Pertz (University of Basel, Switzerland).

Cell transfection

For knockdown experiments, A549-Epac1 cells were seeded sparsely and transfected straight away with 50 nM siRNA oligos (Dharmacon) using HiPerFect (Quiagen) according to the manufacturer's protocol. Transfected cells were left for 48 hours before being analysed further.

Short-term adhesion assays

Short-term adhesion assays were performed as described previously [144]. A549-Epac1 cells were trypsinised, washed in RPMI containing 10% FCS, and kept in suspension for

1.5 hours in RPMI containing 0.5% FCS, glutamine, antibiotics, and 20 mM Hepes, pH 7.4, at 37 °C. 48-well plates were coated with fibronectin overnight at 4°C, and blocked with heat-denatured BSA for 1 hour at 37 °C. Cells were plated into the fibronectin-coated wells and allowed to adhere for 30 minutes at 37 °C in the presence or absence of 100 μM 007. All conditions were performed in quadruplicate. After 30 minutes, non-adherent cells were removed and adherent cells were washed once with pre-warmed PBS. Cells were lysed in alkaline phosphatase buffer (0.4% Triton X-100, 50 mM sodium citrate, and 10 mg/ml phosphatase substrate (Sigma-Aldrich)). The total number of cells adhering was determined by phosphatase assay [157]. Aliquots of the cell suspension added to each well were taken, pelleted by centrifugation and then lysed to determine the total number of cells added per well. The adhesion of cells to wells blocked with heat inactivated BSA but not coated with fibronectin was taken as background, and subtracted from the readouts for basal and 007-induced adhesion. The adhesion over 30 minutes was expressed as a fraction of the total cells added to the wells.

Inhibiting antibodies, Pelicluster CD61 (used at a 1:100 dilution), AIIB2 (used at a 1:10 dilution) and GOH3 (used at a 1:10 dilution) were added to cells just prior to plating out onto fibronectin. In controls, 1% FCS in DMEM was added in a 1:5 dilution and 10 mg/ml BSA was added at a 1:100 dilution to take into account any effects of the storage buffer of the antibodies.

Spreading assays

In spreading assays, either for live-cell imaging or for fixed immunofluoresence assays, cells were trypsinised using a 1:4 dilution of the trypsin stock, washed once with the appropriate media with 10% FCS and then kept in suspension for up to 1.5 hours at 37 °C in media containing 0.5 % FCS, glutamine, antibiotics and 20 mM Hepes. Cells for immunofluorescence were maintained in RPMI, while cells used for live-cell imaging were kept in suspension in Leibovitz's L15 medium (Gibco). For spreading assays with human umbilical vein endothelial cells, the cells were kept in full growth media. During the time in suspension, cells were incubated with inhibitors (20 μM PP2 or 1 μM PF573228) as required. Following recovery, cells were plated onto glass which had been coated with fibronectin overnight at 4 °C at a density of 1.25×10^4 cells/cm^2. For immuofluoresence, cells were applied to coverslips in 24-well plates or, for live-cell imaging experiments, into LabTekII 8-chambered slides (Nalge Nunc International).

For live-cell imaging, cells were plated out in the presence or absence of 100 μM 007 and imaged from approximately 30 minutes after plating, for the following 3 hours. Cells did vary in the extent to which they had already spread at the commencement of imaging, but cells were always captured during the time when the spreading rate over the first 30 minutes of imaging was linear. Imaging was managed using Metamorph software, with images being captured every 5 minutes using a Zeiss Axiovert 200M microscope in a climate-controlled incubator. Stage positions were controlled using a Zeiss MCU 28 robotic stage. Images of GFP-Lifeact-expressing cells were collected using a Lambda DG-4 Ultra High Speed Wavelength Switcher (Sutter Instruments) as a light source and a Coolsnap HQ CCD camera (Photometrics) through a Zeiss Fluar 20× objective or a Zeiss PLAN NeoFluar 63× objective. For each experiment, at least five different stage positions were acquired for each spreading condition.

In immunofluorescence assays, cells were allowed to adhere and spread for 3 hours in the presence or absence of 100 μM 007. After 3 hours, the cells on the coverslips were fixed in

cytoskeletal buffer (0.5% Triton X-100, 10 mM Pipes, pH 7, 50 mM KCl, 2 mM CaCl2, 2 mM MgCl2, 300 mM sucrose) with 4% (v/v) paraformaldehyde for 15 minutes. Coverslips were blocked overnight in 2% (w/v) BSA in TBS at 4 °C. Focal adhesion proteins were detected using the appropriate antibodies and Alexa 568- or Alexa 488- coupled secondary antibodies. Actin was visualised using phalloidin coupled to Alexa 488 (Invitrogen). Immunofluorescence images were acquired using a Zeiss Axioskop 2 microscope fitted with a Zeiss Axiocam CCD camera and 40× and 100× Plan APO objective lenses.

Automated Image analysis and quantification

For automated analysis, a detection and tracking algorithm was implemented in MatLabR2008a (Mathworks Inc). Cells were detected in images using local watershed segmentation upon smoothing. To ensure that all data was collected for the same, single cell over the course of a time-lapse movie, images captured through the 63× objective lens were cropped so that only one cell was visible in each frame. To maximise the number of cells for statistical analysis, we used the 20x objective to image cells which had been transfected with siRNA or cells where PP2 was to be added post-spreading. In images taken through the 20× objective, multiple single cells were analysed for each frame. Individual cells were tracked in time, linking cells from one frame to the next using the overlap of detected objects between consecutive frames. In situations where the detection of a cell was lost between frames, and, therefore, an overlap could not be detected, the object was linked with the five subsequent time-frames so that the tracking of the object could be continued as long as possible. To remove erroneously detected background structures, objects with an average intensity similar to the average intensity of the whole image were discarded. All tracks were validated manually. The size of the spread area of a cell was evaluated by determining the number of pixels within the region of detection, and plotted over time to analyse the spreading kinetics. In 20× images, the spreading areas of all the tracked objects were averaged to obtain the mean spread area of cells in the entire field of view. In a single experiment, the final result for a particular spreading condition was the average of five different 20× fields of view. The average spreading rate was calculated by determining the gradient (m) of the increase in spread area per hour during the first 30 minutes of imaging. Due to differences in imaging conditions, the m values calculated from images collected using the 20× objective lens are not directly comparable to those obtained from images gathered by the 63× objective lens. Statistical analyses on time course data were performed by two-way ANOVA with replication.

Protruding and retracting areas in the 63× images were determined by subtracting the segmented image at a particular time point from the subsequent segmented image in the time-lapse movie to produce an image showing regions gained, lost or unchanged between the two frames. In this image, pixels that were unchanged between frames had a value of 0, pixels that were lost in the subsequent frame (retractions) had a value of -1, while pixels that appeared in the succeeding frame (protrusions) had a value of +1 (Supporting Information, Figure S1) and the total number of pixels with value -1 or +1 was determined. Total area of protrusion and retraction per image was then calculated as percentage of the total cell area in the second frame used in the image calculation. The circularity (circle ratio) of a cell was calculated by quantifying the ratio between the cell area and the area of the circle with a radius measuring the same distance as that between the cell centre and the most distant pixel detected on the edge of the cell at that time point (Supporting Information, Figure S1). For the quantification of the changes to spread area shape over time, at each time point, the standard deviation of the distribution of the distances from the cell centre to every pixel on

the cell edge was determined and normalised to the mean distance to correct for differences in cell size (Supporting Information, Figure S1). The normalised standard deviation (σ_n) was calculated using the standard equation. The variance at time **t** was subtracted from variance at time **t**+1 and the average difference of the variance ($\Delta\sigma_n$) between consecutive time-lapse frames for all analysed cells was determined.

Quantification of cell spread area in immunofluorescence assays

ImageJ (NIH) was used to quantify cell spreading of fixed and stained cells as described previously [144]. Briefly, for each spreading condition, images of at least 30 cells taken from a minimum of 3 different fields of view were captured through the 40× objective. The average cell spread area, in pixels, for each condition was calculated per data set. Data for these individual experiments were then standardised to a value determined by averaging the spread area of control cells for all the data sets analysed. Statistical analysis was performed by paired student's t-tests.

Quantification of Focal Adhesions in immunofluorescence assays

To analyse the composition of focal adhesions under different conditions, the fluorescent intensity of immuno-labelled components in fixed cells was measured. In these assays, the levels of focal adhesion-localised paxillin and vinculin were analysed in single immuno-stainings with a phalloidin counter-stain, while the levels of phospho-FAK and phospho-paxillin were analysed by dual immuno-staining with unphosphorylated paxillin. In order to permit comparison between the intensity levels of staining, the same exposure conditions were used to capture all images for a particular staining within an experiment. The secondary antibodies did not stain components of focal adhesions independently of the primary antibody. Focal adhesions were detected, based on the paxillin or vinculin signal, using local watershed segmentation. In the dual stainings, the objects detected by the paxillin staining were used as mask for detecting the region in which to analyse the phospho-focal adhesion protein. The cell outline was determined by thresholding the phalloidin staining, or by thresholding the paxillin signal in the dual focal adhesion stained cells. All measured focal adhesions were within the designated cell area and outside a user specified area, which allowed the false detection of nuclear spots to be excluded. For each image, the average fluorescence intensity outside the cell area was subtracted from the image to remove camera and other noise. The average fluorescence intensity detected within the cell area, excluding the regions detected as focal adhesions, was then taken as the cellular background. The total intensity of all the detected focal adhesions in the cell was determined and normalised to the cellular background. For the paxillin and vinculin single stainings, in each experiment, the average intensity of all cells analysed per condition was determined. Data from multiple experiments were standardised to the value obtained by averaging the intensity of 007-only treated cells from all the data sets gathered. The vinculin composition under different conditions was analysed by determining the ratio between the normalised vinculin and normalised paxillin levels. For the dual stained adhesions, the ratio between the normalised paxillin and the normalised phosphorylated adhesion protein was calculated. Paired student's t-tests were used to perform statistical analysis.

Isolation and analysis of Rap-GTP

Cells were transfected with siRNA for 48 hours and then stimulated with mock or 100 μM 007 for 15 minutes. Cells were lysed in Ral buffer (50 mM Tris.HCl pH 7.5, 200 mM NaCl, 2 mM MgCl2, 1% (v/v) NP40, 10% (v/v) glycerol, 1 mM PMSF, 1 μM leupeptin, 0.1 μM

aprotinin), and the lysates were pre-cleared by centrifugation. The Rap-GTP was captured using the RalGDS-RBD, pre-bound to Glutathione agarose, over 45 minutes as described previously [158]. Endogenous Rap1 was detected by western blotting.

Western blotting to analyse activation of the Src-signaling pathway

As for spreading assays, cells were trypsinised, washed once with the appropriate media with 10% FCS and then kept in suspension for 1.5 hours at 37 °C in media containing 0.5% FCS, glutamine, antibiotics and 20 mM Hepes in the presence or absence of the appropriate inhibitors. Cells were allowed to adhere in the presence or absence of 100 μM 007 for 30 minutes or 3 hours and lysed using Laemmli sample buffer. Depletion of proteins by siRNA was determined by lysing cells transfected for 48 hours in Laemmli buffer.

Protein samples were separated using SDS-PAGE and transferred to PVDF membranes (Immobilon). The membranes were blocked for 1 hour using 2% BSA and then probed with the appropriate primary antibody. The antibodies were detected by anti-mouse or anti-rabbit antibodies conjugated to horseradish peroxidase, and proteins were detected by ECL.

Acknowledgements

We would like to thank Stefan van der Elst, of the flow cytometry facility, Hubrecht Institute, Anko de Graaff of the Hubrecht Imaging Centre and Livio Kleij, Department of Experimental Oncology, University Medical Center, for their technical assistance, and Bastiaan Spanjaard for discussions on image analysis.

Figure S1: Quantification of cell spreading

Cell protrusion and retraction were quantified by detecting areas of pixel gain or loss between successive frames of time-lapse movies (A). Cells edges (shown in red) were detected using local watershed segmentation upon smoothing and the images binarised. The binarised image at time point, t, (I(t), middle panel), was subtracted from the binarised image of the subsequent frame of the movie (I(t+1), left panel) to determine unchanged regions (grey), lost areas (black) or pixels gained (white) between the two frames. Sizes of areas lost or gained were determined, and expressed as fractions of the total area of the cell in frame I(t+1). The circle ratio was used to evaluate cell shape at each frame of a time-lapse movie (B). The area of a circle (dashed circle) with a radius equalling the length from the centre of the cell to the most distant pixel of the detected cell edge (solid red line) was determined. The ratio between the area of the cell and the circle was then calculated. Shape changes were analysed by determining the variance of the lengths from the centre of the cell to each pixel detected on the periphery. In (C), the black lines mark the shortest and longest lengths from the centre of the cell to the periphery for two consecutive frames of a time-lapse movie of a cell spreading without 007 (top panel) and with 007 (bottom panel) to illustrate how these may change over time. The normalised standard deviation for all the points of the cell periphery (σ_n) is written underneath the cell. The difference of the variance ($\Delta\sigma_n$) was calculated by subtracting the σ_n value for time point t+1 from the σ_n at time point t. Cells displaying dynamic shape changes have a higher $\Delta\sigma_n$ over time.

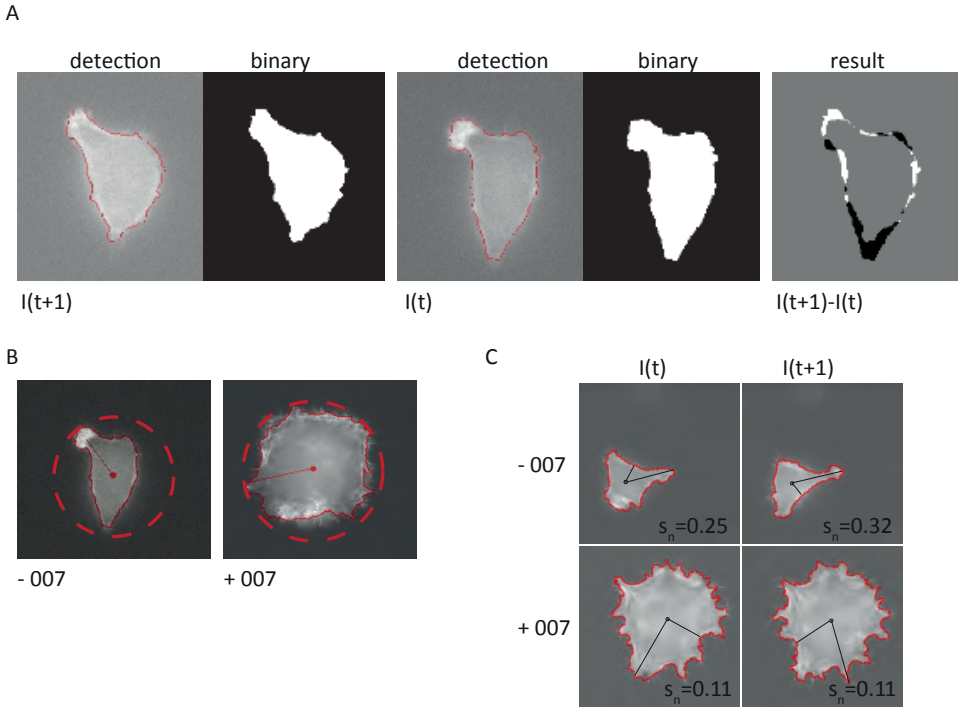

Figure S2: Effect of FAK depletion on cell spreading

A549-Epac1 cells were transduced with either a control (shC002) lentiviral short hairpin, or one targeting FAK (shFAK), and stable expression of the constructs were selected by adding puromycin selection to the growth media. These cells were then subjected to transient transfection of control (siC) or siRNA targeting FAK (siFAK). Depletion of FAK under different conditions was determined by western blot (A). A549-Epac1 cells treated with control and FAK-targeting short hairpins and siRNA were trypsinised and allowed to roll for 1 hour in the absence or presence of 20 µM PP2 and 1 µM PF563228 before being plated onto fibronectin with or without 100 µM 007. They were allowed to spread for 3 hours before being fixed and stained. The FAK content of focal adhesions after 3 hours of spreading was determined by immunofluorescence (B). Representative images of cells treated with 100 µM 007 are shown, with greyscale images of the anti-FAK focal adhesion staining shown alongside the merged images. The scale bars represent 10 µm. Images of at least 30 cells per condition per experiment were captured, and ImageJ was used to quantify the spread area of the cells (C). For each experiment, the spread area of cells in each condition was standardised to the mean area of cells spreading without 007 or inhibitors. The graph in (C) shows the average of 2 experiments ± the range of the means. The P values were calculated using a paired student's t-test.

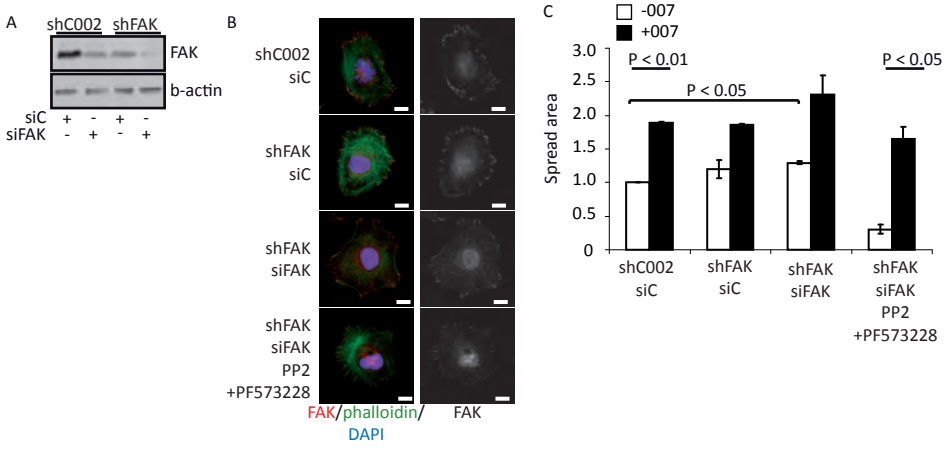

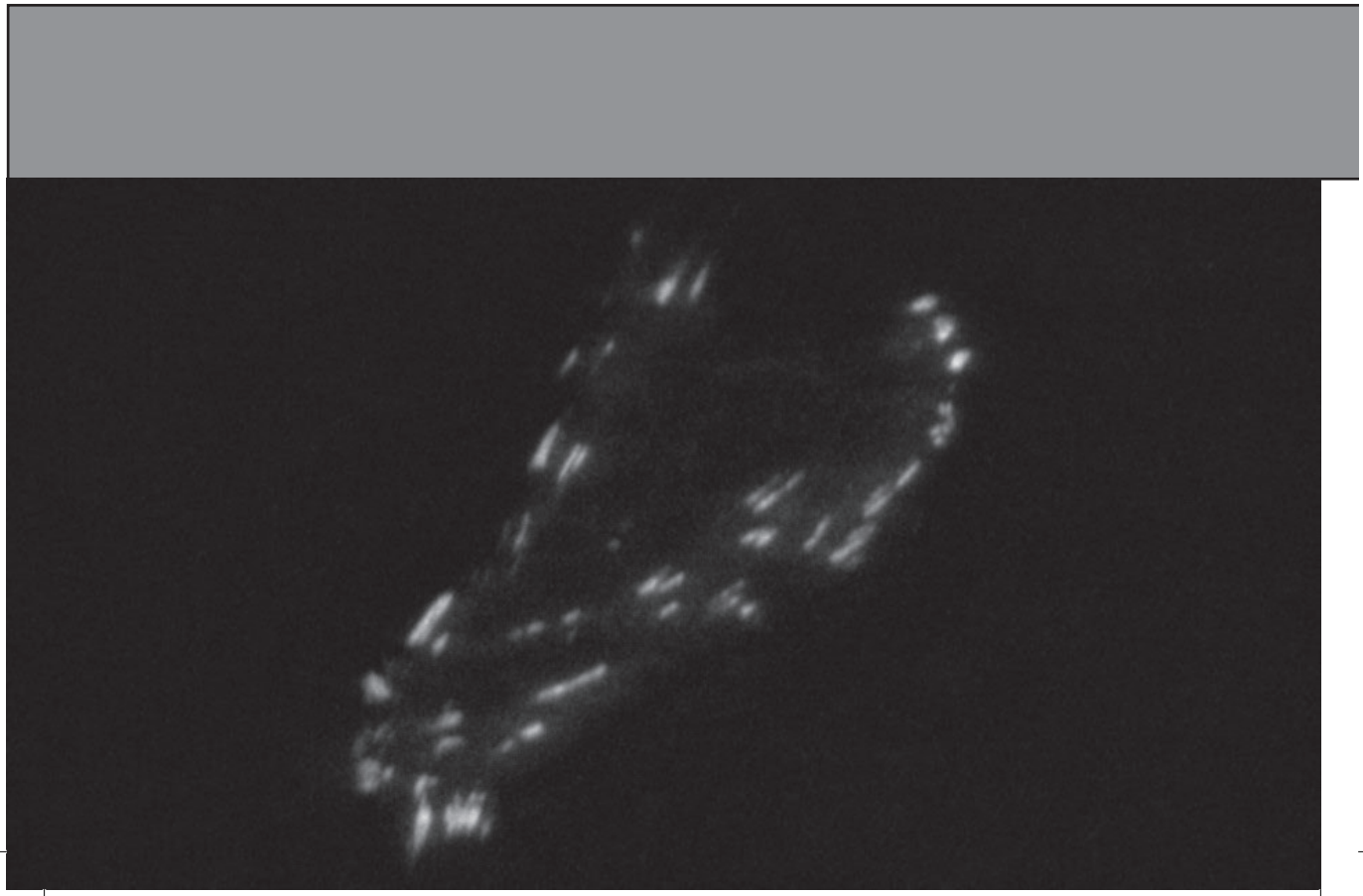

Quantitative imaging uncouples Focal Adhesion dynamics from the regulation of cell migration

3

Emma Spanjaard[1], Ihor Smal[2], Nicos Angelopoulos[3], Ingrid Verlaan[1], Erik Meijering[2], Lodewyk Wessels[3], Hans Bos[1], Johan de Rooij[1]

1 Department of Molecular Cancer Research, Centre for Biomedical Genetics and Cancer Genomics Centre, University Medical Center, Utrecht, The Netherlands.
2 Departments of Medical Informatics and Radiology, Erasmus MC - University Medical Center Rotterdam, Rotterdam, The Netherlands
3 Division of Molecular Carcinogenesis, Netherlands Cancer Institute, Amsterdam, The Netherlands

Submitted for publication

Abstract

Cell migration is crucial in development, tissue repair and immunity and aberrant in pathological process including tumor metastasis. Focal Adhesions (FA) are integrin-based adhesion complexes that form the link between the cytoskeleton and the extracellular matrix and are thought to orchestrate cell migration. A number of major FA proteins, like Src, focal adhesion kinase (FAK) and Paxillin [159-161], have been implicated in development and/or tumor metastasis, underscoring the relevance of their investigation. Here we describe the development of a robust FA tracker that enables the automatic, multi-parametric analysis of FA dynamics, morphology and composition. By automated analysis of freely migrating prostate carcinoma cells, we show that this software recapitulates previous findings that FAs have specific characteristics associated with their lifetime and their cellular location. We then used our software to investigate how FA characteristics are altered when cell migration is induced by the metastasis-promoting hormone HGF and subsequently inhibited by activation of the small GTPase Rap1. We analyzed the data at 2 levels: 1) Bayesian network inference (BNI), using all measured characteristics as input, shows that little correlation exists between changes in cell migration and FA characteristics. Instead BNI indicates a concerted coordination of cell size and FA parameters. 2) At the level of individual FA parameters, we identified FA size, sliding and intensity as primary targets of Rap1, which is in agreement with recent data showing that Rap1 inhibits cytoskeletal contractility [91]. Thus our results question a direct relation between the regulation of cell migration and the regulation of FA dynamics.

Introduction

Regulated cell migration is vital for embryonic development and tissue morphogenesis and underlies pathological processes like tumor metastasis. 2D culture has been instrumental in the elucidation of the fundamental principles, proteins and regulatory mechanisms involved in cell migration. Integrin-based adhesion complexes, collectively called Focal Adhesions (FA), are the mechanical units that connect the intracellular cytoskeleton to the extracellular matrix (ECM) and provide the traction necessary for productive cell migration. FAs are also signal transduction centers that relay mechanical information from the extracellular matrix (stiffness, density) to the intracellular machinery. FAs contain a number of proteins that regulate cytoskeletal organization and dynamics to alter local and global cell mechanics and a number of proteins that regulate signaling cascades to alter nuclear processes such as proliferation and differentiation. Over 1000 putative FA inhabitants have been identified by proteomics [162] and at least 150 have been established as true FA proteins in detailed studies [108]. FAs have also been identified in 3D culture of tumor cells [163] and in vivo in vascular endothelium (unpublished observations). The relevance of the investigation of FAs for cancer cell migration is further underscored by the fact that expression levels and/or signaling activity of FA proteins are often found deregulated in metastastic cancer [164, 165]. Furthermore, inhibitors of 2 master regulators of FA dynamics, FAK and Src are being developed as clinical inhibitors of cancer progression [166-168].

FAs come in a range of different sizes and although generally described as elliptic, their shape also varies largely upon close inspection. Differences in size, shape and dynamics have been associated with involvement in different aspects of the migratory process. Small FAs (then called Focal Complexes) form in the front of a migrating cell, where they stabilize the actin-polymerization driven protrusion (lamellipodium) by linking it to the extracellular matrix [7, 9, 11]. At the base of the lamellipodium, FAs can either turnover or mature into larger FA. These FAs are static structures that provide the anchor points on which traction force can be exerted to pull the cell body forward. As a cell migrates over its FAs they become more centrally located and eventually end up in the rear where they need to disassemble to allow retraction of the rear of the cell [169, 170]. At this stage FAs are no longer stationary and display a sliding motion towards the center of the cell.

The formation, turnover, maturation and senescence or death of FAs is subject to regulation by a number of signaling pathways. For instance, key to the decision to mature or turnover is the phosphorylation state of FAK and paxillin[50, 171, 172]. FA growth and elongation (maturation) is a tension sensitive process in which the molecular composition changes due to recruitment and activation of other FA proteins like vinculin and zyxin [77, 79, 171, 173, 174]. FA disassembly in the center and rear of the cell can be mediated by a diversity of mechanisms, including metalloprotease cutting of the integrin ECM connection or calpain-induced proteolysis of FA proteins, like talin, paxillin and FAK [70-72]. Furthermore a decrease of actomyosin-based tension, possibly through microtubule-dependent delivery of relaxation factors [68, 69] is observed in cell-rear-located FAs which underscores their mechanosensitivity. Thus, at FAs mechanical signals and biochemical signals converge to regulate FA size, shape, dynamics and lifecycle (reviewed in [5]).

Because FA characteristics vary with their role in cell migration and signaling factors that regulate cell migration-dependent processes also affect the characteristics of FAs, it is logical to speculate that the regulation of FA characteristics by such signaling factors is a causative step in their regulation of cell migration, but this has never been directly investigated to

our knowledge. To better understand how FA characteristics and dynamics correlate with cell migration and if signaling factors indeed target FAs to regulate cell migration, we have developed a method that automatically detects and tracks individual FAs (in time lapse image series generated by TIRF microscopy of fluorescently tagged FA proteins) and relates those to their cellular region. We have induced migration by the metastasis-promoting hormone HGF and inhibited migration by the subsequent activation of the small GTPases Rap1. Surprisingly, our analyses reveal that very few FA characteristics change upon induction of cell migration by HGF, whereas Rap1 activation, which rapidly blocks cell migration, reduces FA intensity, FA size and FA velocity. Co-analyzing all measured FA parameters and overall cell behavior by means of Bayesian network inference (BNI), showed that cell size and FA behavior are highly connected, whereas cell migration speed and FA behavior are largely uncoupled. In conclusion, we have developed robust automatic FA detection and tracking software, revealed new specific effects of Rap1 on FA behavior and failed to show correlations between the regulation of FA morphology and dynamics and the regulation of cell migration.

Results

Workflow and algorithms of the FA detection and tracking software

The workflow of the detection and tracking software we developed in MatLab is depicted in Figure 1A. The images that served as input for this FA-tracking algorithm were generated by TIRF microscopy using cells that expressed fluorescently tagged FA proteins. (Fig. 1E).
In the first part of the method we determine the localization of the adhesions, using an h-dome based detector [175] (Fig. 1B). This method has been shown to perform well even in images with relative low signal to noise ratio [176]. In three steps of pixel separation, clustering and center of mass determination, the x and y coordinates of the centers of FAs are found. First a marker image is constructed by subtracting a user-defined value **h** from the original image, after a smoothing step with a Gaussian shaped kernel with a user-defined deviation **σ** (Fig. 1B1). Using gray scale reconstruction [177], a background image is produced (Fig. 1B2). The hDome image is then created by subtracting this image from the original. The hDome image

Figure1: hDome detection

A) The framework of the detection method. B) The unprocessed image for hDome segmentation, for further explanation zooming in on the red square. B1) Smoothed image (left) and corresponding 3D intensity plot. B2) Background image (left), created with grayscale reconstruction and its corresponding 3D intensity plot (right). B3) Zoom of the hDome image (left), resulting from subtracting the background image from the smoothed original and its corresponding 3D intensity plot (right). B4) Image upon weight assignment (left) and its 3D intensity plot (right). B5) Spot image formed upon Monte Carlo simulation and upon clustering (left) and its corresponding 3D intensity plot (right). C) Zoom-in of overlay of the markers detected with the hDome method for the watershed segmentation (left), and the watershed segmentation (right). C1) The adaptive threshold line indicating the intensity range and local threshold of the depicted FAs 1 and 2. C2) Result of thresholding each region that was found in the watershed according to the adaptive threshold line (left) and the overlay in red on the original image (right). C3) Overlay of detected FAs on the original image, with the zoom area in green. D) Determination of protruding and retracting cell areas by subtracting the binary cell image at time (t1) from the image at time (t+5) (top). In the result image, newly arisen areas have value 1 (white) and disappeared areas have value -1 (black) (bottom left). In this result image triangles are drawn from the centre (red dot) along the edges of the found regions (green lines) to enlarge the protruding and retracting regions towards the centre with a maximum width of 50 pixels (green area) (bottom right). D1) Color code image of the FAs in the different areas: green in a protruding region, red when in a retracting region and otherwise blue.

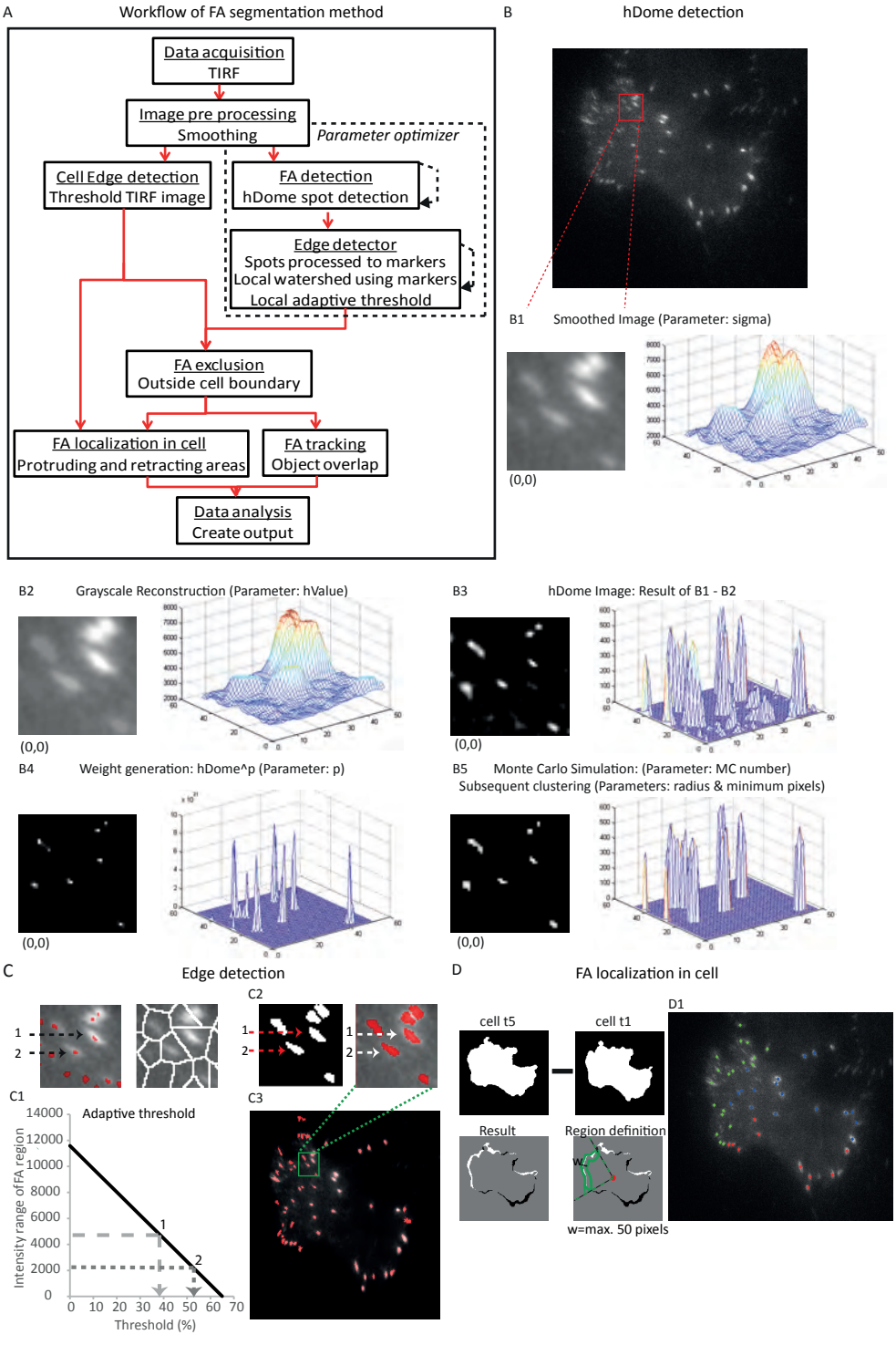
A
Workflow of FA segmentation method
Data acquisition
TIRF
Image pre processing
Smoothing
Parameter optimizer
Cell Edge detection
Threshold TIRF image
FA detection
hDome spot detection
Edge detector
Spots processed to markers
Local watershed using markers
Local adaptive threshold
FA exclusion
Outside cell boundary
FA localization in cell
Protruding and retracting areas
FA tracking
Object overlap
Data analysis
Create output
B
hDome detection
B1
Smoothed Image (Parameter: sigma)
(0,0)
B2
Grayscale Reconstruction (Parameter: hValue)
(0,0)
B3
hDome Image: Result of B1 - B2
(0,0)
B4
Weight generation: hDome^p (Parameter: p)
(0,0)
B5
Monte Carlo Simulation: (Parameter: MC number)
Subsequent clustering (Parameters: radius & minimum pixels)
(0,0)
C
Edge detection
C1
Adaptive threshold
Intensity range of FA region
Threshold (%)
C2
C3
D
FA localization in cell
D1
cell t5
cell t1
Result
Region definition
w=max. 50 pixels

A Manual edge Detection

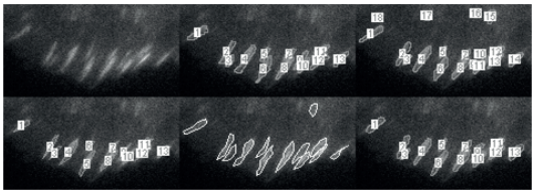

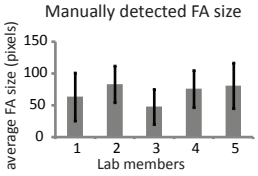

B Optimizer input

Image and outline input (OI)

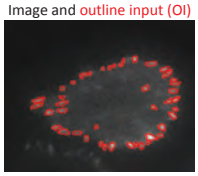

Input and outline input (OI)

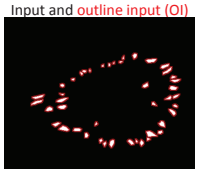

C Adaptive threshold optimizer

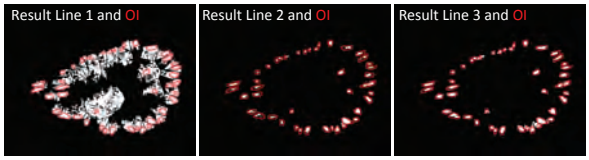

Adaptive threshold lines

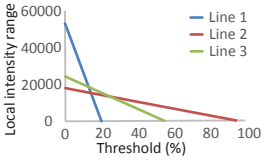

Accuracy	Line 1	Line 2	Line 3
A: r (result vs input)	0.32	0.55	0.72
Total r (sum of 3 different cells)	0.95	1.75	2.18

D hDome parameter optimizer

Segmentation results:

Set 2 (+line 3) and OI

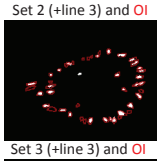

Set 3 (+line 3) and OI

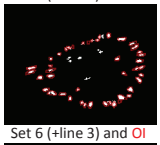

Set 6 (+line 3) and OI

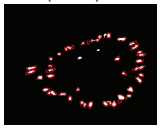

hDome parameters:

Set:	1	2	3	4	5	6	7	8	9	10
hValue	600	650	700	750	800	900	950	1000	1100	1150
sigma	1.5	3	1.5	1.5	3	1	3	2.5	1	2.5
P	8	12	5	8	12	12	8	11	7	11
radius	6	5	4	4	4	3	2	6	5	4
min #	6	5	6	6	2	3	2	5	4	5

Accuracy	Set 2	Set 3	Set 6
A: r (result vs input)	0.64	0.70	0.69
B: FA count	0.64	1	0.98
(A+B) for 1 cell	1.28	1.70	1.67
Total precision value (sum of 3 different cells)	3.61	4.52	4.41

Total precision values of several sets

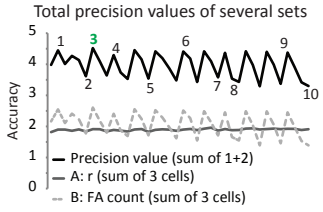

E Accuracy measures

$$r = \frac{\left(\sum(P(input)\times P(result)) - \frac{\sum P(input)\sum P(result)}{\#P(cell)}\right)}{\sqrt{\left(\frac{\sum(P(input))^2 - \sum(P(input))^2}{\#P(cell)}\right)\left(\frac{\sum(P(result))^2 - \sum(P(result))^2}{\#P(cell)}\right)}}$$

FA count

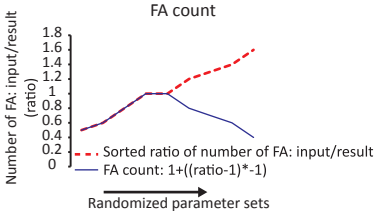

contains peaks that all have a value of **h** or lower (Fig. 1B3). To define which of all these domes belong to an FA, a form of Monte Carlo sampling is adopted. All pixels in the hDome image are given a weight of its grey value to the power of a user-defined number **p.** This weight is then normalized to the total sum of weights (Fig. 1B4). Those weights represent a probability distribution in the image space. We found that sampling 5000 positions according to the weights reliably reconstructed all FAs while keeping computation time limited. Thus 5000 pixels are selected that have a high chance to belong to a FA in the original image. To finally localize the FAs, pixels within a user-defined distance **rad** are clustered together**.** If this cluster contains a user-defined number of pixels **minNum**, it is considered to be a focal adhesion (Fig. 1B5). This new binary image of clustered FA pixels gives the localization of the adhesions and the centers of mass of these clusters are used for the next step**.**

The second part of the detection consists of finding the boundary of the focal adhesions. Defining these is not trivial, shown by the difference in focal adhesion size upon manual detection by several people from our lab, studying related topics, who can be considered relative experts (Fig. 2A). For precise FA boundary detection (which is not achieved by the hDome segmentation by itself), the original image is segmented by a local watershed, using the centers of the hDome clusters as marker (Fig. 1C1 upper panels). In each region of the resulting watershed image a relative intensity threshold is applied to define the area of the focal adhesion (Fig. 1C2). The threshold depth is adaptive to the intensity range in the region (Fig. 1C1 lower panel), which is calculated as the difference between the average intensity of the 2% highest intensity pixels (this averages out outliers) and the average intensity of a user-defined percentage (**lowpart**) of the lowest intensity pixels within the region**.** The threshold depth (x) for each region is then defined by the line y=**-a**x+**b**, where y is the intensity range, **a** and **b** are user defined. Thus regions with a high intensity range (bright FAs) get a low threshold depth (eg. pixels with values > 10% of the intensity range are included), whereas regions with a low intensity range (dim FAs) receive a high threshold depth (i.e. pixels with values >30% of the intensity range are included, see Fig. 1C1 lower panel). In addition, regions that have an intensity range below 1/65th of the bitdepth of the image are excluded (this was found to eliminate detection of background fluctuations, while not discarding dim FAs). Once all regions are analyzed, the boundaries of the focal adhesions are defined (Fig. 1C2-3 and Figure 2B). This is all the information needed for linking and further analysis.

In total the detection method contains 8 user defined parameters. 5 Parameters (**h**, **σ**, **p**, **rad**

Figure2: Optimization of detection settings

A) FA boundaries manually drawn by 5 different people (top) and the average FA size per manual detection (bottom). Bars 1-5 correspond randomly to the top images. B) The original image overlaid with the outline of the input image (red) for the threshold and detection optimizer (top) and the binary input image overlaid with its outline (red). C) The threshold optimizer: example results of segmentation, with an overlay of the outline of the input image (top), with three different adaptive threshold lines (bottom left) and the accuracy of these segmentations (bottom right). Line 3, in green, yielded best result. D) The hDome parameter optimizer: examples of different parameter sets for the hDome detection (top left). Segmentation results of three sets are shown (bottom left) with an overlay of the input image in red. Overview of the accuracy values of the three sets shown (top right), with in green the set that yielded best result, and the accuracy values of the ten sets in the table in a graph (bottom right). E) Definition of the accuracy measures. Top: the formula of the pearson correlation coefficient, where P(input) are the pixels of the input image, P(result) the pixels of the segmented image and #P(Cell) the total amount of pixels in the cell. Bottom: number of detected FAs for different parameter sets, sorted on increasing FA number (red dotted line). For the measure of FA count the number of FA of the input image/result image (ratio) was mirrored using 1+((ratio)*-1), thus resulting in 1 when there is equal amount of FAs in both input and result image and the number of detected FAs differ more towards FAcount=0.

and **minNum**) for the hDome segmentation and 3 parameters (**lowpart**, **a** and **b**) for the boundary-detection. Besides of setting the values of these parameters based on educated guesses, an automated parameter value optimizer was programmed that can be run before doing the analysis. This optimizer uses 3 manually segmented images, representative for the experiment to be analyzed, as input (example in Fig. 2B). First, the optimal values for the parameters of the FA boundary detector are determined by repeating the algorithm with different parameter values, calculating the Pearson correlation coefficient between the software generated image and the manually segmented version, and choosing the values that generated the highest correlation value. As shown in figure 2C, optimizing the threshold parameters is very important for determining edges correctly and consistently in both low and high intensity FAs. Next, using these optimal threshold parameter values, the five hDome parameter values (**h**, **σ**, **p**, **rad** and **minNum**) are optimized by calculating the accuracy of detection as the sum of the pixel overlap correlation (Fig. 2D-grey line) and the number of found adhesions (Fig. 2D-dotted line). See equations in Fig. 2E and black line in the graph in Fig. 2D. The results of this optimization are illustrated by representative images in Fig. 2D. The advantages of running this, slightly time consuming, pre-analysis are the increased detection of low intensity focal adhesions (Fig. 2D) and the more accurate definition of focal adhesion boundaries (Fig. 2C).

Tracking the focal adhesions is the third part of the analysis. FAs generally do not move very fast. This implies that the image of a given FA will have considerable overlap from frame to frame if the time resolution of the imaging is sufficiently high. This concept is used to track the detected FAs by linking them together in sequential frames if they occupy overlapping pixels. To minimize errors and maximize yield, several restrictions and corrections are applied: first the outline of the cell is determined with a threshold based on the bimodal histogram of the TIRF image and detected objects located outside the cell are excluded from the linking algorithm. Second, if FAs overlap with multiple detected objects in the following frame, they are linked to the object with maximal overlap. Third, if an FA has no overlapping objects in the following frame (t+1), it is compared to the two subsequent frames (t+2 and t+3). If an overlapping object is found, the tracks of these objects are then continued from this new frame onwards. This results in a track with small gaps where no FA was detected that are left as gaps to avoid mistakes in the FA feature measurements. This way tracks are constructed for all the focal adhesions. Center of Mass as well as pixel-coordinates determined to belong to the FA area are stored for each FA that can be tracked for at least 3 frames. Notably, because the minimal frame-rate in our experiments is 30 sec, FAs that live less than 1 minute, like for instance the rapid-turnover population in the leading edge described by Horwitz [9], were excluded from our analyses. Center of Mass and FA area are then used for analyses of FA velocity, lifetime and morphological characteristics.

Differences in behavior and in morphology have been observed for focal adhesions in the leading edge compared to the ones in the retracting area of the cell [178]. Classification of focal adhesion characteristics in different regions requires a distinction of these different cell areas. To define protruding and retracting regions, the binary image of the cell at a certain frame (t) is subtracted from the binary cell image at frame t+4. At a framerate of 30 or 35 sec that we used, 5 frames is 2.5 - 3 minutes and this was found to capture stable protrusions, while neglecting rapid, transient protrusions and fluctations in edge-detection due to imaging instability. In the resulting image, newly formed areas (protrusions) will have the value 1, whereas disappeared areas (retractions) will get the value -1 (Fig.1D). This is not done for every frame but with gaps of 5 frames starting from frame 1. The protrusive and retractive

areas are then enlarged towards the cell center such that the diameter of the area in the direction of the cell center is maximal 50 pixels (i.e. 6.5 µm which is roughly the size of the lamellum in these cells when they are migrating at their average speed of 1.5 µm/min) (Fig.1D). The focal adhesions in the frames of t till t+4 are labelled red when they are in retraction regions, green when they are in protrusive areas and the rest (central areas) is labelled blue (Fig.1D1). With this tool it is possible to separate populations of focal adhesions based on the localization in the cell and to look at the characteristics of FAs in retracting, protruding or central cell areas.

Taken together, the FA tracks and outlines that are generated with this method provide the basis for further analysis of individual FA behavior. FA features like lifetime, size, sliding, intensity, orientation and circularity can be related to the sub-cellular location of the FA and also to cell size and cell migration since the cell itself is also detected and tracked over time. Table 1 shows a complete list of cellular, subcellular and FA parameters included in the analysis software. Next we have used this tool to analyze the effects of HGF and Rap1 signaling on FA behavior.

Table1: Features analyzed by our FA detection and tracking software and the effects of HGF and Rap1 activation on the analyzed cells and whether the feature was taken along for BNI

		Response to HGF*	Response to Rap1 activation*	In Bayesian network?
Cell characteristics	Size	↑ 1/4	↑ 6/6	Yes
	Migration	↑ 4/4	↓ 6/6	Yes
Cell related FA characteristics	Cell region localization			No
	Number of FA s	0/4	↑ 5/6	Yes
	Shortest distance to the cell border	0/4	↑ 5/6	Yes
FA characteristics	Size	↑↓ 2/4	↓ 6/6	Yes
	Velocity	↑ 2/4	↓ 4/6	Yes
	Intensity	0/4	↓ 6/6	Yes
	Angle between FA axis and line from FA to cell center	0/4	0/6	Yes
	Roundness	↓ 1/4	↓ 2/6	Yes
	Axis length	↑ 1/4	↓ 4/6	Yes
	Solidity (area/convex area)	↑ 1/4	↓ 2/6	Yes
	Lifetime	↓ 2/4	↑ 1/6	Yes

* No. of cells that responded/ total no. of cells included for this condition

HGF and Rap1 regulate cell migration

To study the effects of HGF and Rap1 signaling on cell migration and focal adhesion dynamics, we used the HGF responsive humane prostate cancer cell line DU145. This cell line was reported to express endogenous Epac [179], the cAMP-responsive GEF of Rap1 [98] that can be activated by the Epac selective cAMP analog 007 (2O-Me-8CPT-cAMP) [99]. However, the Epac levels we detected on western blot were very low (Fig.3B top) and to boost the magnitude of Rap1 activation by 007, the DU145 cell line was stably transfected with exogenous Epac (Fig 3B bottom). The resulting cell line, DU145-G4, displayed scattering upon HGF treatment (Fig.3A, 2nd column) as cells disrupted their cell-cell junctions and increased their migration velocity (Fig.3D). Upon Rap1 activation by 007, cells flattened

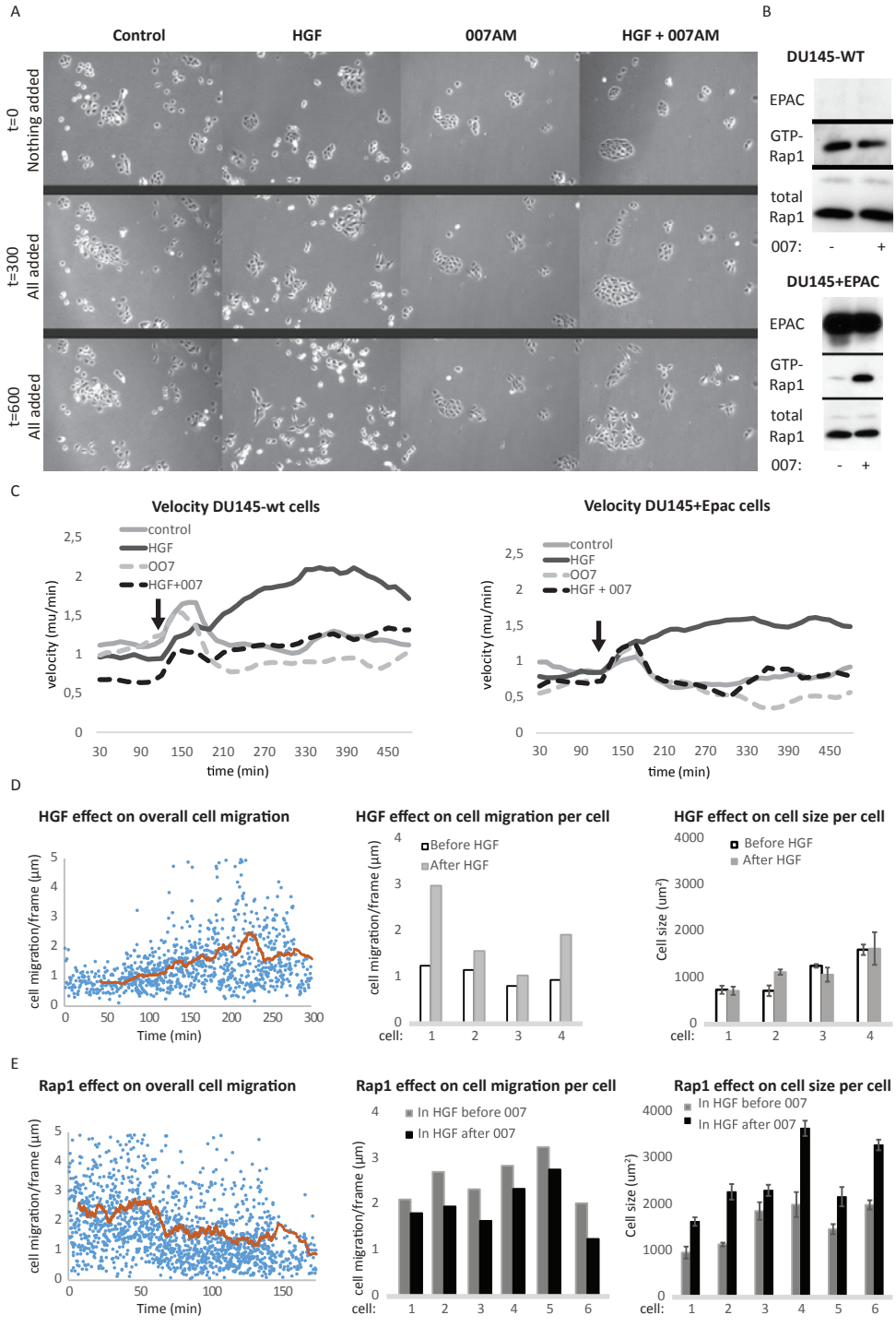
A
Control
HGF
007AM
HGF + 007AM
t=0
Nothing added
t=300
All added
t=600
All added
B
DU145-WT
EPAC
GTP-Rap1
total Rap1
007: - +
DU145+EPAC
EPAC
GTP-Rap1
total Rap1
007: - +
C
Velocity DU145-wt cells
control
HGF
OO7
HGF+007
velocity (mu/min)
time (min)
Velocity DU145+Epac cells
control
HGF
OO7
HGF + 007
velocity (mu/min)
time (min)
D
HGF effect on overall cell migration
cell migration/frame (µm)
Time (min)
HGF effect on cell migration per cell
Before HGF
After HGF
cell migration/frame (µm)
cell:
HGF effect on cell size per cell
Before HGF
After HGF
Cell size (um²)
cell:
E
Rap1 effect on overall cell migration
cell migration/frame (µm)
Time (min)
Rap1 effect on cell migration per cell
In HGF before 007
In HGF after 007
cell migration/frame (µm)
cell:
Rap1 effect on cell size per cell
In HGF before 007
In HGF after 007
Cell size (um²)
cell:

(Fig.3A 3rd column) and cell migration was slowed down (Fig.3D). Simultaneous addition of 007 together with HGF completely prevented the scattering response in the DU145-G4 line (Fig.3A 4th column & 3D) whereas the DU145-wt line showed an impaired HGF response (Fig.3C). Thus, the DU145-G4 cell line is used to study effects on FA dynamics of HGF induced migration and subsequent inhibition of migration by Rap1 activation.
A number of factors limits the long term high magnification TIRF imaging, which would be needed to capture FA dynamics at baseline and upon HGF-induction and subsequent Rap1 activation in one cell: cells migrated out of the field of view; slight drifts in focus reduced FA detection accuracy, bleaching reduced FA detection accuracy, photo-toxicity reduced migration and FA dynamics. Therefore, we separately imaged cells in the transition from baseline-to-HGF and from prolonged HGF-to-Rap1 activation (007 addition). As shown in Fig. 3D, migratory activity - as measured by the displacement of the center of mass of the automatically segmented cell - of the 4 mCherry-Paxillin expressing cells used for further analysis was induced gradually up to 2 fold (on average) within the first 3 hours after HGF. Addition of 007 to 6 further analyzed mCherry-Paxillin expressing cells that were stimulated with HGF for a prolonged period (3 hours prior to the start of imaging), resulted in a rapid, 2 fold (on average) decrease in migratory activity. Concomitant with the reduction in migration, the 007 stimulated cells flattened to increase the size of the area in contact with the ECM-coated glass surface (Fig. 3E).

FA size, intensity and velocity differ between 3 lifetime-based FA subgroups

To define baseline FA dynamics, we used our software to detect and track individual FAs in the 4 untreated mCherry-Paxillin expressing DU145-G4 cells (prior to HGF). We measured in each frame, for each FA, the size, the background-corrected average fluorescence pixel intensity and the frame to frame velocity. In Figure 4, size, pixel intensity and velocity were averaged per FA over their lifetime and the distributions of FA lifetime and these parameters were calculated (Fig.4). A large population of FAs lives up to 4 minutes, whereas only a small subset of FAs lives beyond 30 minutes (Fig.4A). It has been observed in numerous studies that short-lived, newly formed adhesions in the lamellipodia are generally smaller and less motile than longer lived adhesions in the retracting area of the cell, but a systematic investigation into different populations of FAs was to our knowledge not performed. The 4 min and 30 min cut-off we chose is therefore based on [172, 180] [178]. To determine more rigorously how populations of FAs, based on lifetime, differ in characteristics, we divided the FAs into 3 groups: one group of FAs that have a lifetime of less than 4 minutes (short lived),

Figure 3: 007 blocks HGF-induced scattering in Epac-expressing prostate carcinoma cells

A) Stills from image serie of a representative scatter assay using the Epac-overexpressing DU145_G4 cell line at the start (top row), and at 2 distinct time points after the indicated treatments. B) Western Blots revealing Epac expression in DU145 cells and concomitant activation of Rap1 by adding the Epac-selective cAMP analog 007. C) Quantification of the cell velocity by automated cell tracking in DU145 wild type cells (ref. Science Signalling paper), averages of 3 image series per condition, arrow depicts time of HGF and 007 addition at frame 16. D) Similar to (C) but of the DU145-G4 cell line. D) (Left) The average migration of the 4 different cells that were stimulated with HGF during imaging (red line). Each blue dot is the migration of one of the cells at that moment in time. (Middle) Average cell displacement of the 4 cells prior to (white) and after (grey) HGF treatment. (Right) Average cell size of the 4 cells prior to (white) and after (grey) HGF treatment. E) (Left) Similar to (D Left) but then showing the 6 different cells that were stimulated with HGF 3 hours prior to imaging and in which Rap1 was activated during imaging. (Middle) Average cell displacement of the 6 cells before (grey) and after (black) Rap1 activation. (Right) Average cell size of the 6 cells before (grey) and after (black) Rap1 activation.

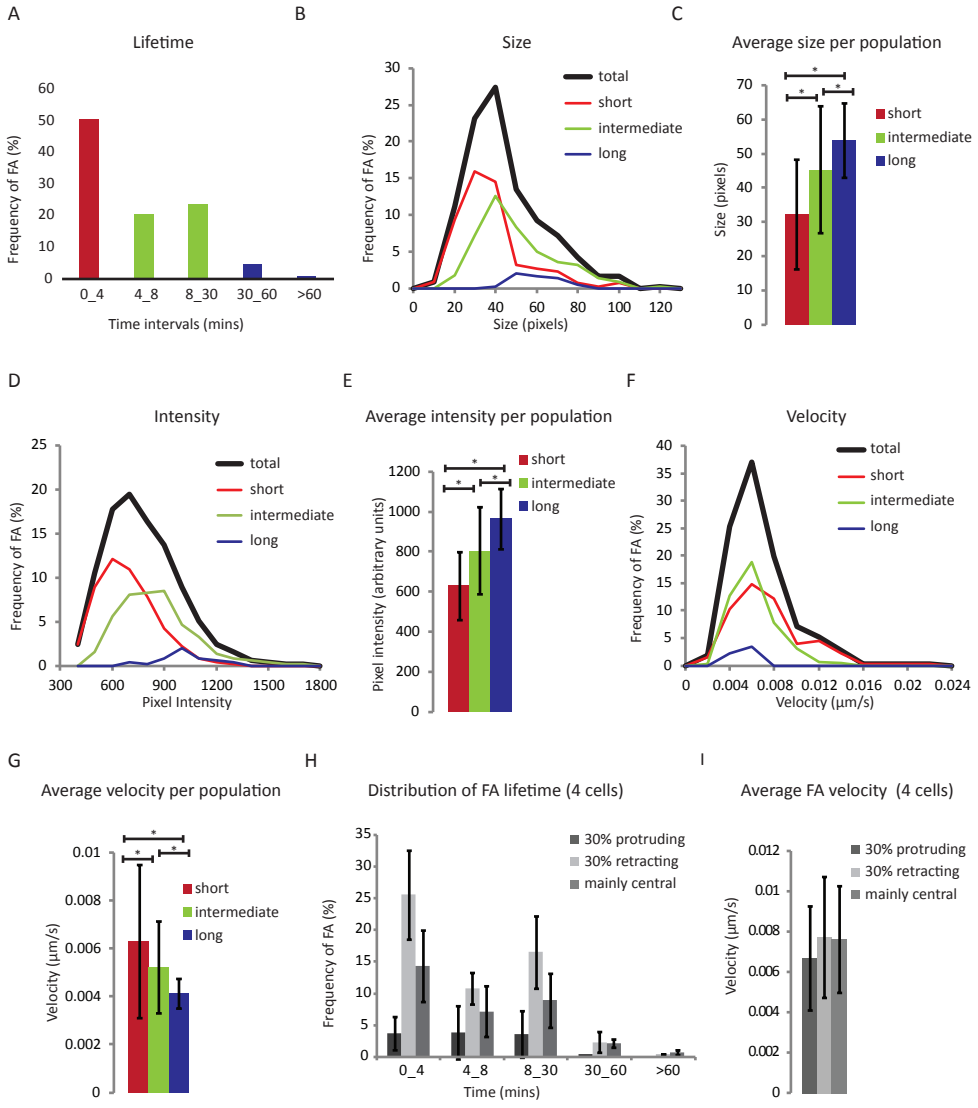

Figure 4: Three lifetime based FA populations show differences in FA characteristics

A) Histogram of lifetime distribution within a representative untreated cell. B) Distribution of average FA size of all FAs and of the 3 lifetime-based subpopulations within a representative untreated cell. C) The average and standard deviation of the distributions of these 3 populations in (B). D) Distribution of average FA pixel intensity of all FAs and of these 3 subpopulations within a representative untreated cell. E) The average and standard deviation of the distributions of these 3 subpopulations in (D). F) Distributions of average FA velocity of all FAs and of these 3 subpopulations within a representative untreated cell. G) The average and standard deviation of the distributions of the 3 subpopulations in (F). Histogram of lifetime within the 3 location-based populations of FAs in untreated cells, with a zoom of the group of FAs that live over 30 minutes (Error bars=standard deviation between cells). B) Average FA velocity of the 3-location-based populations of FAs in untreated cells. (Error bars=standard deviation between cells).

one group of FAs that have a lifetime of 4 to 30 minutes (intermediate lived) and a group of FAs that have a lifetime of more than 30 minutes (long lived). The distribution of average FA size, average FA pixel intensity and average FA velocity is significantly different for the 3 groups of FAs (Fig.4B-G). Both average FA size and average FA intensity increase in the intermediate and long lived population (Fig.4C&E) whereas average FA velocity decreases in these groups (Fig.4F&G). Although there is overlap between populations, this indicates that FA size, intensity and velocity differ depending on how long FAs live.

Our observation that long lived FAs are more static than short lived FAs is in apparent contrast with the described relative immobility of short-lived FAs in the lamellipodia [172, 180]. This difference may arise from the fact that in our analysis the FAs are grouped together independent of subcellular location. To further test this, we formed 3 sub-populations of FAs based on their location: the FAs that spend at least 30% of their lifetime in a protruding area (protruding), at least 30% of their lifetime in a retracting area (retracting) or less than 30% of their lifetime in either and therefore mainly in a central region (central). The few FAs that were located both 30% of their lifetime in a retracting area and 30% of their lifetime in a protruding area have been left out of the analysis. The characteristics of these groups were averaged between cells. This showed that the short lived FAs from the prior analyses were equally present in all 3 location-based populations. This was similar for the intermediate lived group. The long lived population contained relatively few FAs that spent at least 30% of their time in a protruding area (Fig. 4H). Also in general, when no lifetime filtering was applied, FAs in protruding regions displayed a slightly decreased mobility compared to those from central and retracting areas (Fig. 4I). This is consistent with the general notion that FAs in protruding regions of the cell are less motile than in other regions. Thus, these analyses indicate that different lifetime or location-based FA populations can be distinguished in our data with characteristics that are in agreement with previously described FA features.

Because the lifetime-based FA populations differ in intensity, velocity and size, we next determined whether a direct relation exists between FA lifetime, FA size and FA pixel intensity using paired correlation analyses per cell. Strikingly, no paired correlations were found between FA lifetime and FA pixel intensity or FA lifetime and average FA size (Supp. Fig.S1A, B&E). Average pixel intensity and average FA velocity showed opposite behavior in the 3 populations of FAs, but they did not show a paired correlation (Supp.Fig.S1D&E). A low level of linear correlation existed between average pixel intensity and average FA size (Supp.Fig.S1C&E), for which it should be noted that the intensity measure is the average pixel intensity within an FA, the calculation of which is therefore not influenced by the size of the FA. In conclusion, although we observed no clear pairwise correlations between lifetime and measured FA characteristics, we define 3 lifetime-based FA populations that differ in size, intensity and velocity. Furthermore, with our method we can detect and track FAs successfully and reproduce findings earlier reported in literature.

HGF-induced cell migration and subsequent inhibition by Rap1 signaling entail little differences in FA dynamics and morphology

HGF and Rap1 have opposite effects on cell migration in 2D culture [86] and we hypothesized, that their activity would thus affect specific measurable parameters of FA morphology and FA dynamics. To test this, we used our tracking software to detect and track all FAs in the 4 untreated cells that were stimulated with HGF, and the 6 prolonged HGF-stimulated cells (HGF added 3 hours prior to imaging), in which Rap1 was then activated by 007. The features that were measured in these experiments and whether and how they changed in response to

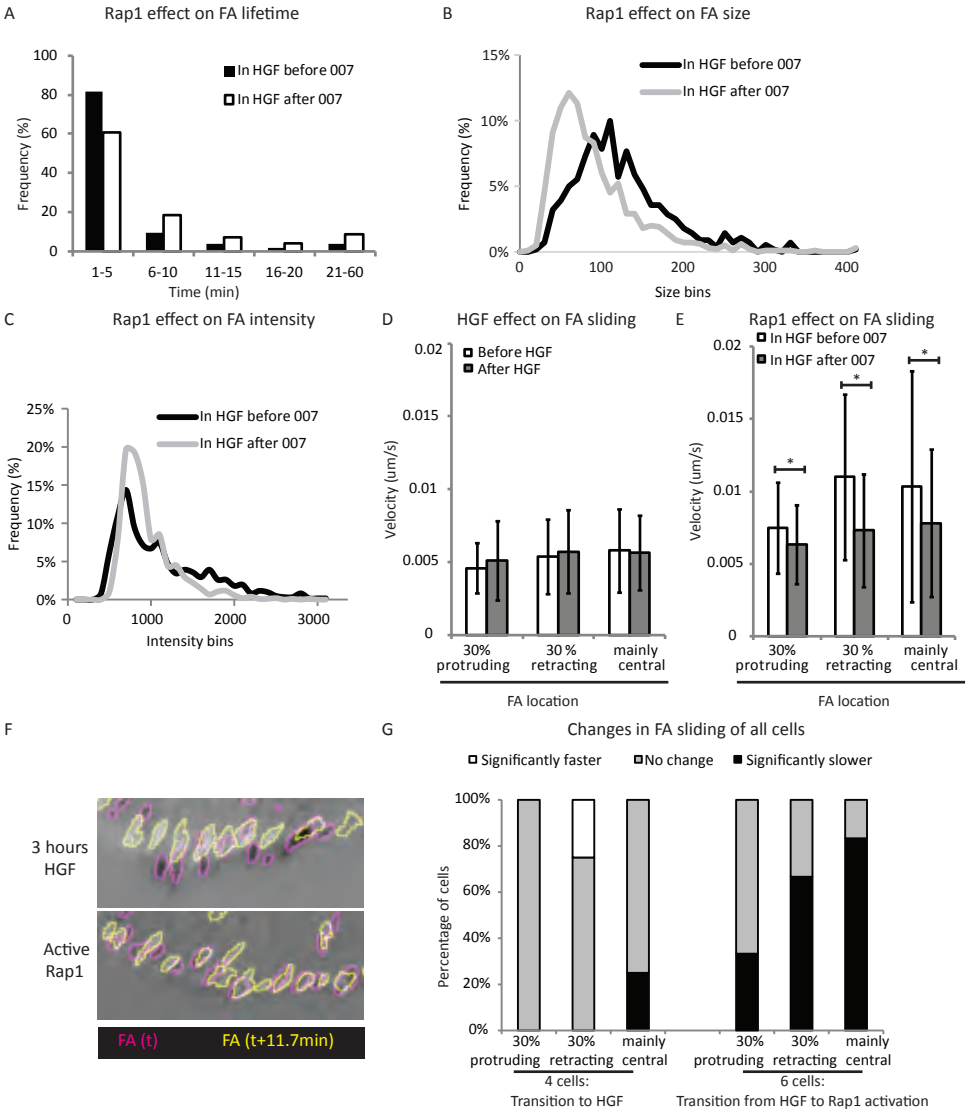

Figure 5: HGF and Rap1 signaling affect only a few FA features

A) Histograms of the lifetime of FAs in cells that were treated with HGF 3 hours prior to imaging, before and after Rap1 activation. B) Distribution within one representative cell of the average FA sizes, HGF was added 3 hours before imaging, before (black) and after (grey) Rap1 activation. C) Distribution of the average FA intensities, within one representative cell , HGF was added 3 hours before imaging, before (black) and after (grey) Rap1 activation. D) Average FA velocity in a representative cell before (white) and after (grey) adding HGF, divided into three populations: FAs that spend at least 30% of their lifetime in a protruding area, at least 30% in a retracting area or FAs that remain mainly central. E) Average FA velocity per region in a representative cell before (white) and after (grey) Rap1 activation, HGF was added 3 hours prior to imaging. G) The result of subtraction of 2 images (t2-t1) at time 't' and 't+11.7min' of the same area of a migrating cell showing FA movement in HGF (top) and loss of movement upon Rap1 activation (bottom). The subtraction image is overlaid with the outline of the detected FAs in 't' (magenta) and in 't+11.7min' (yellow). H) The percentage of cells in which the adhesion velocity per population was either significantly increased (white), significantly decreased (black) or was unchanged (grey).

HGF and Rap1 activation are indicated in Table 1.
Despite a clear induction of cell migration (Fig. 3D), none of the cell-related or independent FA parameters strongly changed upon treatment of cells with HGF (Table 1). On the other hand, Rap1 activation did result in a number of clear changes in FA characteristics. Consistent with the induction of cell-spreading (Fig. 3E), new FA formation was induced for a short period of time upon activation, enlarging the total number of FAs for the duration of imaging (Fig S2). Consistent with earlier observations [86], Rap1 activation caused a shift in the distribution of FA lifetimes averaged over all cells in that the percentage of short-lived FAs decreased and a population of long-lived FAs appeared (Fig. 5A). Most striking, however, are the effects of Rap1 activation on FA size, intensity and velocity (table 1). As shown in Fig 5B and C, the average reduction in size after 007 is a result of a loss of the population of largest FAs. The reduction in average intensity represents a loss of a population of highly intense FAs. Whereas size measurements could be influenced by altered edge detection due to overall decreased FA intensity, intensity and velocity are robust parameters not directly influenced by image detection parameters. Because FA sliding is found higher in the rear compared to the front of a migrating cell (Fig. 4I), we further analyzed regional differences in FA sliding velocities and the effects of Rap1 thereon. To this end, first the velocity was averaged per FA over time and then this average velocity was averaged over all FAs within the 3 populations both before and after treatment (representative examples are shown in Fig. 5D&E). Within the first 3 hours of stimulation, HGF signaling showed little effect on FA sliding in any cellular region (Fig. 5D&G). In the HGF pre-treated cells, however, FA sliding was increased and Rap1 activation decreased FA sliding velocity in the protruding, retracting and central populations of respectively 2, 4 and 5 of the 6 cells analyzed (Fig.5E, F, G). The fact that FA sliding was higher in cells treated with HGF for > 3hours in comparison to the first 3 hours of HGF treatment (Fig. 4E), suggests that sliding increased as a result of increased migration after a few hours of stimulation.
In conclusion, Rap1 activation inhibits the sliding of FAs that is observed in the rear of migrating cells as well as the presence of a population of intense and large FAs. These specific effects could be explained by a reduction in tension in the FA-associated actomyosin cytoskeleton through the activation of a recently identified Rap1 effector pathway that results in ArhGAP29-induced inactivation of Rho. Surprisingly, most FA parameters were not clearly affected by HGF within the first 3 hours of stimulation, even though cell migration was induced. As a consequence, no FA characteristics could be identified that clearly correlated with the migratory capacity of cells.

Bayesian network inference reveals dependence between FA characteristics and cell size but not migration

The fact that effects on cell migration by HGF and Rap1 were not clearly correlating with effects on FA parameters led us to employ BNI to assess dependencies between changes in FA parameters and cell migration parameters in an unbiased, systematic manner. For each cell, and per frame, the FA characteristics, except lifetime, (table 1) and the cell related FA characteristic ‘FA distance to the cell edge’ were averaged over all the FAs present; the cell related FA characteristic ‘number of FAs’ was included; and cell size and migration rate (distance between center of mass in frame (t) and frame t+10) were included. As shown in Fig. 6, a negative correlation was calculated by this model between cell size and cell displacement that decreased upon stimulation by HGF. Strikingly, hardly any direct correlations between cell displacement and any of the FA characteristics were observed in any of the conditions.

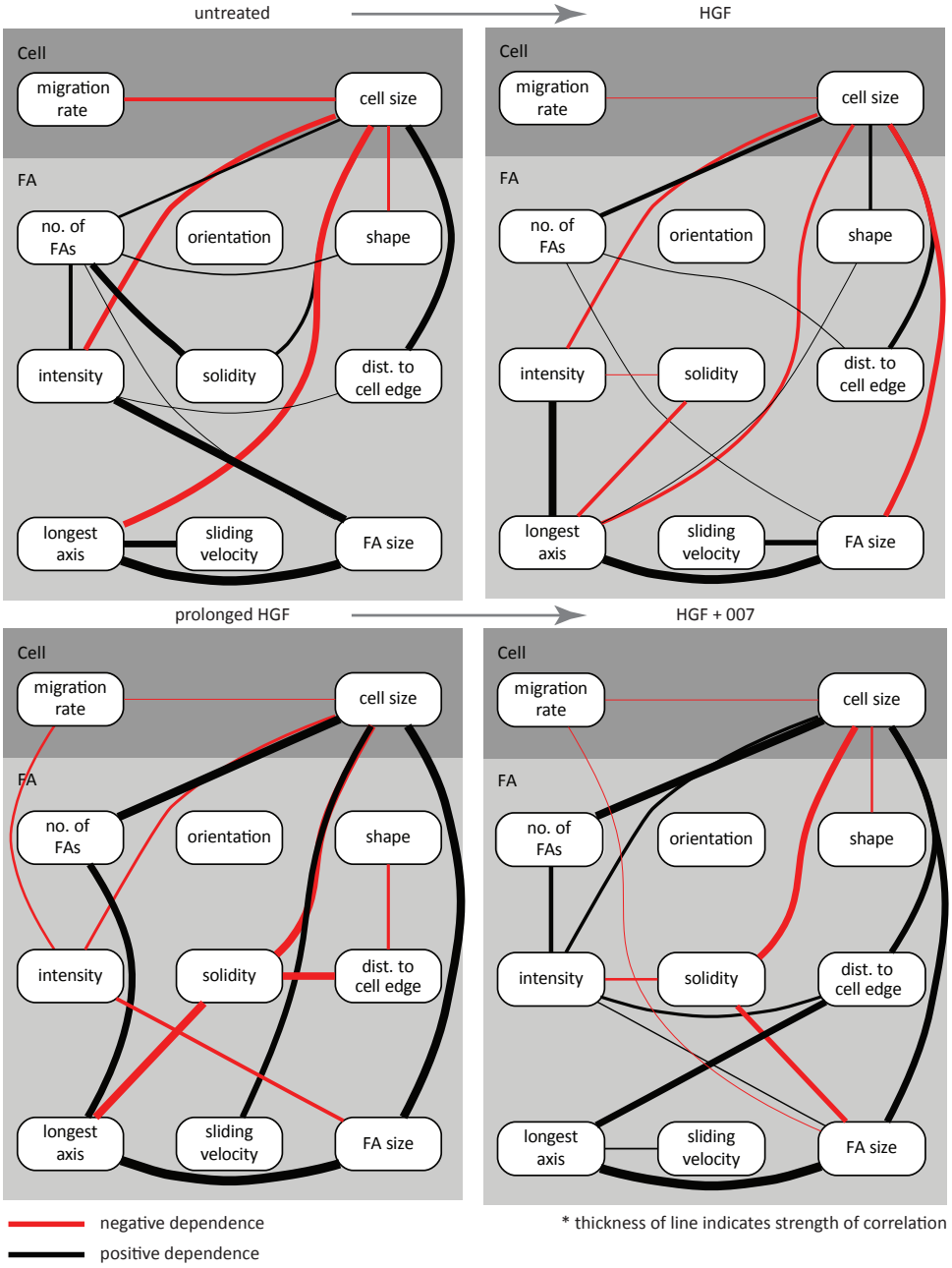

Figure 6: Bayesian Network Inference shows correlation between cell size and FA behavior
Graphical representations of the correlations between FA dynamics and cell behavior calculated by Bayesian Network Inference. Top row: the transition of adding HGF (right) to unstimulated cells (left). Bottom row: the transition of Rap1 activation (right) in cells treated with HGF 3 hours prior to imaging (left). Pairwise correlations are shown in red if negative and in black if positive while the strength of correlations correspond to line thickness. Note that the structure of the graphs is calculated by BNI, whereas correlation is used to visualize the pairwise strength of each line.

Instead 5-7 of the nine FA characteristics included showed correlation with cell size. Some correlations between FA characteristics did change with the acute or prolonged induction of HGF signaling and upon activation of Rap1, but in all of these conditions strong correlations existed between FA characteristics and cell size, but not between FA characteristics and cell migration. Together, these network models indicate that: 1) The correlations between FA characteristics and cell migration rate are surprisingly little. 2) Changes in FA characteristics do not clearly influence cell migration. 3) FA characteristics and cell size do show clear interdependence and 4) The effects of Rap1 on FA characteristics represent its induction of cell spreading (size increase) rather than its inhibition of cell migration.

Discussion

In this study we have developed a software tool to track and analyze characteristics of FAs over time. This method is generally applicable to detect and analyze FA features of single FAs over time with high confidence. We used this tool to analyze how HGF and 007-induced Rap1 signaling affect FA dynamics in order to investigate whether these signaling pathways target specific aspects of FA behavior to bring about their opposing effects on cell migration. We found that HGF has surprisingly little effects on FA dynamics and characteristics and that neither in HGF-induced, nor 007-inhibited migratory conditions clear dependencies exist between migratory behavior and FA characteristics. Instead dependence between FA characteristics and cell spreading emerged to be strong. Concomitant with the induction of cell spreading, 007 decreased FA size and intensity and inhibited FA sliding. All of these effects mimic the effects of inhibition of RhoA mediated cytoskeletal contractility, which has recently been identified as a downstream target of Rap1.

Over the years, several custom made FA detection software tools have been written. Recently, different automated FA tracking softwares have been published [181-183]. The segmentation techniques and research questions differ between methods. Wurflinger et al. designed an 8 step method in which they separate foreground objects using top hat filtering, carefully correct for the merging of close FAs objects by an Otsu threshold and track FAs by object overlap with movement correction and gap closure. It is a very carefully designed method that is powerful in both segmentation and tracking, shown by extensive testing, either with manually segmented images as well as by omitting one by one all the steps they use in the algorithm to validate its strength. Furthermore they reproduce findings on FA dynamics using known experimental data. So far, this method has not been used for the analysis of FA in the context of a biological question. Möhl et al. developed a method to compare measurements from traction force microscopy, actin flow microscopy and fluorescent microscopy monitoring of FAs. For FA segmentation they use a method that has been described previously [184] in which cytoplasmic background staining is reduced by highpass filtering and adhesion patches are segmented by thresholding and linked over time using object overlap. For length aspect ratio measurements, they fit ellipses to the found objects. For comparison between actin flow, FA dynamics and force traction images, they map the datasets into a cell shape restricted to a unit circle. Using this normalization, they find that at the largest adhesion sites f-actin flow is low and traction force is high, which is consistent with previous studies [11, 12, 57, 185]. Berginski et al. also base their FA detection on the above mentioned algorithm [184], which they slightly adapt, and include a nearest neighbor linking to complement object overlap [181]. As proof of principle they analyze the FA dynamics in NIH3T3 cells stably expressing a paxillin mutant that cannot be phosphorylated anymore by c-Jun N-terminal kinase (JNK)

on S178, which inhibits cell migration. In this setting they find that FAs live longer in the paxillin S178A expressing cells.
In our new method, we use a 3-step segmentation and detection algorithm, which is quite different from the above described ones. For the initial identification of the FAs we chose to use the hDome method, because it was previously found to perform the best in a comparison of spot-detector algorithms [176]. Then we defined separated image regions, each containing one FA, by watershed segmentation using the hDome detected spots as markers. FA boundary was determined using a unique, local adaptive threshold. FA linking was by object overlap and gap closing, which is very similar to other methods. Compared to other methods, we have specifically focused on reliably determining the boundaries of FAs, which are intrinsically hard to discriminate from the surrounding basal cell area due to the diffusive nature of the transition. The use of a local adaptive threshold increased the precision and consistency of boundary determination and we developed an optimizer that identifies the best set of parameters for the hDome method as well as the adaptive threshold. We have extensively controlled the robustness and accuracy of our tracker by manual detection and inspection. The boundary detection renders our method specifically useful for the measurement of FA morphology features and for the investigation of signal intensities and fluctuations therein within FAs. We have included the automated generation of such measurements within our software. A second specific feature of our tool is that it uses whole-cell dynamics to define protruding and retracting areas of the cell, which allowed the correlation of FA dynamics to their cellular location. Thus 3 image analysis methods were published in time that we developed our method. Image segmentation algorithms and FA detection and tracking capacity of these methods appears comparable to ours and FA lifetime and dynamics could be measured by these methods for our current study as well. Our method however has a specific focus on detecting FA boundaries accurately and allows investigation of FA morphology and dependent parameters like size and intensity, which is not readily available in the previous methods.
To proof the power of our method, we used our software for the analysis of FAs in DU145-G4 cells in 2D TIRF microscopy. Consistent with a wealth of earlier studies that have built a general perception of FA dynamics and behavior in relation to cell migration, we found that small, immobile FAs concentrate at the cell-front, whereas larger, sliding FAs concentrate at the rear. Additionally, we determined the effects of HGF and Rap1 signaling on FA dynamics and investigated the relation to their effects on cell migration. This revealed a surprising resilience of FAs against altering their characteristics even though cell migration was clearly induced within the first hours after HGF. The BNI further emphasized the lack of correlation between cell migration and FA characteristics and indicated that dependencies with cell size are much stronger. It is obvious that requirements on FA function and dynamics do exist to allow cells to migrate. Eg. traction force needs to be developed and FAs need to form and disassemble at sufficient rate and in a polarized manner [9, 26, 50, 76, 186]. But it stems from our current analyses that these functional properties are not primarily targeted to cause alterations cell migration, at least not in the case of its induction by HGF. Rather, they may change over time to accommodate increased cell migration as dictated by other driving factors such as leading edge actin polymerization [4].
Effects of 007-induced activation of Rap1 on FA characteristics are more apparent than effects of HGF. But also here, correlations between migration and FA characteristics as determined by BNI remained minimal. Again, the strongest correlations existed between cell size (spread area) and FA characteristics. Rap1 was shown to modulate the actin cytoskeleton and increase

cell spreading in numerous studies [86, 122, 124, 144, 187] and it was recently shown that this is mediated by its activation of the RhoGAP ArhGAP29 [91]. In this light, it is interesting to note that all of the FA parameters strongly affected by Rap1 (size, intensity and sliding velocity) were previously shown to be regulated by Rho-dependent cytoskeletal contractility. Thus, using this unbiased, systematic analysis of FA behavior, which was developed and conducted prior to - and completely independent of - the identification of ArhGAP29 as a Rap1 target, we identified features that would be predicted to be affected based on the current knowledge.

In conclusion, we have developed a new and robust FA tracking and characterizing software. We have used it to investigate HGF and Rap1 regulated cell migration and this has identified - as Rap1 targets – FA size, FA intensity and FA sliding. This lends confidence to the general applicability and power of the method. In addition and surprisingly, this has uncoupled the regulation of overall cell migration from the regulation of FA characteristics commonly associated with migration. Our software will be made publically available and can be used for the further investigation into the relation between cell migration and FA dynamics and other systematic approaches to understand FA regulation.

Materials and methods

Cell lines and culture

DU145-G4 cells were transfected with a lentiviral delivery system. Lentivirusal particles were produced by transfection of HEK293 cells with third-generation packaging construct [188]. DU145-G4 cells were plated in full medium in a 6-well plate overnight and then transduced with mCherry-Paxillin or mCherry-Vinculin virus supernatant in the presence of 40µg/ml polybrene for 24 hours before returning the cells to full medium. mCherry-Paxilin or mCherry-Vinculin expressing cells were selected by fluorescence-activated cell sorting (FACS) by their mCherry levels.

48 hours prior to imaging DU145-G4 cells were plated in Roswall Park Memorial Institute (RPMI) medium (Gibco) supplemented with 10% fetal calf serum (FCS) (Sigma) in collagen-type 1 (10µg/ml; PureCol)-coated, Lab-Tek® #1.0 Borosilicate Chambered System, 8 units. 24 hours prior to imaging, the medium was replaced by 0.5% FCS containing RPMI. 25ng/ml HGF was added either 3 hours prior to imaging or after approximately an hour of imaging. 8-pCPT-2'-O-Me-cAMP-AM (007AM) (Biolog Life Sciences) was added, at a concentration of 1µM, to HGF pretreated cells after an hour of imaging.

For the scatter assay, cells were treated similarly but plated in a coated 48-well plate. Before imaging the wells were completely filled with medium and the plate was sealed using silicon grease and a glass plate. Either HGF alone, 007AM alone or a combination of HGF and 007AM was added to the cells after 1 hour of imaging.

Microscopy

For imaging we used a NIKON Ti microscope equipped with a total internal reflection fluorescence (TIRF) system, a CFI Apochromat TIRF objective, 60x oil with an NA of 1.49, a 12-bit electron multiplying CCD (EMCCD) Luka camera (Andor) and controlled by company software (NIS-elements).

We have created a dataset of image series of the DU145-G4 cells with mCherry Paxillin in the two different transitions. The data set consists of 12 cells imaged from epithelial to migratory induced by HGF and of 18 cells that were incubated with HGF 3 hours prior to imaging and in which Rap1 was activated during filming via Epac by the cAMP analog 007AM. Within this dataset there are 4 out of 12 cells that clearly responded to HGF, shown by average cell displacement before and after adding HGF (Supp.Fig.S8) and 6 out of 18 that were migratory at the start of imaging and in which Rap1 activation inhibited migration (Supp.Fig.S8).

The scatter assay for the characterization of the Du145-G4 cell line was carried out on a Leica AF7000 microscope, with a 10x objective. Images were taken every 10minutes and the analysis was carried out using CellTracker, a custom developed Matlab analysis tool [189].

Parameter measurement

FA Intensity: To determine the average pixel intensity in the FA, it is necessary to correct for a certain background level. To negate fluctuations in the measurement of FA pixel intensity, preferably the background should be measured locally around the FA. In order to do so, we determined a watershed on each frame with the found adhesions as markers and the found cell edge as outer edge. The average pixel intensity in each region, minus the area that belongs to the FA, was used as the local background and this was subtracted from the average intensity of the accompanying adhesion.

Lifetime normalization: For normalization of the lifetime to 100, each time point on the

intensity profile of the FA and its accompanying intensity was rescheduled to point: (x*100)/ frames_FA-1, where x is an increasing point on the x-axis ranging from 1 till the maximum of number of frames the FAs existed and frames_FA is the number of frames the FAs existed. Thus the appearance of the FA will be set to point 1 and the last to point 100. Gaps that formed in between these data points in the tracks that contained less than 100 time points were filled by interpolation between 2 subsequent data points, using the interpolation function (interp1) of MatLab.

Statistics

Statistical tests on distributions of FA velocity, FA size and FA intensity in untreated cells were carried out using the "Two-Sample Assuming Unequal Variances" student's t-test of the statistical add-in of Excel (Fig.4). The statistical tests on FA intensity distribution per cell were carried out using the Mann-Whitney-Wilcoxon test from MatLab R2013 statistical toolbox (Fig.7). Input per cell were the average FA pixel intensities averaged over the entire lifetime of the FAs, comparing prior to and after addition of HGF or 007.The statistical analysis of the FA sliding data was carried out using the Mann-Whitney-Wilcoxon test in R (Fig.6). Input per cell was the average velocity per FA, comparing prior to and after the addition of a compound. The FAs were divided over the three subclasses, protruding, retracting and central, and the test was done for each set separately.
R Core Team (2013). R: A language and environment for statistical computing. R Foundation for Statistical Computing, Vienna, Austria. URL http://www.R-project.org/.

Bayesian Network Inference

The FA characteristics (table 1) were averaged per frame and collected along with the cell size and cell displacement, calculated as travelled distance from frame (t) to (t+11), into datasets used in learning the network structures. Each variable in these datasets was discretized to four distinct values. The default settings of the Banjo software (Bayesian Network Inference with Java Objects) [190] were used to run its simulated annealing learning algorithm. Families were constrained to a maximum of 5 parents and annealing moves were made randomly from local perturbations. The fitness of networks to the data was calculated with Banjo's standard likelihood function. There were 1000 re-starts per learning run and the networks presented here were those that best fitted the data of the respective microscopy experiments.
Graphviz [191] was used for visualizing the networks and R was used to compute the Pearson correlation between variables. Scripts to coordinate these tasks were written in SWI-Prolog [192] and its Real package*.

* Integrative functional statistics in logic programming.
Nicos Angelopoulos, Vitor Costa Santos, Joao Azevedo, Jan Wielemaker, Rui Camacho and Lodewyk Wessels In Practical Aspects of Declarative Languages (PADL'13) January, 2013. Rome, Italy.

Supplemental Figure S1

Scatter plots of different features of all FAs within a representative, untreated cell. Each dot represents an FA. A) Average FA lifetime versus average FA intensity. B) FA lifetime versus average FA size. C) FA intensity versus average FA size. D) Average FA intensity versus average FA velocity. E) Correlation coefficients for each of the 4 shown correlations, averaged over 4 untreated cells (Error bar= standard deviation between cells).

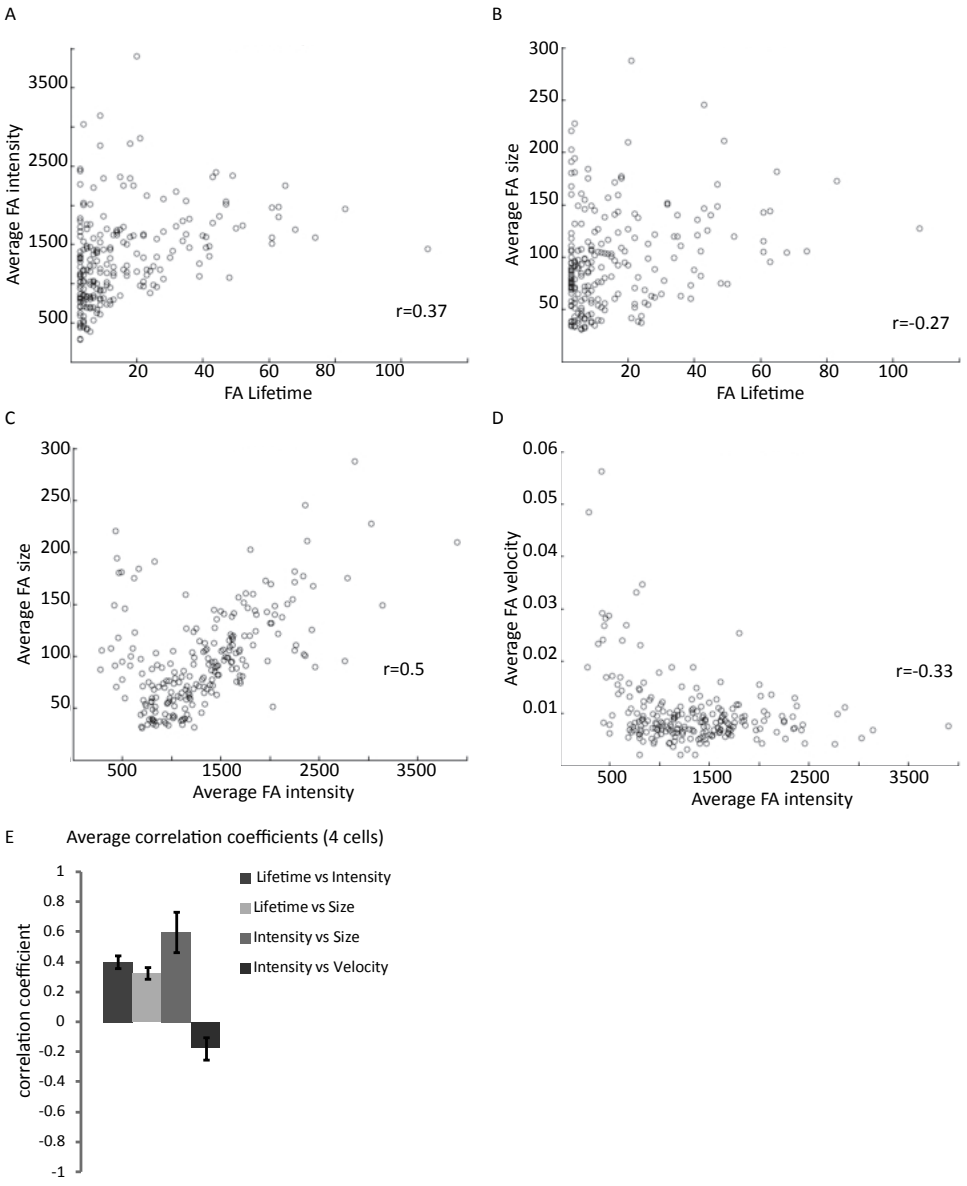

Supplemental Figure S2

A) The total number of FAs per frame divided by 10 (grey line), the number of newly appearing (black dots) and disappearing (red crosses) FAs in each frame of 20 frames of the non-treated state (untreated), the first 20 frames just after adding HGF (early HGF) and the 20 last frames of the image series (long HGF), data from one representative cell. B) Similar to (A) but showing FA numbers for a cell, treated with HGF 3 hours prior to imaging, in 20 frames of HGF only (3 hours of HGF prior to imaging), followed by the first 20 frames upon 007 addition (early Rap1) and the last 20 frames of the image series (prolonged Rap1).

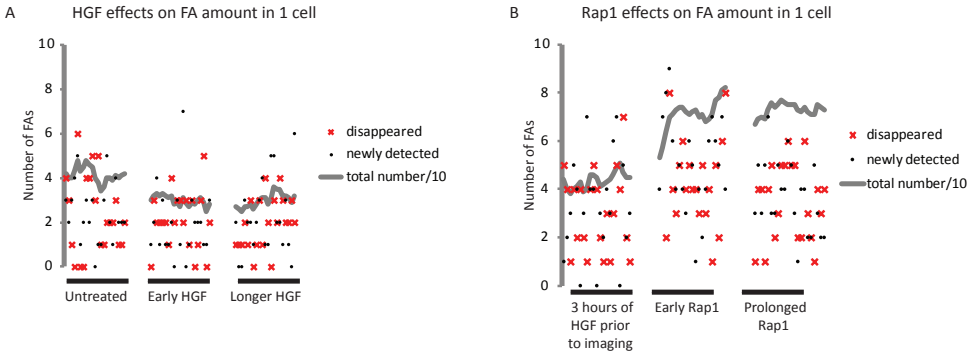

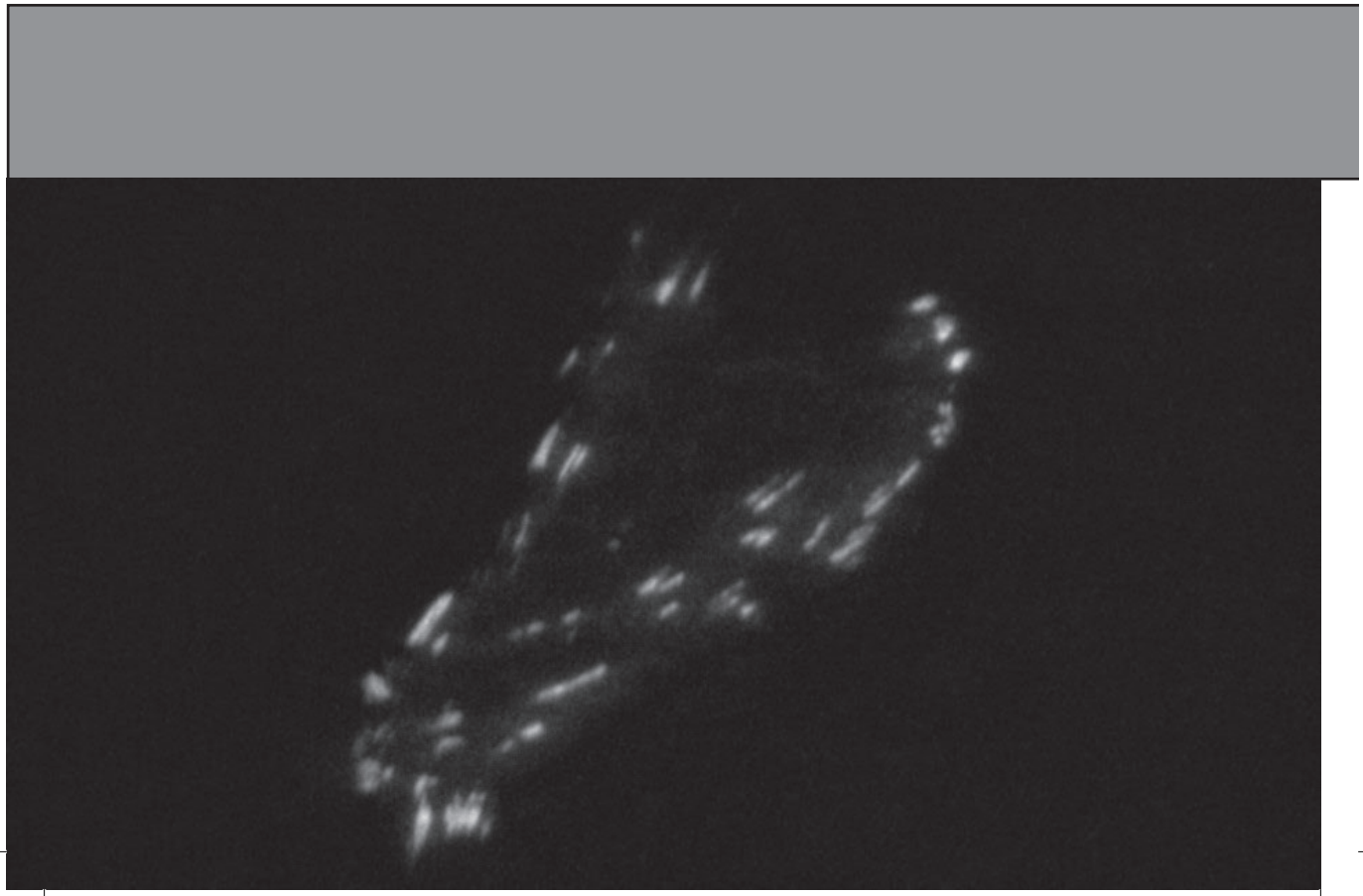

Focal Adhesions display a characteristic lifetime dependent compaction profile that is affected by HGF and Rap1 signaling

4

Emma Spanjaard, Johannes L. Bos and Johan de Rooij

Abstract

Integrin-based Focal Adhesions link the intracellular actomyosin cytoskeleton to the extracellular matrix. As such, they are crucial for the mechanics that support tissue morphogenesis and drive cell migration. FAs are also signaling centers that integrate biochemical and mechanical information and regulate cellular reponses such as survival and lineage differentiation or stemness. A number of FA associated signaling proteins, like Src kinase, focal adhesion kinase (FAK) and Paxillin [159-161], have been implicated in tissue morphogenesis as well as tumor metastasis, underscoring the relevance of their investigation. Using our recently developed FA tracking software (AdQuant, chapter 3), we have systematically investigated the development of FAs from their nascence to their final turnover by live imaging of the constitutive FA protein paxillin. This identified a life-cycle dependent, biphasic increase and decline in protein density within FAs that we call FA-compaction. We then investigated how the metastasis promoting hormone HGF, which induces cell migration, and the small GTPase Rap1, which counteracts the migratory effects of HGF, affected the FA lifecycle. Whereas HGF steepened both the compaction and de-compaction rates, activation of Rap1 impaired both the increase and the decline of FA compaction. In both cases, effects of average total FA lifetime were minimal. Thus we identified FA-compaction as a novel FA feature that is targeted in opposing directions by signaling pathways that induce or inhibit cell migration.

Introduction

Integrin-based focal adhesions (FA) connect the extracellular matrix (ECM) to the intracellular actomyosin cytoskeleton. FAs are complex, multi-protein structures that consist of approximately 150 different proteins [108] and can be roughly divided in 3 functional layers. In the basal layer, at the cell membrane the adhesive, integrin proteins are located, as well as their activators kindlin and talin (head domain), a number of adaptor proteins like paxillin and P130Cas and signaling proteins like Focal Adhesion Kinase (FAK) and Src. In the intermediate layer, multiple proteins and combinations of proteins form the link between the basal layer and the actin-cytoskeleton. These include talin (rod domain), vinculin and parvin. Higher up in the FA (the upper layer) are regulators of actin polymerization and structure located, like α-actinin, VASP and zyxin [39]. FAs are subject to inputs from the extracellular environment as well as the interior of the cell. Tensile forces across the FA that are generated by the contractile actomyosin cytoskeleton and the relatively immobile ECM. The magnitude of this tension is influenced by myosin activity from the inside and ECM stiffness from the outside and there is a clear feedback, mediated by FA signaling proteins like FAK, which ensures that cytoskeletal contractility and stiffness are adapted to ECM stiffness [193]. Thus physical properties of the ECM, sensed by FAs, result in alterations in intracellular physical environment and this affects many cellular functions including cell-cell adhesion, cell migration and the programming of transcriptional networks that regulate processes like stemness and lineage differentiation [21]. Extracellularly activated, hormone driven signaling pathways and cell intrinsic signaling pathways, which also control these basal cellular functions impinge upon FA organization and signaling by controlling the phosphorylation of its constituents and by controlling the physical properties of the connected cytoskeleton [5]. Thus FA are sites where mechanical signals and biochemical signals converge to regulate the behaviors that allow cells to function properly in multicellular tissues. Defective inputs and defective activities of these signaling pathways are driving a range of pathological processes including cancer metastasis [73]. The combined input of chemical and mechanical signals into FAs is also affecting their own morphology and dynamics and these measurable properties thus serve as a straightforward read-out for the investigation of the signaling mechanisms that control FA function (reviewed in[5]).

Different populations of FAs have been described based on protein content, morphological characteristics and dynamics and a number of molecular mechanisms have been identified that regulate FA morphology and dynamics. Close to the leading edge of a migrating cell, new adhesions form in an actin-polymerization dependent manner [9, 11]. At the base of the lamellipodium, adhesions can either turnover or mature into larger FAs. The short lived adhesions, that turnover in the lamellipodium, show a discrete paxillin intensity profile from formation till disassembly, reaching a plateau phase of an intensity level similar in all these adhesions [9]. Key to the decision to maturate or turnover is the phosphorylation state of FAK and paxillin [50, 171, 172].The tyrosine residues 31 and 118 of paxillin are FAK target sites. Expression of mutated paxillin that cannot be phosphorylated on these sites anymore, as well as FAK knock-down inhibits FA turnover and cell motility [9, 50, 63, 79, 194]. FA maturation is partially a tension dependent process. FAs grow when cells are plated on stiffer substrates, and disappear when tension is inhibited, which is commonly achieved by the addition of inhibitors of myosinII activation or activity [5, 76]. However, FA maturation is also regulated by activity of the motor protein MyosinII in a motor independent manner [195, 196], underscoring that myosinII inhibition results in more than

inhibition of cytoskeletal contractility. During maturation FAs grow and elongate. FAK and paxillin phosphorylation levels diminish and the molecular composition changes due to recruitment and activation of other FA proteins like vinculin and zyxin [77, 79, 171, 173, 174]. Several mechanisms are known to regulate final FA disassembly in the centre and rear of the cell, including microtubule involved endocytosis [68, 197] and calpainII recruitment inducing proteolysis of several FA proteins, like talin, paxillin and FAK [70-72]. Strikingly, FAs connected to MyosinIIA containing F-actin bundles turnover more rapidly than FAs connected to MyosinIIB containing F-actin bundles [198], indicating an important role for the actin architecture in FA regulation. Many mutations in FA proteins have been described that affect FA assembly and disassembly and cell migration, demonstrating the tight link between these processes.

Hepatocyte Growth Factor (HGF) signaling has been found upregulated in many tumor types and is associated with poor prognosis [199, 200]. In 2D cell cultures of epithelial cells, HGF signaling induces a scattering response that mimics key aspects of metastatic cell behavior [189, 201, 202]. Crucial for this scattering response is an increase in integrin-mediated adhesion and an increase in contractility of the actomyosin cytoskeleton [203]. Rap1 is a small GTPase that also regulates integrin adhesion as well as actomyosin contractility [93, 204]. Rap1's effect on integrin adhesion was found to be mediated by RIAM [205]. Rap1 can regulate Rho-dependent myosin activity through the activation of the Rho-GAP ARHGAP29 [91]. As our lab showed previously, activation of Rap1 blocks HGF-induced cell scattering and may thus serve as a cell-intrinsic inhibitor of metastasis [86].

To investigate FA dynamics in control, HGF-induced and Rap1-inhibited conditions, we used our recently developed FA-tracking software (adQuant, chapter 3). The analysis of total internal reflection (TIRF) microscopy time-lapse image series of paxillin-GFP-labeled FAs revealed a lifetime dependent, convex-shaped protein intensity profile in all FAs, which we call compaction. This indicated that FA disassembly is a slow process that initiates long before the FA ceases to exist. Such early initiation of disassembly of FAs has not been recognized previously and will have to be incorporated in the current models about FA regulation and function. HGF enhanced the speed of compaction and de-compaction and lead to denser FAs, while Rap1 decreased the dynamics of this density profile resulting in less dense FAs. The correlation between FA compaction and the generation of traction force on FAs needed for cell migration suggests that compaction is a mechanically regulated process influenced antagonistically by positive and negative regulators of cell migration.

Results

FAs show characteristic compaction and de-compaction profiles

Using our tracking software (chapter 3) we measured the life-time-dependent mCherry-paxillin density profile of each individual FA, by calculating the average, background-corrected fluorescence pixel intensity per FA. In order to average data from multiple FAs that all appear and disappear at a different time point during imaging, all tracks from newly detected FAs were synchronized to their frame of first appearance. FAs that existed beyond the end of the image series were not used for these analyses. For each time point in these synchronized tracks, the pixel intensity was averaged of all the FAs of equal lifetime, taken from different cells and cellular regions imaged. The obtained average paxillin intensity profiles had a convex shape: they showed an increase in intensity in the beginning, reached a plateau phase at a time that differed with lifetime, and then declined towards the end

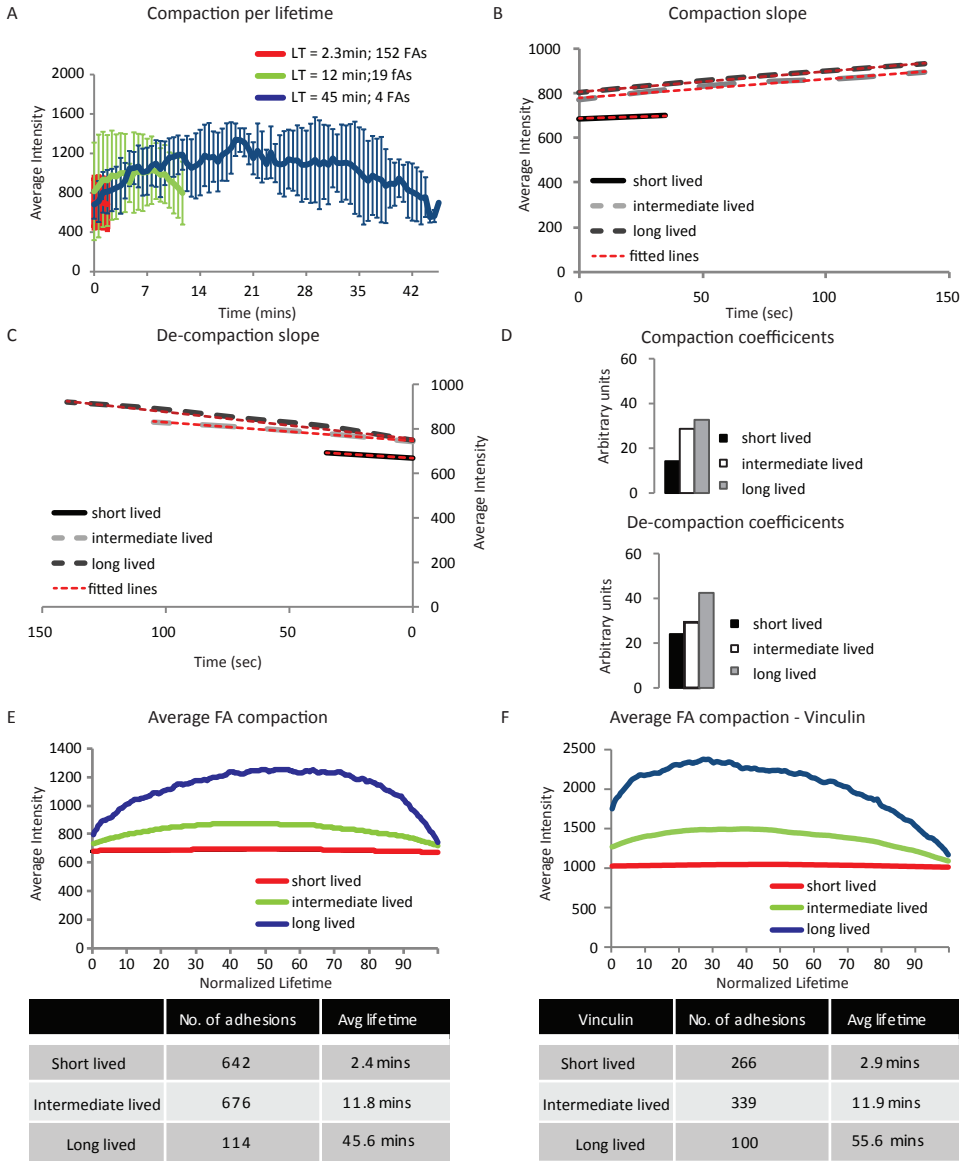

	No. of adhesions	Avg lifetime
Short lived	642	2.4 mins
Intermediate lived	676	11.8 mins
Long lived	114	45.6 mins

Vinculin	No. of adhesions	Avg lifetime
Short lived	266	2.9 mins
Intermediate lived	339	11.9 mins
Long lived	100	55.6 mins

Figure 1: Paxillin intensity profiles reveal life-time-dependent compaction and de-compaction of FAs

A) Examples of paxillin intensity profiles obtained by averaging the intensity of the GFP-Paxillin signal in all FAs with equal lifetime (error bars= standard deviation). B) Line fit on the first data points of the compaction curves, obtained by averaging the first data points of all newly formed FAs within each population until the FA with shorter life dispersed from the longer lived ones. C) Line fit on the final data points of the de-compaction slopes, obtained by averaging the last time points of all dying FA within each population, starting at the moment that the FAs with shorter lifetime converged with the longer lived ones. D) Resulting coefficients of fit on compaction (top) and de-compaction (bottom) data points. E) Overall FA compaction of 3 populations, obtained by normalizing the total lifetime to 100, interpolating missing relative time points in shorter-lived FAs and averaging at each relative time point the intensity of all FAs within each population. In the table the number of FAs per population and the average lifetime are shown. F) Similar to (E) but showing the compaction profile of vinculin in the 3 different populations obtained from a separate experiment of DU145-G4 cells stably expressing mCherry-Vinculin.

(Fig.1A). Although there was variance, the intensity profiles of single FAs (Supp.Fig.S1) were comparable to this average intensity profile. This shows that paxillin density in FAs increases during their maturation, a previously observed feature, which we will now call compaction. It also shows that the reverse process of gradual de-compaction of paxillin occurs before FAs cease to exist. This is not a well described FA feature and it is revealing that an intrinsic property determines FA turnover long before their disappearance is obvious. Since we observed an increase in average paxillin density with FA lifetime (chapter 3), we next investigated in what respects the compaction profiles differ between the populations of short lived FAs (lifetime shorter than 4 minutes), intermediate lived FAs (lifetime between 4 and 30 minutes) and long lived FAs (lifetime longer than 30 minutes). We asked whether FAs from the different populations compact initially at the same speed and the longer lived ones compact longer or whether the rate of compaction varies with lifetime and whether the 3 populations differ in initial, maximum and pre-disappearance density. To analyze the compaction rates, we determined the coefficients of a linear fit on the first few data points of the synchronized and averaged intensity curves of the 3 populations (Fig.1B&D-top). This analysis showed that the rate of compaction increased with lifetime. Similarly, by synchronizing all FAs of each population to their last frame of detection, de-compaction rates were found to increase with lifetime (Fig.1C&D-bottom). The maximum reached paxillin density showed variation within the populations but was on average increased with lifetime (Supp.Fig.S2A). Consistent with this notion, a scatter plot of lifetime versus maximum intensity showed a relation between the two characteristics. (Supp.Fig.S2B). Surprisingly, initial density and the density after de-compaction of the FAs, calculated as an average of the first or last 2 data points respectively of the separate, per lifetime averaged compaction curves, showed a large variance and there was no clear shift between populations (Supp.Fig. S2C&D). A scatter plot showed that little relation existed between initial density and the density just before disappearing (Supp.Fig.S2E) and neither of these intensities showed a relation with the maximum intensity (Supp.Fig.S2F).

To be able to evaluate the overall compaction of each population, we have normalized the lifetime of each adhesion to 100, using interpolation to fill gaps between data points, and averaged all adhesions within each group from different non-stimulated cells. Thus three compaction curves were generated that contain data of 642, 676 and 114 adhesions per category with an average lifetime of 2.4, 11.8 and 45.6 minutes respectively (Fig.1E). The compaction profile increased in convexity in the intermediate and in the longer lived population of FAs, consistent with the observed raise in average FA density and compaction rate in populations of increasing lifetime. Similarly, a separate experiment of DU145-G4 cells stably expressing mCherry-Vinculin showed that vinculin also compacts in a lifetime dependent manner (Fig.1F). Due to the fact that it is data from two independent experiments, direct comparison of the profiles is not possible, but the compaction profiles are similar. A comparable analysis of FA size, again monitoring mCherry-Paxillin, revealed very similar convex curves of growth and shrinkage during FA maturation (Supp.Fig.S3B) also visible in averaged FA size per lifetime (Supp.Fig.S3A), consistent with the earlier described finding of increased average FA size in the intermediate and long lived FAs (chapter 3). This indicates that FA compaction and FA size are analogously regulated features (notably, their calculation is independent). Furthermore, compaction appears not to be single protein, paxillin-specific behavior as it is visible for multiple FA proteins (at least 2; vinculin and paxillin, additional proteins will be investigated).

Taken together this analysis shows that FAs compact and de-compact in relation with their

lifetime; long lived FAs compact and de-compact faster and reach a more compact state than intermediate- and short lived FAs, but this is unrelated to the initial and final density. Strikingly, gradual de-compaction and shrinkage start on average halfway through the lifetime of FA, which indicates that intrinsic signals or physical properties dictate FA dissociation at a much earlier time in their existence than currently appreciated. The physical properties or signaling events that determine this early onset decline are currently elusive. We need to incorporate this notion into the design and evaluation of our investigations into the signaling mechanisms and mechanical inputs that regulate FA dynamics.

HGF and Rap1 signaling affect FA compaction

As described in chapter 3 of this thesis, Rap1 activation induced a loss of highly intense FAs, indicating that Rap1 signaling may affect the process of FA compaction. To address the questions whether HGF signaling also affects compaction and which characteristics of the compaction profile are affected by these signals, we compared paxillin intensity profiles of the different conditions in the 3 lifetime-based populations, each containing a large amount of FAs (Fig.2E). Neither HGF treatment nor Rap1 activation changed the average lifetime within each population (Fig.2D). It should be noted that all tracks existing beyond imaging were excluded, which may lead to an underestimation of the effect of Rap1 on average FA life-time. The convex shape of the compaction curves was maintained upon HGF treatment (Fig.2A left), but the rates of compaction and de-compaction were slightly increased in all populations of FAs (Fig.2B & C left). Rap1 activation in HGF treated cells 3 hours prior to imaging, decreased the maximum compaction of FAs (Fig.2A right), consistent with the observation that Rap1 activation induced a loss of highly intense FAs (chapter 3). Furthermore the rate of compaction and de-compaction was decreased in all groups of FAs in Rap1 treated cells (Fig.2B & C right).

Together these data show that upon HGF treatment compaction and de-compaction become more dynamic. Subsequent Rap1 activation decreases the dynamics of compaction and de-compaction as well as the maximum level of compaction. How this relates to the effects observed on cell migration (chapter 3) remains elusive but some speculations will be discussed below.

Discussion

Consistent with a wealth of earlier studies that have built a general perception of FA dynamics and behavior in relation to cell migration, we found that small, immobile FAs concentrate at the cell-front, whereas larger, sliding FAs concentrate at the rear. The novel finding of this study is that, in all populations of detected FAs, we measured an increase in mCherry-paxillin signal intensity per volume unit over time, which indicates that the density of the paxillin protein within FAs increases (compaction), followed by a decrease in signal intensity indicating that the paxillin-density decreases (de-compaction). Previous studies have determined assembly and disassembly kinetics based on intensity increase of different FA proteins in manually detected subsets of FAs [50, 206, 207]. Here we show that the increase and decrease in intensity occurs overall in all FA populations in the cell and that the dynamics of the compaction profiles are lifetime dependent. We observed these profiles for both paxillin and vinculin, suggesting that it is not limited to a single protein. Thus our data indicate that this reflects a general increase in the concentration of proteins within FAs leading to their compaction. It would be interesting to analyze the compaction behavior of other FA proteins

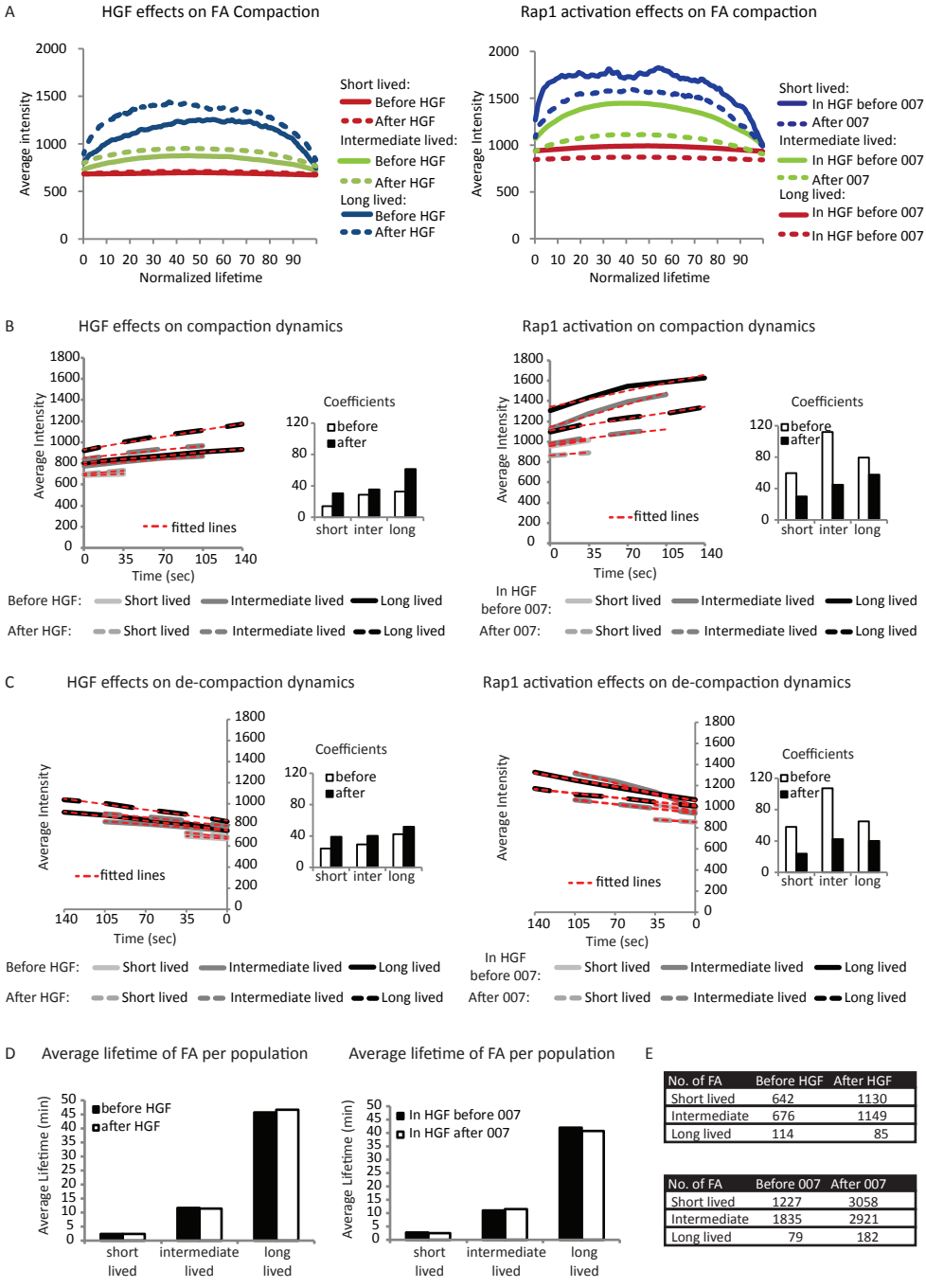

No. of FA	Before HGF	After HGF
Short lived	642	1130
Intermediate	676	1149
Long lived	114	85

No. of FA	Before 007	After 007
Short lived	1227	3058
Intermediate	1835	2921
Long lived	79	182

Figure 2: Compaction dynamics are affected by HGF and Rap1 signaling

A) Overall compaction curves of the 3 FA populations before and after HGF (left) and in HGF treated cells before and after Rap1 activation (right), obtained by normalizing the lifetime of each FA to 100 and averaging paxillin intensity levels of all FAs within a population. B) Line fit on the first 2, 4 and 5 data points of the average of all FA

and identify differences in compaction profiles that may provide clues about FA regulation. What is most striking in our observations is that in all FAs analyzed, a decrease in density (de-compaction) started long before the FAs actually ceased to exist (on average about three quarters of their existence). This indicates that a gradual loss of FA compaction is part of a disassembly process, of which the early onset was to our knowledge not previously reported. As a consequence of this compaction process the increase in structural FA proteins like paxillin will generate more binding sites for other proteins, thereby increasing FA signaling. Furthermore the increase of actin-binding proteins like vinculin reinforces the FAs and the connection between the FA and the actin cytoskeleton [20, 41, 208].

We found that HGF increased the compaction dynamics and the maximum reached density in all three lifetime based populations. On the other hand, Rap1 activation reduced the compaction dynamics and the maximum density reached. Similarly, on cell migration the 2 signaling pathways have opposing effects, where HGF signaling induces migration and Rap1 activation inhibits migration. Previous data suggest that these effects on cell migration are most likely caused by opposing regulation of cytoskeletal contraction, as HGF induces myosin activity [203, 209] and Rap1 reduces myosin activation by activating the ARHGAP29 to inactivate Rho [91]. A likely hypothesis that stems from this is that traction at FAs, resulting from contractile forces in the intracellular actomyosin cytoskeleton and rigidity of the extracellular ECM substrate, correlates with FA compaction. This is further supported by the notion that intensity of vinculin in FAs showed a linear relationship with exerted traction force [75]. Additionally, an increase in tension, concomitant with compaction could also provide an explanation for the onset of de-compaction. Tension dependent FA recruitment of proteins involved in the Calpain-mediated proteolysis pathway has been reported [162, 210], such that prolonged tension (and concomitant compaction) eventually causes FA disassembly [70, 71, 211]. Another explanation for the early onset of de-compaction comes from the model that FAs link to the actin cytoskeleton in a clutch-like manner [11, 12]. If traction force increases, the proteins that form the clutch may not hold and occasionally slippage occurs. With the build of tension, slippage increases exponentially until there is a complete failure of the clutch to hold, which leads to FA disintegration [58]. Combining traction force microscopy to measure traction force directly [194, 212, or FRET-based tension sensors to measure tension at FA-proteins directly [113], with high resolution microscopy of
the FAs will allow us to directly correlate the compaction profile with the traction or tension profiles.

In conclusion, our study revealed a lifetime dependent FA compaction profile that is oppositely affected by 2 pathways that antagonistically affect cell migration. The FA compaction profile maybe tension-dependent and appears to be a general feature of FAs that should be incorporated in our models of FA regulation.

within the short, intermediate and long lived population respectively, synchronized to the frame of first appearance, of non-treated cells before and after HGF (left) and of HGF treated cells before and after Rap1 activation (right). The resulting coefficients of the fitted lines are shown in the small bar graphs on the sides. C) Similar to (B) but a line was fitted through the last 2, 4 and 5 data-points of the average of all FA within the short, intermediate and long lived population respectively, synchronized to the last frame of appearance. D) Average lifetime of the short lived, intermediate lived and long lived population in non-treated cells before (black) and after (white) HGF (left) and in HGF treated cells before (black) and after (white) Rap1 activation (right). E) Table showing the number of FAs within each population.

Materials and methods

Cell lines and culture

DU145-G4 cells were transfected with a lentiviral delivery system. Lentivirusal particles were produced by transfection of HEK293 cells with third-generation packaging construct [188]. DU145-G4 cells were plated in full medium in a 6-well plate overnight and then transduced with mCherry-Paxillin or mCherry-Vinculin virus supernatant in the presence of 40µg/ml polybrene for 24 hours before returning the cells to full medium. mCherry-Paxilin or mCherry-Vinculin expressing cells were selected by fluorescence-activated cell sorting (FACS) by their mCherry levels.

48 hours prior to imaging DU145-G4 cells were plated in Roswall Park Memorial Institute (RPMI) medium (Gibco) supplemented with 10% fetal calf serum (FCS) (Sigma) in collagen-type 1 (10µg/ml; PureCol)-coated, Lab-Tek® #1.0 Borosilicate Chambered System, 8 units. 24 hours prior to imaging, the medium was replaced by 0.5% FCS containing RPMI. 25ng/ml HGF was added either 3 hours prior to imaging or after approximately an hour of imaging. 8-pCPT-2'-O-Me-cAMP-AM (007AM) (Biolog Life Sciences) was added, at a concentration of 1µM, to HGF pretreated cells after an hour of imaging.

For the scatter assay, cells were treated similarly but plated in a coated 48-well plate. Before imaging the wells were completely filled with medium and the plate was sealed using silicon grease and a glass plate. Either HGF alone, 007AM alone or a combination of HGF and 007AM was added to the cells after 1 hour of imaging.

Microscopy

For imaging we used a NIKON Ti microscope equipped with a total internal reflection fluorescence (TIRF) system, a CFI Apochromat TIRF objective, 60x oil with an NA of 1.49, a 12-bit electron multiplying CCD (EMCCD) Luka camera (Andor) and controlled by company software (NIS-elements).

We have created a dataset of image series of the DU145-G4 cells with mCherry Paxillin in the two different transitions. The data set consists of 12 cells imaged from epithelial to migratory induced by HGF and of 18 cells that were incubated with HGF 3 hours prior to imaging and in which Rap1 was activated during filming via Epac by the cAMP analog 007AM.

The scatter assay for the characterization of the Du145-G4 cell line was carried out on a Leica AF7000 microscope, with a 10x objective. Images were taken every 10minutes and the analysis was carried out using CellTracker, a custom developed Matlab analysis tool [189].

FA tracking and calculations

The FA tracking method and ensuing image analysis algorithms have been described in detail in chapter 3 of this thesis. Specific for the analyses in this chapter are the below parameters:

FA Intensity: To determine the average pixel intensity in the FA, it is necessary to correct for a certain background level. To negate fluctuations in the measurement of FA pixel intensity, preferably the background should be measured locally around the FA. In order to do so, we determined a watershed on each frame with the found adhesions as markers and the found cell edge as outer edge. The average pixel intensity in each region, minus the area that belongs to the FA, was used as the local background and this was subtracted from the average intensity of the accompanying adhesion.

Lifetime normalization: For normalization of the lifetime to 100, each time point on the intensity profile of the FA and its accompanying intensity was rescheduled to point: (x*100)/

frames_FA-1, where x is an increasing point on the x-axis ranging from 1 till the maximum of number of frames the FAs existed and frames_FA is the number of frames the FAs existed. Thus the appearance of the FA will be set to point 1 and the last to point 100. Gaps that formed in between these data points in the tracks that contained less than 100 time points were filled by interpolation between 2 subsequent data points, using the interpolation function (interp1) of MatLab.

Supplemental Figure S1

Randomly picked examples of single FA intensity curves of the short lived (left), intermediate lived (middle) and long lived (right) populations in untreated cells.

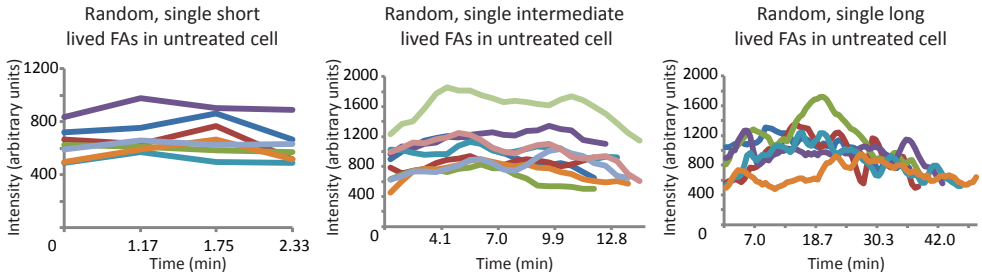

Supplemental Figure S3

A) Examples of average FA size obtained by averaging the size of all FAs with equal lifetime, coming from different regions and different, untreated cells (error bars= standard deviation). B) Overall FA growth curves of 3 populations, obtained by normalizing the lifetime to 100 and averaging for each relative time point the sizes of all FAs within each population.

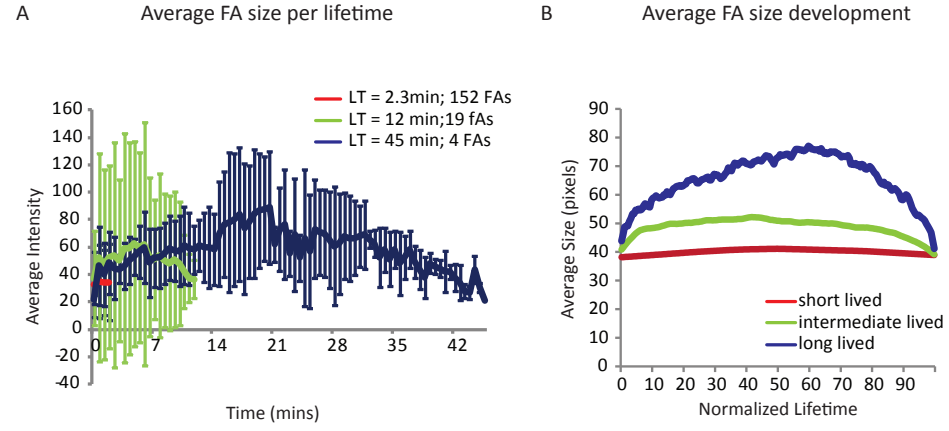

Supplemental Figure S2

A) Distribution of maximum compaction of the 3 lifetime based populations from untreated cells. The highest intensity is the maximum of each, per lifetime averaged compaction curve after smoothing with a running average of 6. B) Scatter plot of the lifetime versus maximum density. Each dot represents the maximum density of one per lifetime averaged compaction curve. C) Distribution of the initial compaction density, the average of the first 2 data points of the per lifetime averaged compaction curves. D) Similar to (C) but for the final de-compaction density, measured as an average of the last 2 data points. E) Scatter plot of initial density versus the final de-compaction density. F) Scatter plot of maximum density versus initial density (blue dots) and versus final de-compaction density (red dots).

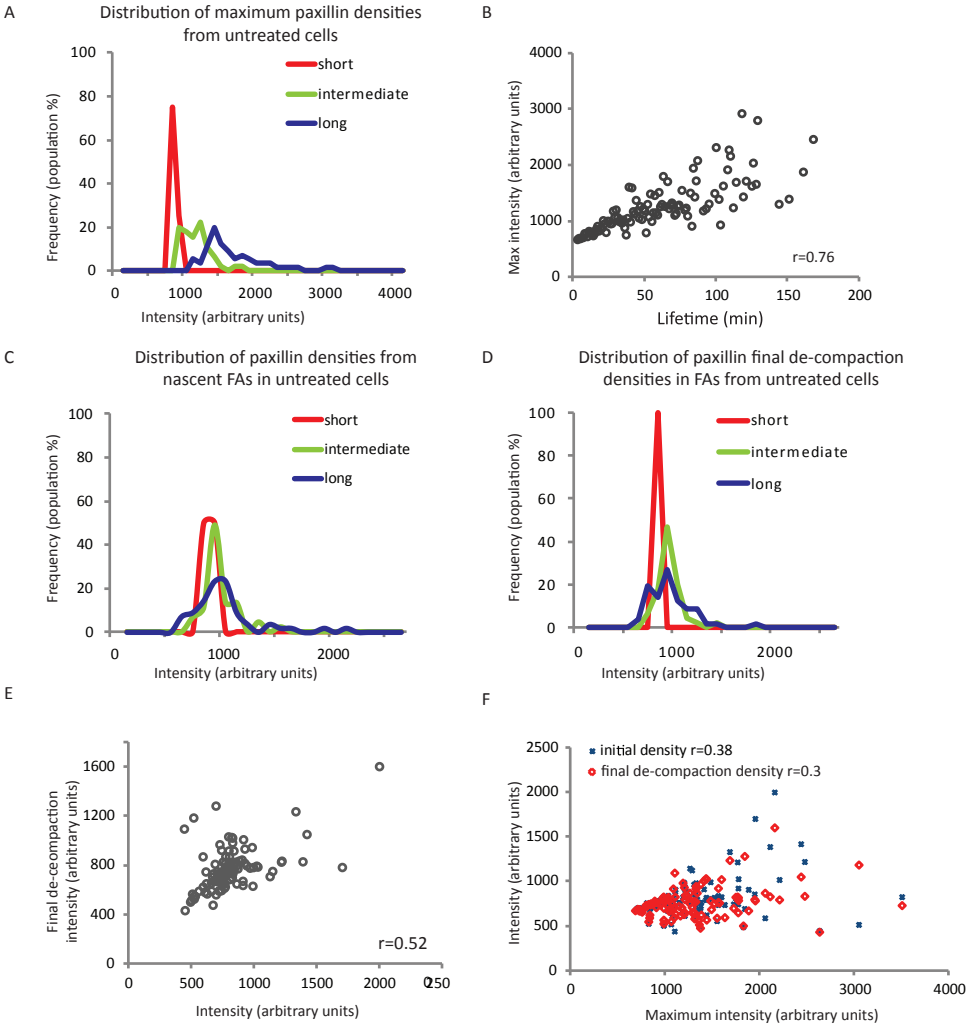

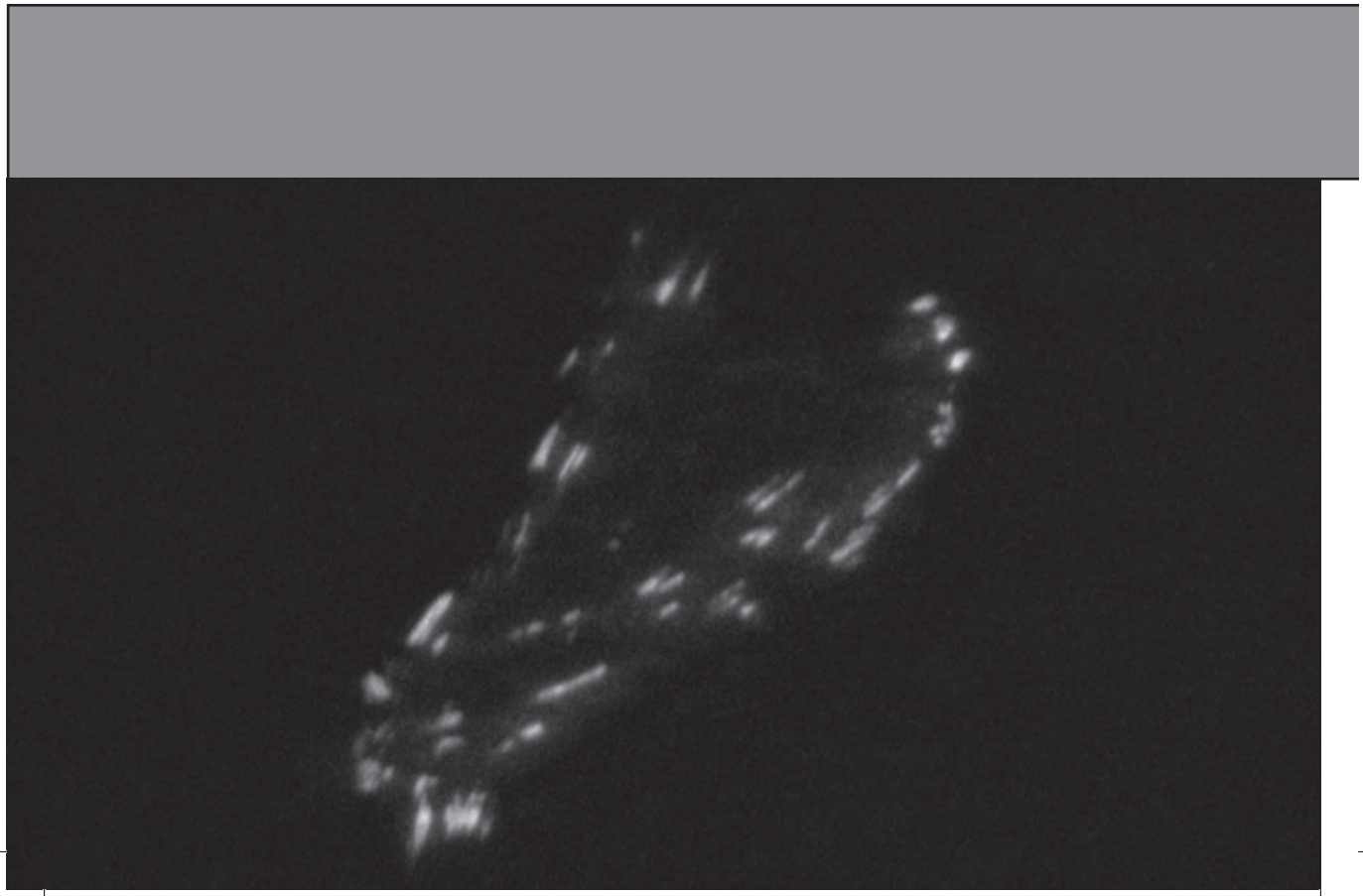

Quantitative, automated analysis of the immediate response of focal adhesions to loss of tension reveals a faster decrease of paxillin compared to vinculin

5

Emma Spanjaard and Johan de Rooij

Abstract

Integrin-mediated Focal adhesions (FA) are pivotal for cell adhesion, migration and tissue integrity. FAs form the link between the cytoskeleton and the extracellular matrix (ECM) and transduce mechanical input from the ECM into cellular responses. In turn, cytoskeletal tension and signaling cascades from within the cells are important for the regulation of FA properties like size, dynamics and turnover. A central protein in these processes is vinculin whose presence and activity at FAs are reported to depend on actomyosin-based tension and are found to influence FA size and dynamics. Detailed, time-resolved investigation of vinculin concentration at FAs under fluctuating tension has not been reported and therefore the direct relation between FA-tension and vinculin presence remains controversial. Here we investigated the immediate effect of tension release on the abundance of vinculin at FAs and on the abundance of the structural FA protein paxillin that is thought to be an upstream regulator of vinculins presence. To this end we have analyzed by live cell TIRF microscopy, automated image segmentation and FA-tracking, the FAs of the prostate cancer cell-line DU145, expressing mCherry-paxillin and GFP-vinculin, upon inhibition of cytoskeletal contractility by simultaneous wash-in of the ROCK inhibitor (Y27632) and the myosin light chain kinase inhibitor (ML7). Conform the literature, we measured cell spreading and decreased FA number, size and intensity upon tension release. Also the biphasic compaction profile, previously described by us as a feature of the FA lifecycle, of already existing FAs was disrupted by loss of tension. Our analysis showed that both vinculin as well as paxillin intensity in FAs decreased upon release of tension. Surprisingly however, the decrease of paxillin was in general more rapid than that of vinculin. Only in very few FAs vinculin decreased more rapidly. Together these data challenge the notion that vinculin is a distinct tension sensitive member of the FA.

Introduction

Cells experience a constant bidirectional play of forces between them and their extracellular environment, which underlies many developmental and physiological processes. On the outside of the cells, the stiffness of the extracellular matrix (ECM) and the concentration of ligand determine the resistance that cells sense. Within the cells, force is for a large part generated by the motor activity of MyosinII acting on the actin cytoskeleton, which is regulated by biochemical signals [32, 213]. Focal adhesions (FAs) provide the anchor point for these forces by connecting the cytoskeleton to the relatively stationary ECM via integrins. On the intracellular side, more than 1000 proteins participate in the connection of the integrins to the cytoskeleton [162], of which 250 have been established as true FA proteins [108], including adaptor proteins, kinases, phosphatases and small GTPases. Together they form the 'integrin adhesome' [37] that transmits tensile forces and translates these mechanical signals into cellular responses. The FAs themselves are also modulated by the tension between cytoskeleton and ECM, which affects their size, dynamics and lifecycle [171]. The mechanosensitive signals that FAs transduce determine crucial cellular functions like stem cell plasticity and lineage differentiation in healthy tissues [214] and epithelial mesenchymal transitions in cancer [215]. One of the key intracellular mediators of mechanotransduction in these processes is the transcriptional co-activator YAP [216]. A major gap in our understanding is how mechanosensitive processes within FAs are transduced to cytoplasmic and nuclear cascades. A better understanding of the molecular details of FA mechanosensing may help to close this gap.

Although many proteins function in the FAs, a small subset can be seen as the core proteins and these core proteins have distinct roles and positions within the FA. These core proteins include the integrins, stretchable adaptor proteins like talin, signaling-involved proteins like focal adhesion kinase (FAK) and paxillin, actin regulators like zyxin and VASP. Recently, with the use of super-resolution microscopy these proteins were shown to reside in specific, functionally different layers of the FA [39]. The head domain of talin and the proteins FAK and paxillin are positioned close to the cytoplasmic tails of the integrins, forming a basal layer of integrin stabilization and signal transduction. This basal layer is followed by an intermediate layer that regulates the kinetics of the interaction between the basal FA layer and the associated F-actin cytoskeleton. The tail of talin positions in this intermediate layer, directly linking integrins to the actin cytoskeleton. Talin is indispensable for functional adhesion as its head domain regulates the strength of the integrin-ECM binding [56, 59]. Vinculin is positioned in the same layer and can bind to talin, paxillin, FAK and to actin, through interactions that are regulated by tension (see below). By working as a clutch between inward flowing actin and static integrin-ECM complexes the intermediate layer contributes to the development of traction on FAs for which vinculin is important [42]. The third layer contains actin regulators like α-actinin, VASP and zyxin. This layer may function to alter local cytoskeletal dynamics and organization in response to feedback signals from the FAs. New adhesions can form in a tension independent manner [9]. But FA maturation is a tension dependent process. The FAs in cells that are plated on soft substrate are smaller than on stiffer substrate, indicating that FAs grow upon tension [5, 217]. FAs disappear when myosinII activity is inhibited [76], indicating that tension is required for FA stability. Thus, FAs form complex mechanosensitive entities and mechanosensitivity plays an important role in the lifecycle of the FA.

As an explanation for mechanosensitivity of FAs, stretchable proteins have been put forward.

These include talin, p130Cas and vinculin. One hypothesis, supported by biophysical experiments in vitro, predicts that tension mediated unfolding of talin exposes binding sites for vinculin to induce its recruitment and thus strengthen the integrin-actomyosin connection [21]. In addition, vinculin abundance in FAs was shown to be regulated by activity of FAK, activated via myosinII mediated tension. Here FAK-induced phosphorylation of paxillin increased its affinity for vinculin [79]. To be localized to adhesions, vinculin must uncouple its head and tail regions, which are folded onto each other, masking its major protein binding sites. In the head domain the binding site for talin is located, whereas the binding sites for paxillin and actin are located in the tail [44]. Carisey et al (2013) showed that not only the abundance of vinculin is mechanosensitive, but also its activity, as vinculin was shown to promote integrin adhesion in an actin-binding and myosin-promoted manner [41]. Stretching of p130CAS may regulate associated signaling pathways like Src and Rap1 to enhance integrin activity [81]. A recently uncovered connection between p130Cas and vinculin may interconnect these 2 stretch activated systems [46, 80]. Thus, multiple mechanosensitive routes converge on the regulation of the abundance and the activity of vinculin at FAs, implicating vinculin as a central mediator of FA mechanotransduction.

Since tension on the FA and vinculin presence appear so closely related from numerous previous studies, we hypothesized that loss of tension would affect the presence of vinculin at FAs differently than the presence of basal layer FA proteins that have a less direct relation to tension, like the adaptor protein paxillin. To our knowledge there is no study that has systematically investigated the immediate, time-resolved effect of release of Rho-mediated tension on the abundance of vinculin compared to the abundance of paxillin. We hypothesized that vinculin abundance would rapidly decrease upon tension release prior to that of paxillin. To test this hypothesis, we have extended our recently developed FA detection and tracking method to analyze dually labeled FAs specifically over time. We then used this to investigate the intensity change of mCherry-paxillin and GFP-vinculin upon release of tension by wash-in of myosin-activity inhibitors in live-cell TIRF-microscopy recordings. Similar to previous observations, inhibition of myosin activity induced cell spreading, FA size decrease and FA intensity decrease [32, 79]. Furthermore, FA compaction, which we previously described as the biphasic increase and decrease in protein density during the live-cycle of FAs, was disturbed. The initial effects of inhibitor wash-in on the presence of proteins in the FAs occurred rapidly, within 30 seconds, confirming the immediate release of tension by these inhibitors. Surprisingly, in contrast to our hypothesis the average decay of paxillin abundance preceded the decay of vinculin. Within 6 minutes the balance was restored and only at longer timepoints after drug wash-in vinculin levels were found reduced more than paxillin levels. A large population of FAs in which paxillin and vinculin decrease was equal was also detected, whereas only few FAs showed faster vinculin decay. Thus, contrary to common notion in the field, our data imply that vinculin is not an exquisite or rapid tension-responsive member of the FA.

Results

Dual Color-based detection for ratio analysis

To study whether loss of tension has a differential effect on the abundance of vinculin compared to paxillin, we used the DU145-G4 cell line (DU145 prostate carcinoma cells that overexpress Epac) stably expressing, mCherry- paxillin and GFP-vinculin. To maximize the precision and reliability of our analyses we extended our detection and tracking method of

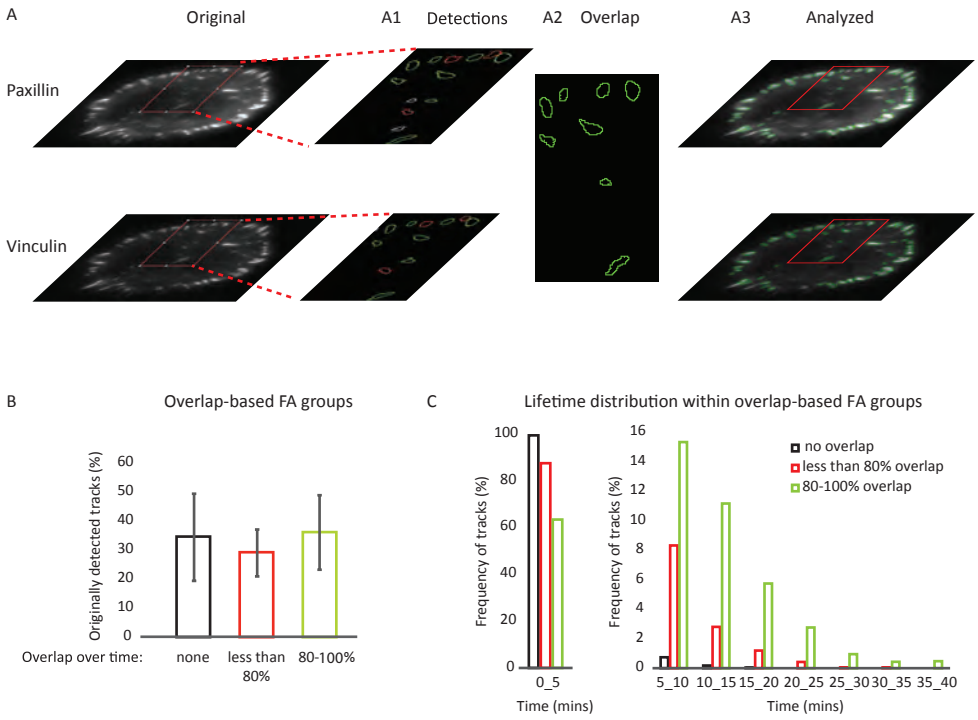

Figure 1: Selection method for dually labeled FAs

A) Grey images of paxillin (top) and vinculin (bottom) in which FAs are separately detected (close-up in red). A1) Detected FAs in the paxillin (top) and vinculin (bottom) channel of the close-up in (A). In green FAs that overlap in 80% of the track or more, in red FAs that overlap in less than 80% and in white the FAs that do not overlap. A2) Detection result of the close-up in (A) after the overlap analysis. A3) Original images of mCherry-paxillin signal (top) and GFP-vinculin (bottom) with overlay (green) of the detected FAs (close-up in red). B) Percentage of FA that either do not overlap (black bar), overlap less than 80% of the track (red bar) or overlap of 80-100% of the track (green bar) (error bars: standard deviation of 15 cells, imaged with the same framerate). C) Lifetime distribution of the 3 different groups of FAs as depicted in (B).

FAs in time lapse image series, described in a previous study (chapter 3), with a module to select FAs that are simultaneously detected in sequential images recorded in the 2 channels used to monitor the differentially labeled proteins. To achieve this, first FAs (and possibly other objects) are detected and tracked in each channel using our detection method with a set of parameters optimized for that channel. Next, for each time point all detected objects in the paxillin channel are probed for overlapping objects detected in the other channel (Figure1A &1A 1). Objects that do not overlap (Figure 1A 1, white) are discarded. For all overlapping objects, the number of frames this overlap lasts is determined. Based on this information, tracks of objects that are detected in both channels for 80% of the paxillin-based track are kept for further analysis (Figure1A 1&1A 2, green) and the other objects are discarded (Figure1A 1&1A 2, red). The 80% cut-off criterion was chosen, since inconsistencies like laser-power fluctuations or uneven reflection of the TIRF beam (resulting in uneven evanescent wave and illumination of FAs) could introduce gaps in the detection in one channel and using too stringent criteria (like eg. 100% overlap) would result in unnecessary discarding of bona fide FAs. Approximately 36% of all initially detected objects

have a >80% track overlap in the 2 channels. These are further analyzed below. The group of tracks that did not overlap at all (34%) (Figure1B, black) mainly consisted of very short lived objects (less than 5 minutes) (Figure1C). Visual inspection indicated that this group includes fluctuations in signal intensity in the paxillin channel (causing detection of objects that do not look like FAs), which are not paralleled in the vinculin channel. These detected objects could be regarded as noise that needs to be filtered out. It also seems to include a subset of integrin adhesions (objects that do look like FAs) that contain paxillin, but not vinculin, as has been postulated to be the case for focal complexes that have not yet established contact with the contractile actomyosin cytoskeleton [77]. We did not further investigate this set of FAs in this study. The group of tracks with less than 80% track-overlap (30%) (Figure 1B, red) contained short lived, mostly FA-shaped objects but also FA-shaped objects of longer lifetime (Figure 1C, red). It is obvious that single or 2-frame imaging and/or detection errors in one channel would affect the percentage of overlap of short tracks much more than that of longer tracks. This <80% overlap group likely includes bona fide FAs that contain both vinculin and paxillin, but tracking of which was affected by inconsistencies in the imaging. Thus this selection eliminated noise-induced objects as well as bona fide FAs predominantly in the group of FAs with a lifetime up till 10 minutes. Nevertheless, sufficient FAs survived this stringent selection to allow analysis of FA intensity in all categories. For this, FA features were collected for the > 80% overlap FAs based on the FA outline as detected in the paxillin channel. Running the analysis based on the outline as detected in the vinculin channels yielded similar results for the FA feature analysis over time (not shown). Thus a stringent detection-pipeline was defined to collect FA data containing information on both vinculin and paxillin, which was further used to study the relation between paxillin and vinculin intensity upon inhibition of myosin activity.

Inhibition of Rho-mediated tension affected cell size and FA features

To study the effects of tension release on the abundance of vinculin and paxillin in FAs, we imaged paxillin and vinculin by TIRF microscopy in unstimulated conditions for maximally 15 min. Then we added the Rock inhibitor Y27632 and MLCK inhibitor ML-7, to inhibit myosin-dependent cytoskeletal contractility and release tension from FAs, and continued imaging until most FAs had disappeared (Figure 2A). For the characterization of the effects of tension release, the following features were averaged per cell before and after addition of the inhibitors: cell size, the number of FAs, average FA size and average paxillin and vinculin intensity. In previous studies it was shown that inhibition of Rho mediated contractility induces cell spreading and a decrease of the number of FAs [32, 79]. In our case, most of the 18 recorded cells increased in size after inhibition of contractility (Figure 2B). We also observed disappearance of FAs, resulting in a lower amount of FAs (Figure 2C), but new FAs were still formed in the presence of the inhibitors. In the process of disappearing, FAs decrease in size and proteins leave, which was observed as a decrease in average FA size (Figure 2D) and reduction of paxillin intensity (Figure 2E) and vinculin intensity (Figure 2F), measured as the average per FA and subsequently averaged over all FAs per cell before or after addition of inhibitors. Inhibition of contractility was also shown to decrease FA lifetime, but we did not include this feature for the characterization, due to the short amount of time of imaging prior to inhibition. The fact that the responses of these cells recapitulate previously described effects of inhibition of Rho-mediated contractility on cell size and FA features, lends confidence to the wider relevance of the relative response of vinculin and paxillin concentration in FAs in these cells to release of tension, which we study below.

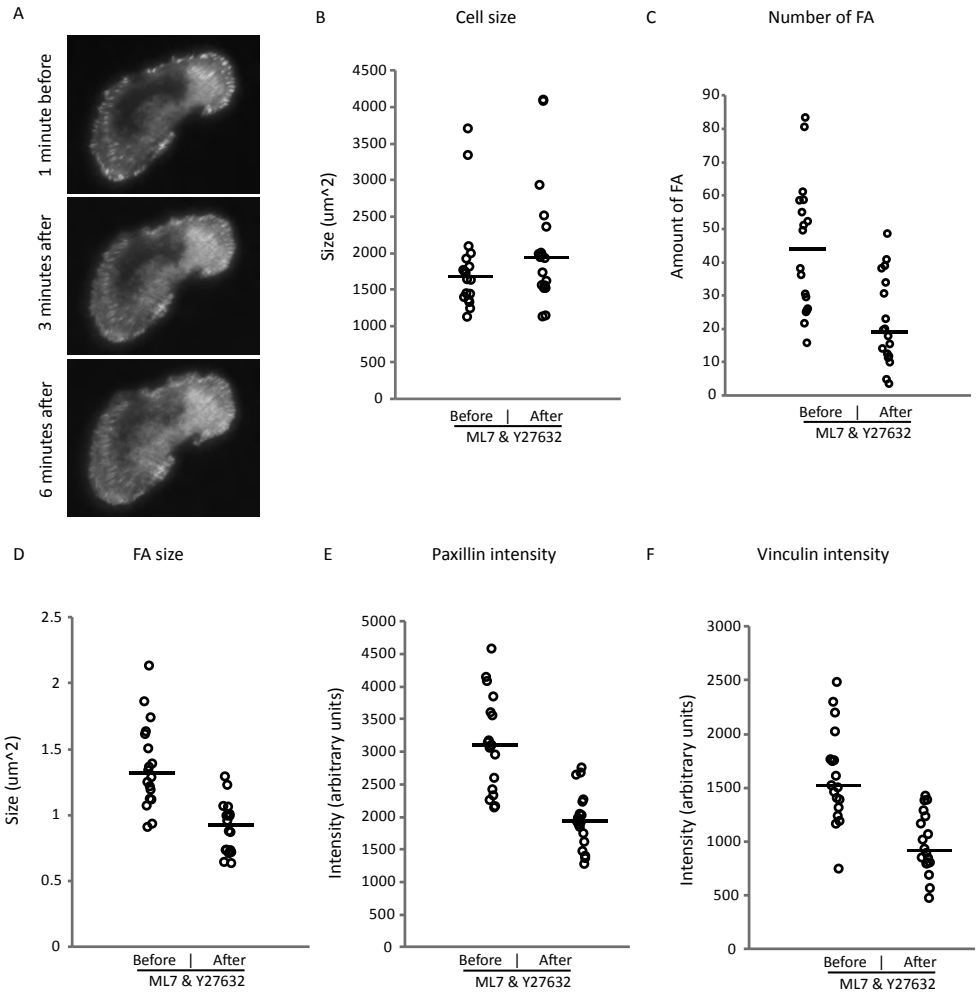

Figure 2: Characterization of the effects of inhibition of Rho-mediated tension

A) Stills from image serie (paxillin labeled FA) 1 minute prior to wash-in of ML7 and Y27632 (top) and respectively 3 and 6 minutes after addition of the inhibitors (middle and bottom). B) Cell size per cell averaged over all the frames prior to inhibitors (before inhibitors) and after addition of inhibitors (after inhibitors). C) Number of FAs per cell averaged over time similar to (B). D) Average FA size per cell, where first for each FA the size was average and then all FAs were averaged per cell prior to and after inhibitors. E) Similar to (D) but for the average pixel intensity of Paxillin. F) Similar to (D) but for the average pixel intensity of vinculin.

Inhibition of Rho-mediated contractility interrupts FA compaction

Previously we have described a lifetime-dependent biphasic intensity profile of overall fluorescent intensity in FAs, indicating that FAs compact while growing and that their turnover starts gradually by de-compacting far before the actual disappearance. We speculated that this compaction profile is a tension dependent process, as had been previously postulated for FA maturation, since activation of the small GTPase Rap1, which was recently shown to reduce Rho activity [91], decreased both the rate and degree of compaction (chapter 3). To determine the compaction profiles, all films with a similar frame rate were grouped together. From

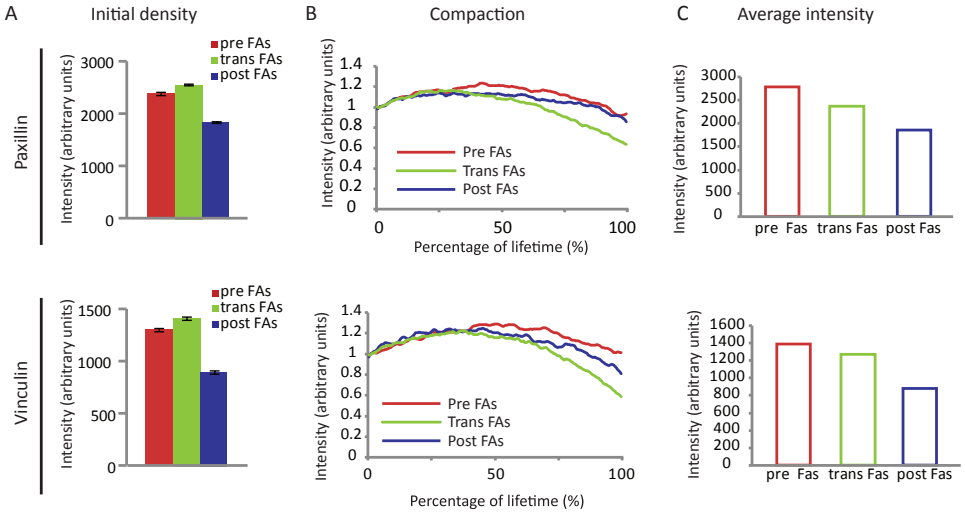

D FA amount

	No of FAs
Pre FAs	46
Post Fas	115
Trans FAs	126

Figure 3: FA compaction is disturbed upon inhibition of Rho-mediated tension

A) Initial intensity (average over the first 5 data points) of the pre, trans and post FAs that live between 4 and 30 minutes of the 15 cells imaged with the same frame rate (top= paxillin, bottom = vinculin). Error bars = standard deviation. B) Compaction profiles of paxillin (top) and vinculin (bottom) for the pre FAs (red), the post FAs (blue) and the trans FAs (green), normalized to the average of the first 5 data points of the compaction curve. C) Intensity of the compaction profiles, averaged over the all data-points, per category. D) The number of FAs that each category contains.

these combined films, FAs were divided in 3 groups dependent on the time of existence: FAs that only existed before adding the inhibitors (pre FAs), FAs that only lived after adding the inhibitors (post FAs) and the group of FAs that appeared before addition and disappeared after addition (trans FAs). Next, within these 3 groups, FAs were sorted for lifetime as previously described (chapter 3) and the FAs that live between 4 and 30 minutes (intermediate lived) were used for the analysis, because shorter-lived FAs do not display strong compaction and because the full lifetime of longer-lived FAs could not be captured in these time-lapses due to limited time of imaging (maximally 15 minutes before and maximally 40 minutes after wash-in of inhibitors). The FAs were synchronized to their frame of first appearance. The lifetimes of the FAs were normalized between 0 (frame of appearance) and 100% (last frame of detection). Thus, the longest-lived FAs (30 min) defined the number of data points (intensity versus relative lifetime) in these graphs. Intensity values were interpolated (using the linear interpolation function of Matlab) for the gaps that occur in shorter lived FAs in order to be able to calculate the average FA intensity for each data point along the graph. Finally, the averaged compaction curves were normalized to their initial intensity.

The average initial intensity of both paxillin and vinculin in nascent FAs was lower after addition of ML7 and Y27632 (Figure 3A, compare red and green bars to blue bars). Normalization of the compaction curves nevertheless showed that the initial steepness of compaction is similar between FAs in unperturbed conditions (pre and trans) and in

myosinII-inhibited conditions (post) (Figure 3B). Also the steepness of final de-compaction is comparable between FAs that disappeared in unperturbed versus myosinII-inhibited conditions, indicating that myosin-based tension is not required for the rate of compaction. However, FAs do compact to a higher maximal density in unperturbed conditions (Figure 3B). For the FAs that were formed under normal myosinII activity, but then experienced release of tension (NB. at a random timepoint during their lifecycle) (Figure 3B, trans FAs) de-compaction on average started earlier and followed a steeper profile in comparison to the FAs in unperturbed conditions (Figure 3B, green and red lines). All of this is reflected in the average intensities over the entire FA lifetime (Figure 3C) that are highest in unperturbed, lowest in inhibited and intermediate in "trans" conditions.
Taken together these analyses show that initial stages of FA compaction are not dependent on myosinII-activity, whereas a second phase is dependent on myosinII activity. The increase in de-compaction of the "trans" FAs indicates that release of tension functions as a direct signal for the disassembly of the FAs. This underscores the notion that FA maturation and turnover is the combined result of biochemical and mechanical regulation.

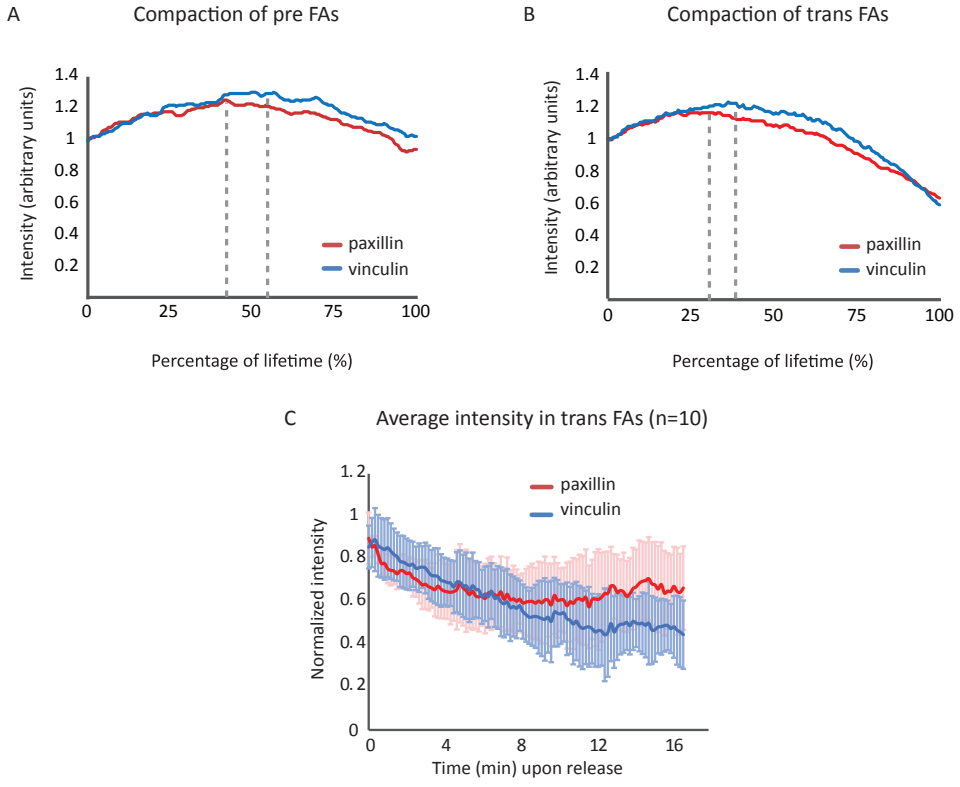

Figure 4: The abundance of paxillin and vinculin in FAs is differentially regulated
A) Compaction profiles of the pre FAs of paxillin (red) and vinculin (blue), normalized to average intensity of the first 5 data-points of the curve. The start of de-compaction is indicated by a grey, dotted line, B) Similar to (A) but for the trans FAs. C) Over time, the average paxillin and vinculin intensity over the 10 cells imaged with the same frame rate normalized to the average of the first 5 time points per cell (error bars=standard deviation).

The abundance of paxillin and vinculin in FAs is differentially regulated

Interestingly, although overall behavior and responses of paxillin and vinculin concentration were similar, close inspection revealed that in unperturbed conditions, paxillin de-compaction started on average after ~45% of the lifetime, whereas vinculin intensity continued to increase and decompaction was initiated slightly later at ~55% of the lifetime (Figure 4A). This indicates a difference between the density regulation of paxillin and vinculin. Also upon tension release, in the "trans" FAs, vinculin decrease sets in later than paxillin decrease (Figure 4B). This indicates a difference in response to tension release. To further analyze this differential response to tension release, the paxillin and vinculin intensities of all FA's that lived after inhibitor addition were averaged per cell and normalized to average FA intensity in the first 5 frames of imaging. Values from 10 cells imaged at equal frame rate were then synchronized to the time of drug wash-in and averaged per frame. As shown in Figure 4C the average paxillin response to release of tension was faster than the vinculin response. However, vinculin decrease continued longer resulting on average in a lower relative concentration of vinculin in the FAs that were still detected after more than 10 minutes of myosinII inhibition (Figure 4C).

Paxillin responds faster than vinculin to a release of tension from FAs

Because many reports exist that link vinculin recruitment and function with tension on the FA [21, 41, 79], the general impression has emerged that vinculin is a specific rapid responder to fluctuations in tension at FAs. Following this, we initially hypothesized that vinculin would show a more rapid dissolution from FAs compared to paxillin whose presence is not thought to be exquisitely mechanosensitive. The intensity decay curves in Figure 4C, however indicate that directly after drug addition, in the first instances of tension-release, paxillin intensity on average decreases more rapidly and more strongly than vinculin intensity. One explanation for this surprising result, could be that the responses of vinculin and paxillin differ between sub-populations of cells or FAs and that the average behavior measured in our systematic analyses shielded a subset of FAs in which vinculin and paxillin did display the expected behaviors (i.e. stronger response of vinculin to release of tension). To investigate whether differential behaviors existed among cells, we analyzed in which of the 18 recorded cells the average FA-intensities changed from 1 minute before drug-addition to 1 minute after. As a control for drug-specific effects, we performed the same analysis for 2 minutes around a randomly chosen time point in untreated conditions. Whether a significant change in intensity occurred in these short transitions, was determined per cell with a Mann-Whitney-Wilcoxon test. During the 2 minutes in untreated conditions, there was a variety of changes, while in many cells no change occurred (Figure 5A left). From the minute before to the minute after addition of ML7 and Y27632, the type of change was much more consistent: in 13 cells both proteins decreased in FA-intensity (Figure 5A right). This shows that significant (although small) changes in FA-intensity occur at random, through cell-intrinsic fluctuations and confirms that tension release affects FA-intensity quickly, driving the decrease of both vinculin and paxillin in a short period of time. Only one cell showed a decrease of vinculin but not paxillin and we considered this cell to be an exception and not studied it further. Thus this analysis did not reveal clear cell-specific responses to tension release.

We then determined the distribution of the relation between vinculin and paxillin per FA over time to investigate whether differential behaviors may occur between different subsets of FAs in the cells in which both vinculin and paxillin decreased. To obtain a distribution centered on 0 (abundance of paxillin and vinculin unchanged), the intensity of each FA at

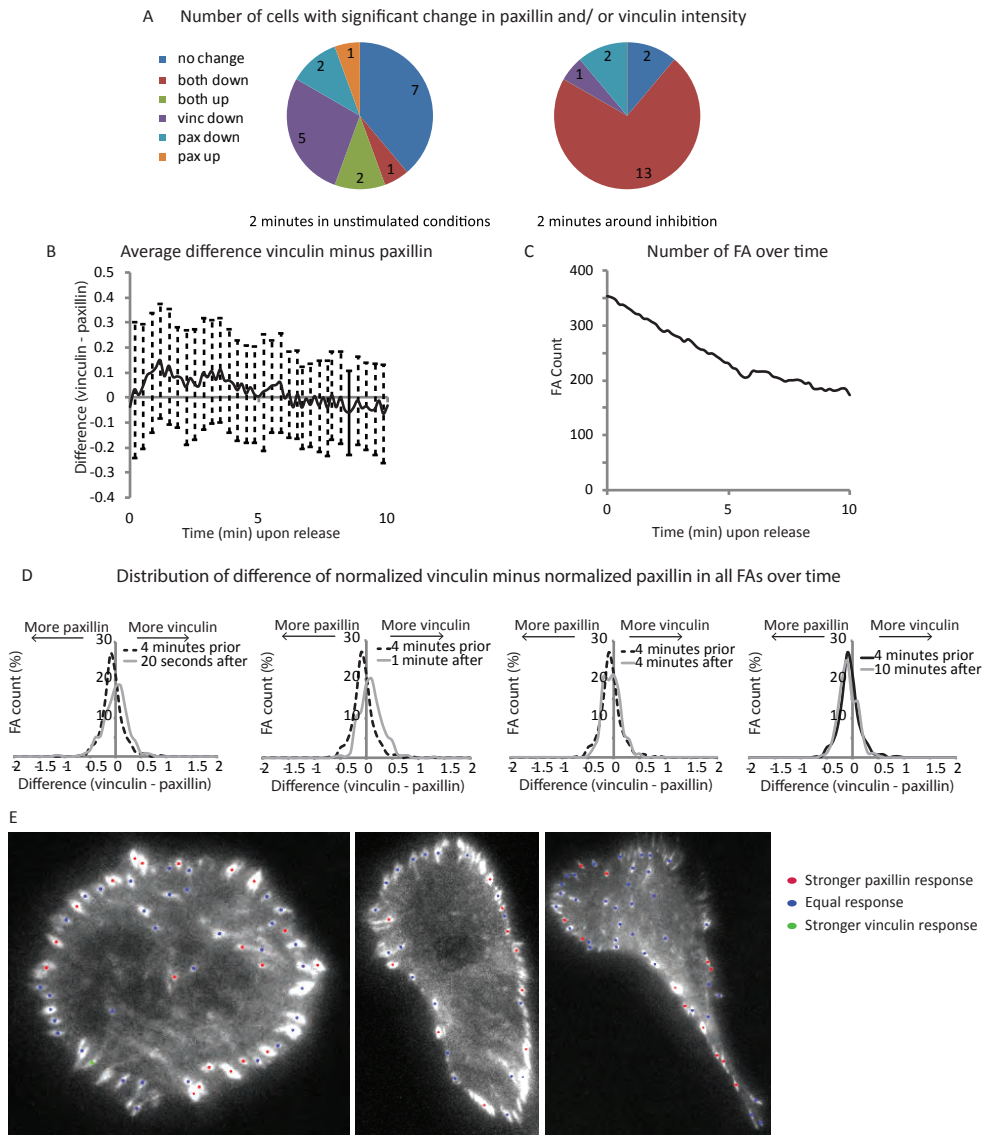

Figure 5: Inhibition of tension vastly affects both paxillin and vinculin FA abundance, with paxillin responding first in general

A) Number of cells in which the abundance of paxillin or vinculin or both changed either between 1 minute before and 1 minute around a time point in untreated conditions (left) or between 1 minute before and 1 minute after addition of the inhibitors (right). B) Average of the difference of normalized vinculin intensity minus normalized paxillin intensity over time of the 10 cells in which both vinculin and paxillin intensity decreased (A) and that were imaged with equal frame rate. C) FA count over time in the 10 cells of (B). D) Distributions of normalized vinculin intensity minus normalized paxillin intensity compared to 4 minutes prior to tension release (dotted line). E) Color marker on the FAs for the change in difference of vinculin minus paxillin from 1 minute before till one minute after tension release, plotted on the image at the moment of wash-in of the tension inhibitors: red for a stronger paxillin response, blue for an equal response and green for a stronger vinculin response.

each time point was normalized to the average intensity of that FA over its entire lifetime. Next, the normalized intensity of paxillin was subtracted from the normalized intensity of vinculin. This resulted in a positive number if relatively more vinculin is present and in a negative number if relatively more paxillin is present. Next, all tracks were synchronized to the frame of inhibitor wash-in. Averaging these differences over time confirmed that paxillin and vinculin were present relatively equal before tension release (difference ca. 0), while just after tension release, paxillin intensity decreased faster than vinculin intensity (difference > 0) (Figure 5B). As predicted by Figure 4C, after 6 minutes the effect was gone and vinculin and paxillin were again equally present in the remaining FAs. The total number of FAs decreased until 6 minutes and then also stabilized (Figure 5C). The distribution of the difference in normalized intensities in all FAs is shown for a few key time points in Figure 5D. In the first minute after tension release the whole distribution curve shifted positively, indicating that the number of FAs with more vinculin than paxillin increases in favor of the FAs with more paxillin than vinculin. From this analysis there is no emergence of a specific sub population of FAs in which vinculin responds faster than paxillin to release of tension.
Finally, we calculated per FA the change in difference of vinculin minus paxillin between 1 minute prior to addition of tension inhibitors and 1 minute after. On the image prior to inhibitor-addition, the FAs were color-marked accordingly (red: more vinculin, many FAs; green: more paxillin, very few FAs; blue: no significant change, many FAs). Also this analysis did not reveal any specific subsets of FAs in which changes could be related to cellular geometry. Whether the cell was round or appeared more polarized, red- and blue-marked FAs were mixed throughout the cell and very few green marks appeared (Figure 5E).
In conclusion, our analyses showed that cytoskeletal tension differentially affects the abundance of paxillin and vinculin at FAs. Immediately upon tension release in a large fraction of FAs the decay of paxillin is more rapid than that of vinculin. This is in contrast to our expectations and implies that vinculin-release is not a prominent immediate response to loss of tension at FAs.

Discussion

FAs are dynamic, mechanosensitive entities that anchor cells to the cytoskeleton. They grow in response to tension [218, 219] and disappear when tension is inhibited [5, 76, 79]. One of the most acclaimed molecular results of mechanical force (tension) being applied to FAs is the recruitment and presence of vinculin [21, 41, 79]. Several molecular mechanisms were put forward explaining the tension-sensitive behavior [21, 79]. Subsequent to its recruitment, the function of vinculin itself, strengthening of FAs, depends on its own mechanosensing- and actin-binding properties [24, 41, 42]. Thus, vinculin's relation to FAs is affected by tension at several levels. Therefore, we hypothesized that tension release would primarily affect the abundance of vinculin in the FA compared to another core protein of the FA that has a different role: paxillin. Paxillin is an adaptor protein present in all types of FAs that binds to vinculin, was proposed to regulate vinculins tension-sensitive recruitment and is important for FA signaling and turnover. Paxillin has no direct link to actin and there are no indications in literature that paxillin's abundance at FAs is distinctly mechanosensitive [50, 54]. Surprisingly, however, our results have shown that the decrease of paxillin from FAs in response to a release of tension, induced by myosinII inhibition, is faster than the decrease of vinculin. This argues against the hypothesis that vinculin's presence at FAs is specifically dependent on tension.

First of all, to increase accuracy of FA-detection we have added a 'dual color' tool to our previously described FA detection and tracking method. The dual detection method strongly increased the reliability of the data on the FAs that live up to 10 minutes, by stringently eliminating detected areas possibly not representing FAs. The fact that our measured effects on cell spreading, reduction of FA number and FA size recapitulated previous reports showed both the functionality of our method and the wider relevance of our dataset.

During the course of their life, FA intensity shows a convex profile. FAs grow denser initially and start to disassemble far before their disappearance. We have described this compaction behavior previously (chapter 4) and hypothesized that tension on the FAs plays a role in the process. Here we found that the FA-density of both paxillin and vinculin decreased upon addition of the inhibitors (Figure 3C). Release of tension initiated a steep, early de-compaction of pre-existing FAs. Newly formed FAs in myosinII inhibited conditions still compacted and de-compacted, but they compacted to lesser degree than FAs in control conditions (Figure 3B). This suggests that the final level of density of FAs is tension dependent and that release of tension is a signal for de-compaction. However, new FAs can form in the absence of tension. Such a tension independent density increase of FAs has been shown for a population of short-lived adhesions that form in the lamellipodium of a migrating cell [9], but in general FA-maturation is clearly associated with actomyosin based tension. Our current results indicate that tension-independent and tension-dependent regulatory mechanisms cooperate to generate the characteristic lifetime-dependent compaction profile of FAs.

Regarding our hypothesis that vinculin would respond to loss of tension prior to paxillin, it was surprising that the presence of vinculin was not affected prior to paxillin abundance. Instead, immediately upon tension release the average loss of paxillin from FAs was more rapid than that of vinculin. This was a general effect, independent of lifetime or cellular location, as we could not detect a subpopulation of FAs in which the reverse, expected behavior occurred (more rapid decrease of vinculin). After this immediate imbalanced response, within 6 minutes, the relation between paxillin and vinculin stabilized again, while at later stages the intensity of vinculin continued to decrease so that after ~12 min of inhibition, the ratio of vinculin over paxillin was lower than before inhibition (figure 4C). One explanation for the apparent discrepancy between our data that show no strong difference between the response of vinculin and paxillin to loss of tension, and previous studies that showed a strong loss of vinculin, may be that most studies have measured at a fixed timepoint after inhibition and that this may have captured the late stage rather than the early stage difference we describe here between vinculin and paxillin [41, 79]. To our knowledge, the immediate, relative responses of vinculin and paxillin to release of tension from FAs have never been systematically investigated and our current analyses show that the notion that vinculin-decrease is a distinct response is false.

The observation that paxillin presence decreased prior to vinculin presence in tension-released FAs could be related to the observation from Fluorescence recovery after photobleaching (FRAP) experiments that paxillin turnover (t1/2 =11s) is faster than vinculin turnover (t1/2=20s) [25]. Also, Carisey et. al. (2013) showed that paxillin localization to FAs is unperturbed in cells expressing vinculin mutants that cannot bind to actin, which perturbed the turnover of vinculin, indicating that paxillin recruitment is independent of vinculin dynamics. Differences in paxillin and vinculin responses to tension release between individual FAs could be caused by differences in the amount of tension at these FAs prior to inhibitor wash-in. Measurements using a tension-deformable FRET module (TS-Mod) inserted in vinculin showed that vinculin experiences less force in disassembling or trailing

FAs [113]. In addition, laser cutting experiments showed that FAs experience more tension when located at actin stress fibers at the periphery than when located at central stress fibers [220]. Whereas these studies were able to pinpoint specific, spatially defined sub populations of differential tension, we could not find a clear difference in the cellular localization of the FAs that showed different responses in vinculin over paxillin abundance.

In conclusion, we have developed a robust addition to our FA-detection and tracking software that can be used to investigate the relation between the concentrations of pairs of FA proteins over time. We have used it in cells dually-labeled for vinculin and paxillin to investigate their relative responses to release of tension by inhibition of Rho-mediated myosinII activity. We have found that myosinII activity contributes to FA maturation by setting the degree of FA compaction and that inhibition of contractility, resulting in release of tension is a signal that initiates FA turnover. Surprisingly, paxillin initially decreased more rapidly than vinculin upon release of tension from FAs, which questions the designation of Vinculin as a distinct tension sensitive member of FAs.

Materials and Methods

Cell lines and culture

The prostate cancer cell line DU145, stably expressing Epac and mCherry-Paxillin (that has been described in Chapter 3), was co-transduced with a lentiviral delivery system. Lentivirusal particles were produced by transfection of HEK293 cells with third-generation packaging construct [188]. DU145-G4 cells were plated in full medium in a 6-well plate overnight and then transduced with GFP-Vinculin virus supernatant in the presence of 40µg/ml polybrene for 24 hours before returning the cells to full medium. GFP-Vinculin expressing cells were selected by fluorescence-activated cell sorting (FACS) based on the levels of both mCherry and GFP.

Cells are cultured in RPMI (Gibco) supplemented with antibiotics and 10% fetal calf serum (FCS) (Sigma).

48 hours prior to imaging DU145-G4 cells were plated in full medium (Gibco) in collagen-type 1 (10µg/ml; PureCol)-coated, Lab-Tek® #1.0 Borosilicate Chambered System, 8 units. 24 hours prior to imaging, the medium was replaced by 0.5% FCS containing RPMI. A combination of 3µM ML7 and 10µM Y27632 was added after 10 to 15 minutes of imaging.

Microscopy

For imaging we used a NIKON Ti microscope equipped with a total internal reflection fluorescence (TIRF) system, a CFI Apochromat TIRF objective, 60x oil with an NA of 1.49, a 12-bit electron multiplying CCD (EMCCD) Luka camera (Andor) and controlled by company software (NIS-elements).

We have created a dataset of 18 sets of image series of dually labeled DU145-G4 in which tension was inhibited after 10-15 minutes of imaging. 15 out of 18 cells were imaged with a framerate of 10 seconds, 3 were imaged with a framerate of 13 seconds.

FA detection and statistics

For FA detection and tracking we used the hDome based, custom devised method described previously (Chapter 3). The method was extended for detection of dually labeled FA (described in results). Standard MatLab functions were used to extract object size and average pixel intensity, the latter was corrected by subtraction of the local background, for which the regions of the earlier determined local watershed were used. Compaction profiles were calculated as described previously (Chapter 3 The FA lifetime was measured as the number of frames the FA was detected. For overall description, features were either averaged first per FA and then per cell (Figure 2) or per cell per time point over all FA and subsequently normalized to the average of the first 5 timepoints (Figure 4B). The change in intensity was tested per cell using the Mann-Whitney-Wilcoxon test of MatLab between the intensities of one minute before to 1 minute after addition of the inhibitors, or 2 subsequent minutes in unstimulated conditions (Figure 4A). The difference of the paxillin vinculin intensity was calculated for each FA as the difference at each time point of the normalized vinculin signal minus the normalized paxillin signal. For normalization each track was normalized to its average intensity. The histogram was determined using the histogram command of MatLab.

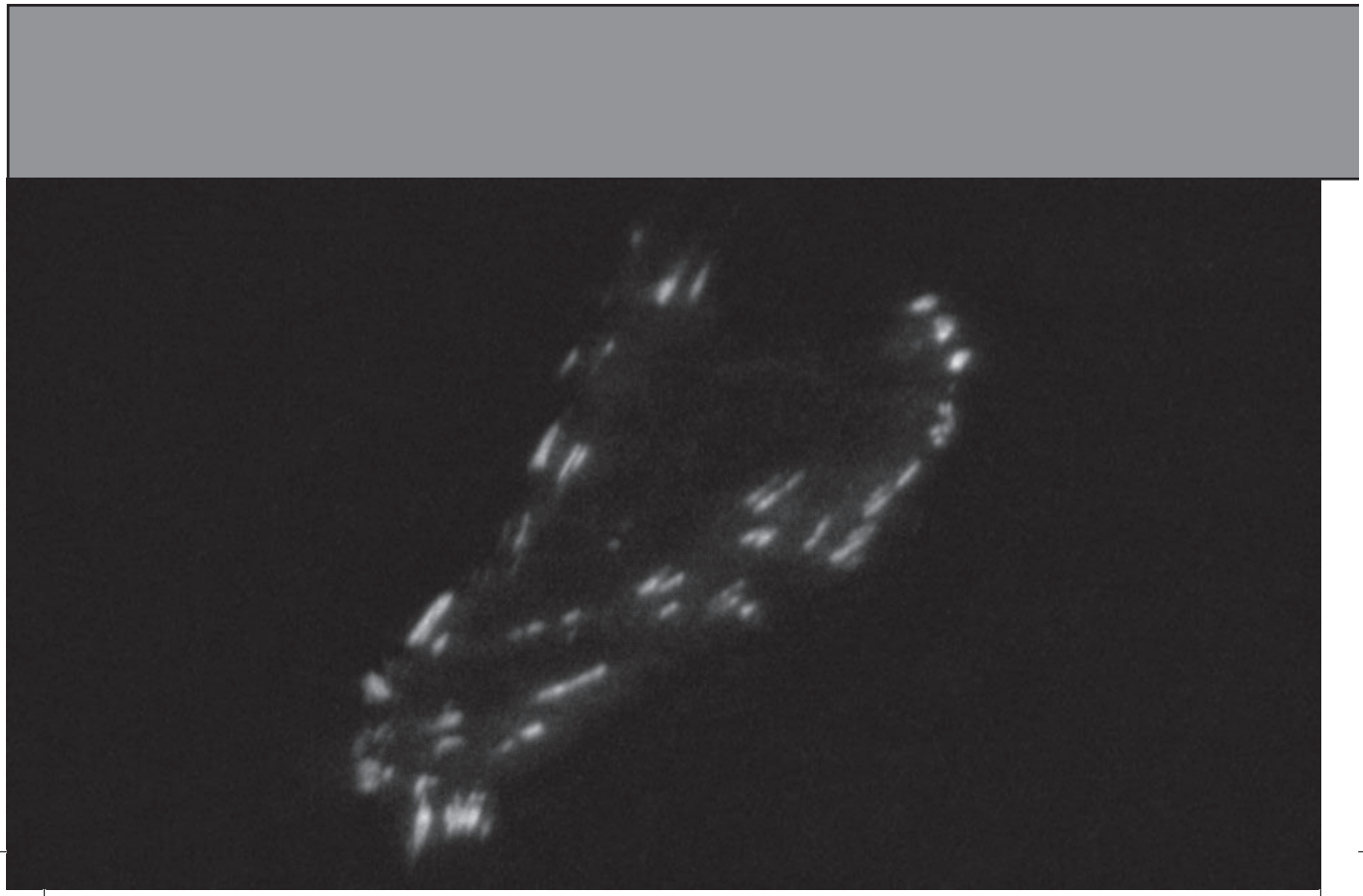

General Discussion 6

General Discussion

Cell adhesion and cell migration are of great importance to development, the immune system and several processes that occur throughout the life of an organism. Deregulation of adhesion and cell migration processes underlie many pathological developments, including tumor metastasis. Live-cell imaging allows highly detailed observations of the processes of adhesion and migration. Manual analysis of this kind of images is time consuming and can be prone to bias. A more systematic approach for the quantitative analysis requires automated methods to detect the structures of interest in the images. This thesis contains the description of a custom developed cell adhesion image analysis toolbox, Adquant, and the analyses for which it was used.

Adquant consists of a set of 5 image analysis tools. In chapter 2 a cell adhesion and spreading toolset is used to characterize Rap1 dependent spreading. This study further showed that Rap1 activation can bypass Src-FAK signaling to induce cell spreading and formation of FAs that contain vinculin, which is regarded as a marker for mature FAs. In chapter 3 an FA detection and tracking method is described for the investigation of FA dynamics. This analysis revealed that FAs overall show a biphasic densification pattern, which we called compaction, and is described in chapter 4. We further investigated the effects of HGF stimulation and Rap1 activation on FA dynamics. Although both influenced cell migration, effects found on FA dynamics could be rather related to cell spreading than to cell migration, uncoupling them from the regulation of cell migration. In chapter 5, we extended our FA detection and tracking method for the analysis of FAs that are labeled for 2 proteins. Using this stringent selection, we analyzed the relation between the abundance of the mechanosensitive FA protein vinculin and the central FA adaptor protein paxillin at the FAs while inhibiting RhoA induced contractility. To our surprise, overall paxillin decreased rapidly upon tension release and preceded vinculin's disappearance from the FAs. Although vinculin's decrease continued longer, these results question vinculin as a distinct mechanosensitive protein in FA disassembly. Finally, the last 3 image analysis tools of Adquant will be explained in the addenda that follow, consisting of a method to track cell migration, a method to analyze cell-cell adhesion protein localization and a tool to analyze the activity of the Hippo-pathway by comparing YAP localization in the nucleus versus the cytosol. Thus, we have developed image analysis methods for the investigation of adhesion processes ranging from cell adhesion and spreading (and some thereby influenced signaling pathways) to cell migration. This software tool will be made publically available.

The main advantage of developing image analysis tools is that bias in the analysis is avoided. In addition, it allows for systematic investigation of topics that when manually analyzed, would cost much more time. For our study of the effects of HGF and Rap1 on FA dynamics the automated analysis has shown that there are minor direct effects on FA dynamics, in contradiction to our initial hypothesis. Although this was studied only in 1 cell line, the analysis involved a large number of FA. With our software now available, analysis of questions related to FA dynamics can be readily addressed. In combination with advanced microscopic techniques and the availability of biosensors that can, for example, induce or report local effects [113, 221], unbiased analysis remains pivotal to address fundamental questions on cell adhesion and migration.

Rap1 and HGF effects on cell migration

The continuous assembly and disassembly of FAs is essential for cell migration and aberrant signaling and expression of several FA proteins are correlated to tumor development, suggesting that FA dynamics could form a good predictive model for the early steps of metastasis. HGF, via its receptor cMet, is one of the inducers of invasive tumor growth and is found upregulated in many cancers. Downstream signaling pathways of HGF regulate proliferation, survival and migration [222]. In 2D cell culture HGF induces cell scattering, associated with an increase in Rho mediated contractility [203]. The positive effect of HGF on cell scattering can be blocked by Rap1 activation [86]. In chapter 3 we set out to analyze the effects of HGF and Rap1 activation on FA dynamics. However, in our cell line of choice, HGF did not show clear effects on the FA dynamics within the first 3 hours of treatment, although it did induce cell migration. Subsequent Rap1 activation affected some aspects of FA dynamics, but a direct correlation with the inhibition of cell migration was not obvious. Rather, these effects appeared correlated to the inhibition of RhoA activation, as was recently shown to be a downstream effect of Rap1 via its GAP ArhGap29 [91]. This was confirmed by Bayesian Network Inference that related the changes we observed to cell spreading rather than cell migration. These results question the general notion that regulation of FA dynamics and regulation of cell migration are interdependent, coordinated processes. Therefore they also question the value of FA dynamics as a proxy for the early steps of metastasis.

FA Compaction

The lifecycle of an FA starts at the moment of assembly. They can turnover shortly upon appearance, or mature and disassemble after a longer time period. During maturation, FAs grow and elongate. In chapter 4 and 5 we describe another, novel feature of the FA lifecycle; a lifetime dependent, densification of FAs over time, which we called compaction. A similar biphasic profile has been described for short-lived adhesions in the lamellipodium [9] and earlier studies have shown assembly and disassembly kinetics based on intensity increase of different FA proteins in manually detected FAs [50, 206, 207]. But here we show that this is a process that occurs overall in all different populations of FAs. It may not be such a surprise that we found compaction of the FA upon initial assembly; as it is well established that during maturation of FAs, FA proteins are modified and recruit other proteins, thus increasing again FA signaling and protein recruitment. However, we found a lifetime dependent level of compaction, where longer lived FAs compact faster and to a higher degree than short lived FAs and, intriguingly, de-compaction starts long before the FAs disappear (chapter 4). What mechanisms regulate compaction and which signal induces the start of de-compaction, remains an interesting question.

One of the mechanisms that appears to be involved in the regulation of compaction, is cytoskeletal contractility, which results in tension on the associated FAs. In chapter 5 we show that release of tension acutely initiates the de-compaction process. This indicates that loss of tension can be a signal that triggers FA de-compaction. Furthermore, FAs that form after inhibition of contractility compact to a lower degree than FAs that form normally. Additionally, Rap1 activation also reduces the level of compaction of FAs (chapter 4) and this could be due to Rap1's inhibiting effect on RhoA. This indicates that tension determines the level of compaction that FAs may reach. However, as shown in chapter 5, loss of tension does not seem to change the dynamics of compaction. This implies that tension does not influence the compaction and de-compaction rates and FAs still assemble. Concomitantly, FA maturation has been shown to occur in FAs on which tension is very low. Instead, actin

remodeling, cross-linking and actin retrograde flow can be enough to induce FA maturation [196]. It would be interesting to test whether inhibition of these processes would affect the rate of the compaction dynamics.
On average we find that compaction is lifetime dependent, with compaction and de-compaction rates being faster for longer lived adhesions. This implies that for any FA, calculation of the initial compaction rate could be predictable for its lifetime. However, the compaction rates of individual FAs are highly variable which renders such predictive analyses as yet impossible. Further analysis would be required to dissect the different types of compaction underlying the overall curve. In conclusion, compaction is an interesting observation of overall FA behavior that could be investigated further for the individual FAs.

Rap1: Rho-activity associated and Rho-activity-independent effects?

Cell spreading and cell migration are driven by differentially regulated dynamics of the actin cytoskeleton. The small GTPases are important regulators of these processes. Rap1 activation affects cell migration negatively and induces cell spreading. Indeed, Rap1 has been shown to have a role in the modulation of the actin cytoskeleton [86, 122, 124] and it was recently shown that Rap1 can activate the RhoGAP ArhGAP29 [91], thereby reducing contractility. Most of the effects induced by Rap1 activation we observed in chapter 2 and 3 can be explained by reduced RhoA activity. Cell spreading, decrease of FA size, reduction of FA intensity and a decrease in FA sliding can be related to inhibition of RhoA activity. Indeed, in chapter 5 we observed all these effects upon addition of inhibitors of the RhoA signaling pathway, although here we did not look at sliding due to relatively short imaging periods.

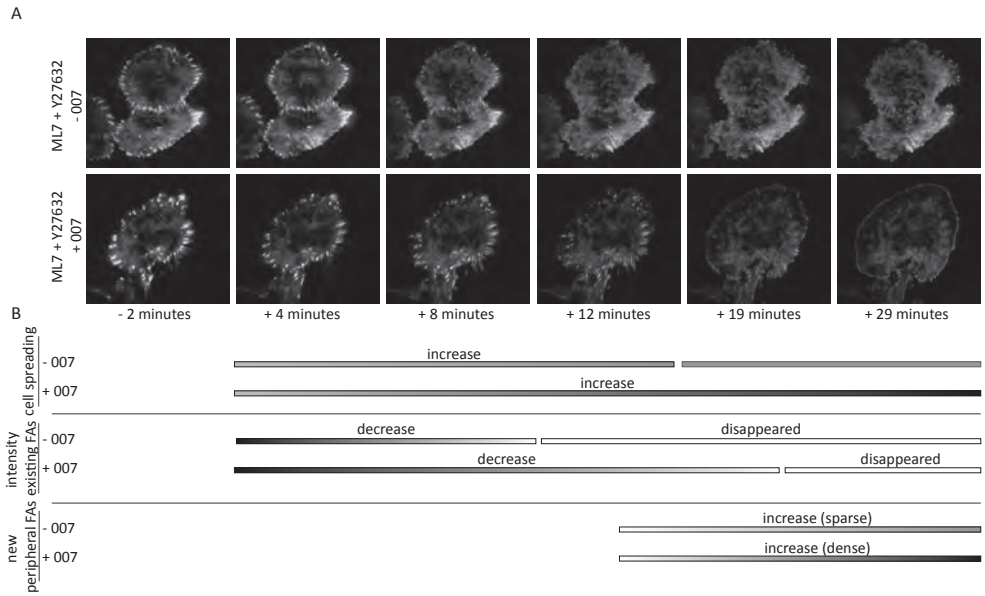

Figure 1: Assay for RhoA-activity-independent effects of Rap1

A) Representative images of DU145 cells, stably expressing Epac and mCherry-Paxillin, to which either a combination of ML7 and Y27632 is added (top row) or ML7 and Y27632 combined with 007, activating Rap1, (bottom row) with the time in relation to wash-in of the compounds underneath. B) Schematic overview of analysis, by eye, of the timing of the effects of RhoA inhibitors with and without 007 on cell spreading, intensity of existing FA and the appearance of peripheral structures labeled by paxillin.

However, there are a few effects that are less easily related to a reduction of RhoA activity. Whereas a decrease of lifetime is associated with loss of contractility, Rap1 activation induces a population of longer lived FAs ([86] and chapter 3). Additionally, the rates of the compaction dynamics are decreased upon Rap1 activation in HGF stimulated cells, whereas loss of tension has no effect on these rates (chapter 4&5). Lastly, Rap1 activation causes formation of new FAs (chapter 3). These RhoA-inhibition-independent effects of Rap1 activation are best illustrated by time lapse recordings of cells that were simultaneously treated with contractility inhibitors and the Rap1 activator 007 (Figure 1A). Here we observed that Rap1 first delays the disassembly of pre-existing FAs. Then it induces even larger cell spreading than RhoA inhibition alone. Furthermore it induces the formation of a rim of very small FAs at the periphery (Figure 1B). FA formation and FA stabilization have been shown to be also regulated by actin polymerization and actin crosslinking in a tension-independent manner [9, 10]. Together, this suggests that Rap1 activation affects these types of actin modulation as well. A few activators of such pathways have been reported to be downstream of Rap1, including Vav2 and Tiam. Vav2 is a Rac-GEF that can bind Rap1 and Rap1-dependent membrane localization of Vav2 has been shown to induce cell spreading [138]. In endothelial cells, Rap1 is reported to induce formation of circumferential actin bundles at the periphery of the cell via Cdc42 [92]. However, whether Rap1 activation also induces these pathways in the DU145 cells used in our studies and whether that induces FA formation and stability, remains to be elucidated. Imaging and analysis of FA disassembly and re-formation in these cells where RhoA-inhibition and Rap1 activation are simultaneously induced, provides a good assay system to further investigate these effects and effectors of Rap1.

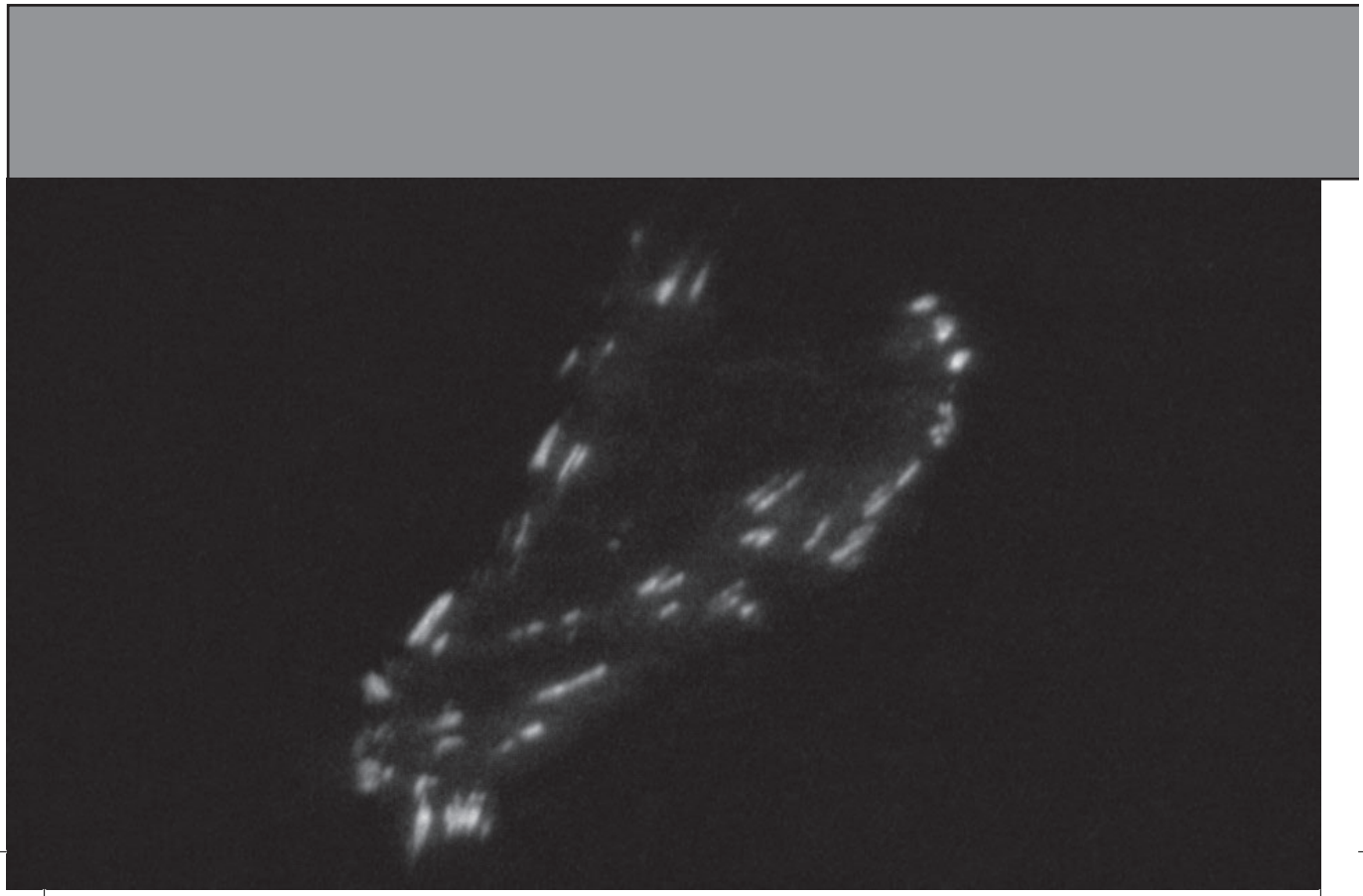

Addendum 1 &

Emma Spanjaard and Johan de Rooij

Analysis of cell migration by tracking of fluorescently labelled nuclei

Here we describe a method that we developed in MatLab for the tracking of fluorescently labelled nuclei. This method is based on a previously custom-developed software tool, ScatterTrack, with which phase-contrast microscopy images of cell migration can be analyzed [189]. In short, two steps lead from image acquisition to analysis: a segmentation step for the localization of the cells and a linking algorithm for the tracking over time. The main difference between the method described here and ScatterTrack is the initial segmentation of the images for the localization of the cells since a different methodology is required for the segmentation of fluorescent- or phase-contrast images. The workflow is outlined in Figure 1A.

For the segmentation of fluorescent nuclei we choose to use marker based watershed segmentation [101]. Three types of images are needed for marker watershed segmentation: a mask image that defines the contours of the objects, a foreground image that marks the objects and a background marker image that defines regions to separate the objects (Figure 1B). For the mask image the gradient of the original image is calculated using a sobel operator on the normalized, original image (Figure 1B middle panel left). To obtain an input image for the foreground markers, the original image is processed using a morphological opening with a small filter for low magnification (10x) images and a larger filter for higher magnification (20x) images. Next, to remove dark spots, a morphological closing operation is applied. The regional maxima of this processed input image form the foreground markers (Figure 1B middle panel middle). A distance transform on the foreground marker image defines the borders of regions that each contains one marker of the foreground image (Figure 1B middle panel; right &bottom panel; left). A watershed segmentation on these three images, detects the cells (Figure 1B bottom panel; middle). The center of mass of the objects detected provides the coordinates of the cell that are used for linking each cell over time (Figure 1B bottom panel; right).

To form tracks of each cell the same code is used as in ScatterTrack. Cells are linked to the cell that is in closest proximity in the next frame (Figure 1C&D). Topological conflicts are solved using neural network algorithms [223-225]. In case a cell is not detected for a few frames but is detected again later, which induces a gap in the track, this gap is closed using linear interpolation of the travelled distance over the number of frames the track was lost. The maximum gap-length is user-defined. The user can also define the minimum number of frames a track should exist. Cells that are tracked over less than this minimum number of frames are discarded (Figure 1B blue arrow). Newly formed tracks will be labeled with an increasing number. This means that once track number 1 has stopped, a newly formed track will not be labeled as track number 1, but will receive the label number following the highest number used (Figure 1C yellow arrow). Thus tracks are formed that can subsequently be analyzed for migration speed (Figure 1E) and persistence. This software is being used for several collaborative projects and will be published in due time.

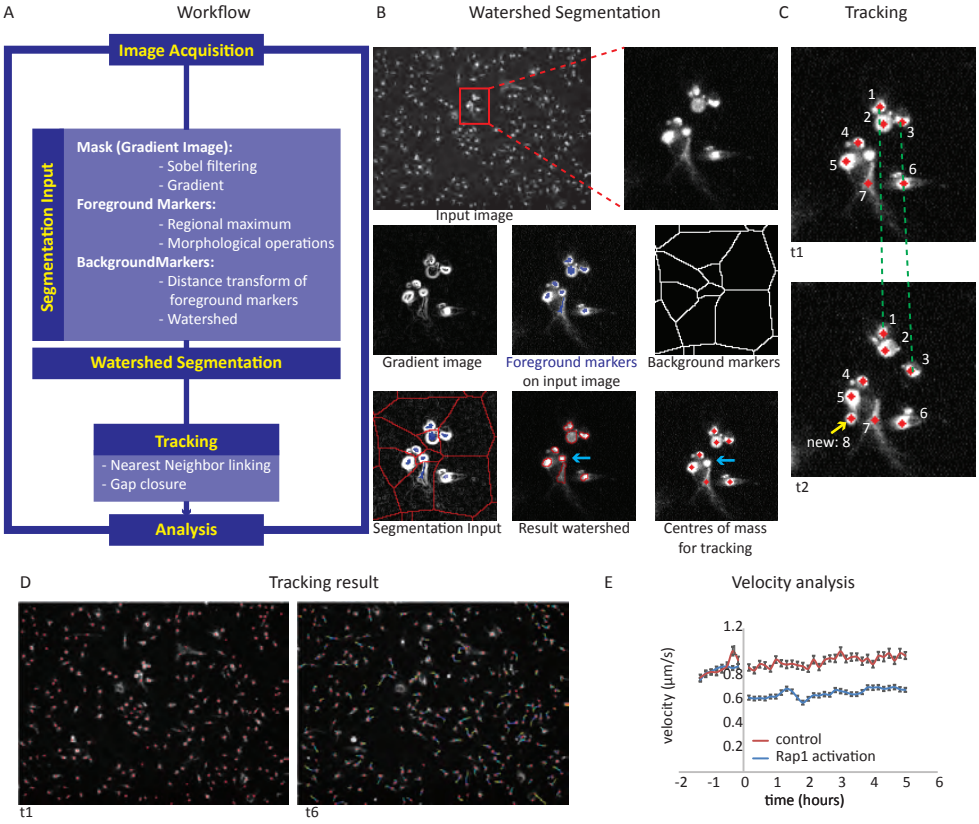

Figure 1: Workflow of segmentation and tracking of fluorescently labelled nuclei

A) Workflow overview. B) Top panel: Image of MDA-MB231 cells labelled with a nuclear dye (SytoDye64 (Molecular Probes)) as input image for tracking analysis (left) and zoom (right). Middle panel: gradient image of the zoom, used as mask for the watershed segmentation (left). Overlay of the foreground markers for the watershed on the original input image (middle). Background markers (right). Bottom panel: total input for the final watershed segmentation: gradient image (grey), the foreground cell markers (blue) and the background region markers (red) (left). The outline of the result of the watershed segmentation in red on top of the original image (middle) and the centers of mass on top of the original image, after tracking (right). Cells that are tracked for less than a user-defined minimum number of frames are excluded (middle & right; blue arrow). C) Linking of the cell nuclei using the nearest neighbor method. The center of mass of the nuclei in image of time-point t1 (top) are linked to the centers of mass of the nuclei in image at time-point t2 (bottom &green lines) based on the cell coordinates most proximal and get the same cell-label. Newly detected nuclei are labeled in an increasing fashion (yellow arrow). D) Visualization of the tracking result: all the tracked nuclei are labeled with a red dot at the center of mass and over time the path followed by each cell is labeled by a per frame growing comet tail. For each frame that the track exists, the tail is prolonged by the travelled distance with a different color. E) Velocity analysis of tracked MDA-MB231 cells in which Rap1 is activated (blue line) or not (red line) (error bars: SEM).

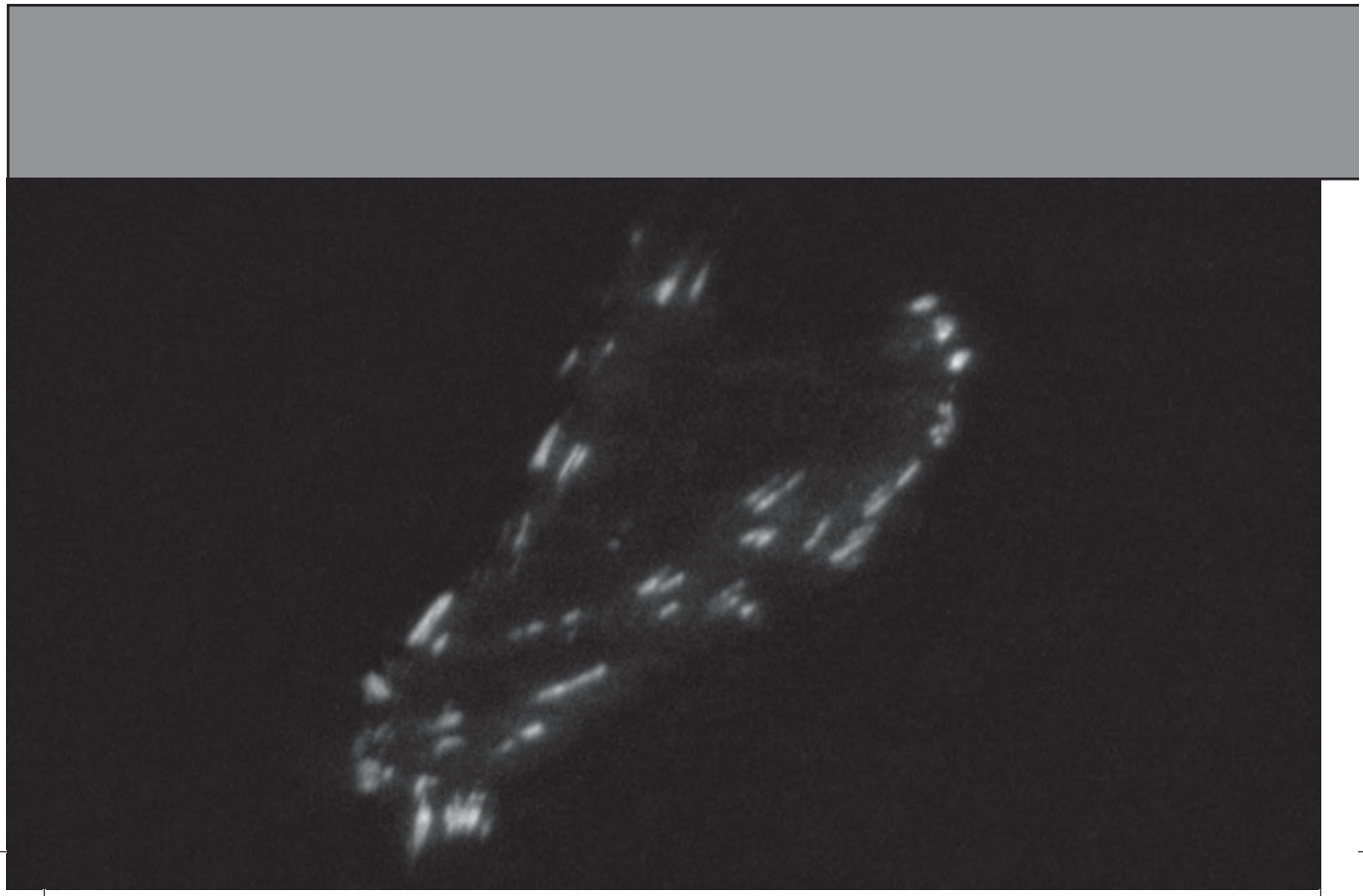

Addendum 2

Emma Spanjaard and Johan de Rooij

Analysis of protein abundance at adherens junctions

One of the protein complexes that connect cells to neighboring cells are adherens junctions, highly important for tissue integrity. They are very dynamic structures that by remodeling can contribute to the passage of molecules into tissue, important for immune responses. Like FAs adherens junctions are regulated by both biochemical and mechanical signals. Two types of junctions can be distinguished: linear junctions, with parallel actin bundles running alongside, and focal adherens junctions (FAJ) that have radial actin bundles running into them. Vinculin has been shown to play a role in the mechanical regulation of adherens junctions and was found to localize to radial-actin contacted junctions [78]. In endothelial cells transformation of adherens junctions into FAJs can be rapidly induced by the endothelial hormone thrombin though the activation of RhoA and subsequent actomyosin contraction [226]. To systematically analyze whether vinculin specifically localized to FAJs, and whether this correlated with Rho-dependent cytoskeletal tension, we developed an image analysis tool to analyze protein abundance at cell-cell contacts on two levels: 1) the ratio between a core cell-cell adhesion protein (VE-cadherin) and a variable cell-cell adhesion protein (vinculin) , averaged over all automatically detected junction fragments and 2) the fraction of vinculin positive junction fragments [226]. Although applied to VE-cadherin and vinculin-labelled images, the method described here can be used for the analysis of any protein combination at cell-cell junctions.

For the detection of cell-cell junctions, we have made use of two separate segmentation methods, based on the hDome method described for the detection of FAs. An overview of the workflow is depicted in Figure 1A. The input consists of two images: an image of the core junction protein that will be the detection channel and an image of the variable protein of interest (Figure 1B). For the analysis of only a small portion of the image, a region of interest (ROI) can be drawn in the detection image, excluding the rest of the image for analysis. Detection of the junction elements will be carried out only on the core protein image, in this case VE-cadherin. Before segmentation, the image is preprocessed by background subtraction and smoothing (Figure 1C). For the first segmentation, a user-defined value x is subtracted from the image and this image is then used as a marker image for grayscale reconstruction [177], as explained in chapter 3 of this thesis, which results in an image in which the intensity peaks are flattened off (compare figure 1C right panel with Figure 1D top right panel). Because the resulting image is basically the lower part of the original image, it is called the downside image (Figure 1D top panel). Next, the edges of the objects in the downside image are detected using a sobel operator, defining edges there where the gradient is maximal (Figure 1D bottom panel left). Final objects of this segmentation are found upon

Figure 1: Workflow of junction detection method

A) Overview workflow. B) Untreated HUVEC cells stained for VE-cadherin and vinculin (top) and close-ups on which the method is shown (Bottom). C) The VE-cadherin imaged after background subtraction and smoothing (left) and a 3D representation of its intensities (right). D) Segmentation 1: the image upon grayscale reconstruction (top left) and the 3D intensity plot (top right). The result of the sobel edge detection (bottom left) and the segmentation result after closing and filling procedures (bottom right). E) k-Means clustering on the upside image (left) and the intensity profile of the upside image (right). K-means clusters shown for the red line in top left (bottom left): pixels clustered in the lowest 2 levels are discarded. The top 3 levels are kept and the image is binarized (bottom right). F) The outline of the final result of junction detection overlayed on the VE-cadherin image (top) and vinculin image (bottom). G) Fraction of vinculin positive junction fragments (right) in untreated HUVECS (top row) and upon 10 minutes of thrombin treatment (bottom row) (Image taken from Huveneers et. al. 2012).

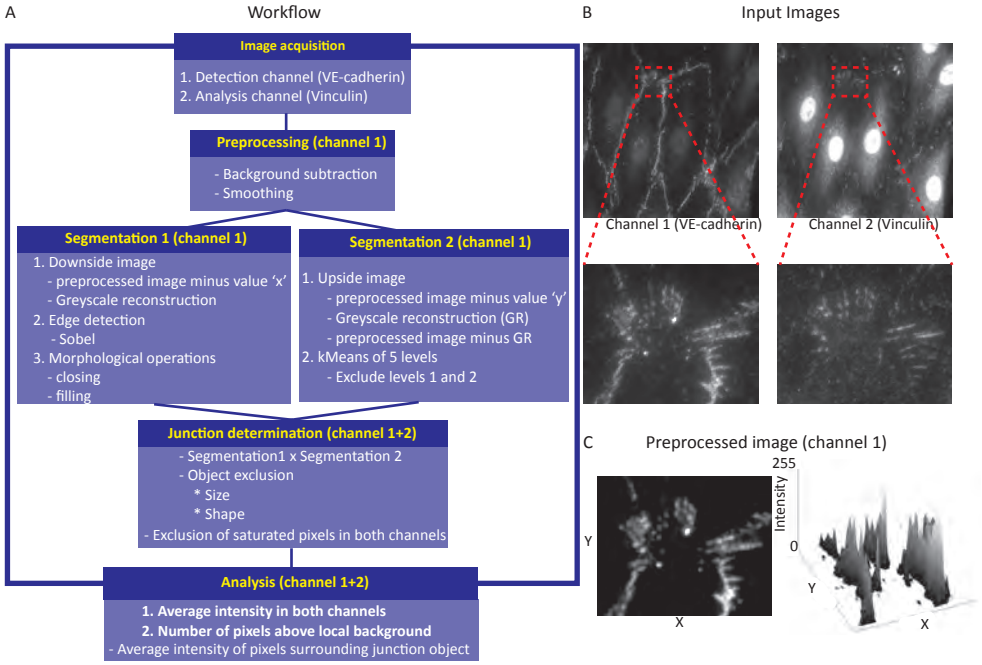
A
Workflow
Image acquisition
1. Detection channel (VE-cadherin)
2. Analysis channel (Vinculin)
Preprocessing (channel 1)
- Background subtraction
- Smoothing
Segmentation 1 (channel 1)
1. Downside image
- preprocessed image minus value 'x'
- Greyscale reconstruction
2. Edge detection
- Sobel
3. Morphological operations
- closing
- filling
Segmentation 2 (channel 1)
1. Upside image
- preprocessed image minus value 'y'
- Greyscale reconstruction (GR)
- preprocessed image minus GR
2. kMeans of 5 levels
- Exclude levels 1 and 2
Junction determination (channel 1+2)
- Segmentation1 x Segmentation 2
- Object exclusion
* Size
* Shape
- Exclusion of saturated pixels in both channels
Analysis (channel 1+2)
1. Average intensity in both channels
2. Number of pixels above local background
- Average intensity of pixels surrounding junction object
B
Input Images
Channel 1 (VE-cadherin)
Channel 2 (Vinculin)
C
Preprocessed image (channel 1)
255
Intensity
0
Y
X

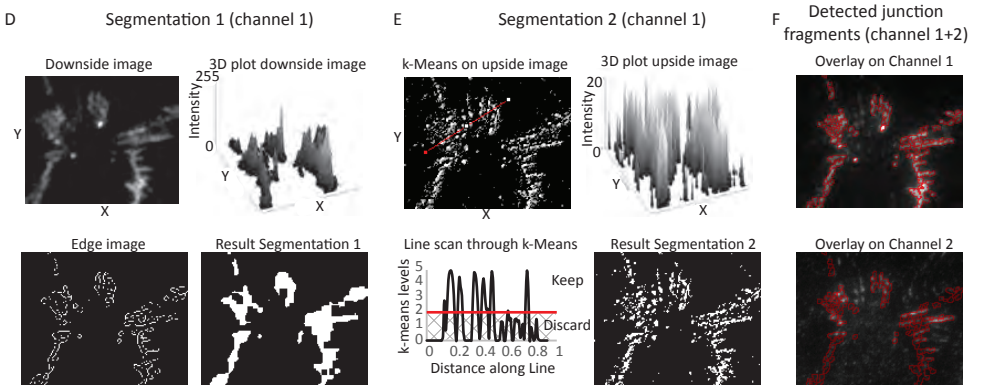
D
Segmentation 1 (channel 1)
Downside image
3D plot downside image
255
Intensity
0
Edge image
Result Segmentation 1
E
Segmentation 2 (channel 1)
k-Means on upside image
3D plot upside image
20
Line scan through k-Means
k-means levels
Keep
Discard
Distance along Line
Result Segmentation 2
F
Detected junction fragments (channel 1+2)
Overlay on Channel 1
Overlay on Channel 2

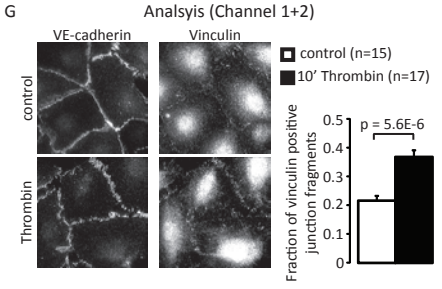
G
Analsyis (Channel 1+2)
VE-cadherin
Vinculin
control
Thrombin
control (n=15)
10' Thrombin (n=17)
Fraction of vinculin positive junction fragments
p = 5.6E-6

a 2 times repeated closing and filling operation (Figure 1D bottom panel right).
For the second segmentation, first a user-defined value y (can be the same as x) is subtracted from the preprocessed image. This image is used as the marker for grayscale reconstruction, similar to segmentation 1, but now the grayscale reconstructed image is subtracted from the preprocessed image, resulting in an image in which the top parts of the intensity peaks are retained (compare figure 1C right panel with Figure 1E top right panel). As this contains the top part of the image, it is called the upside image (Figure 1E top panel right). Next, the upside image is further dissected into 5 levels of intensity, using the K-means clustering algorithm of MatLab (Figure 1E top left). Subsequently, all pixels that are clustered in the lowest 2 clusters are discarded and the resulting image of k-mean levels 3 to 5 is binarized (Figure 1E bottom panel). The final step of this junction detection method is the multiplication of the resulting images of segmentations 1 and 2. Thus objects only detected in both steps are kept for further analysis. Objects, now called junction fragments are excluded if size and/or shape are below a user-defined threshold. In addition, upon measurement of the fragment intensities in channel 1 and 2, saturated pixels are discarded to exclude clipping. The average pixel intensity is determined for each junction fragment in both channels (Figure 1F).
Finally, a junction fragment was called vinculin positive if a user-defined percentage of its pixels had an intensity value that exceeded that of the local background by 50% (for this experiment). This local background is calculated as the average background pixel intensity of a region defined by a dilation of the fragment (fragment pixels excluded). In this way, it was determined that the localization of vinculin to focal adherens junction in endothelial cells increased upon thrombin stimulation (Figure 1G) [226]

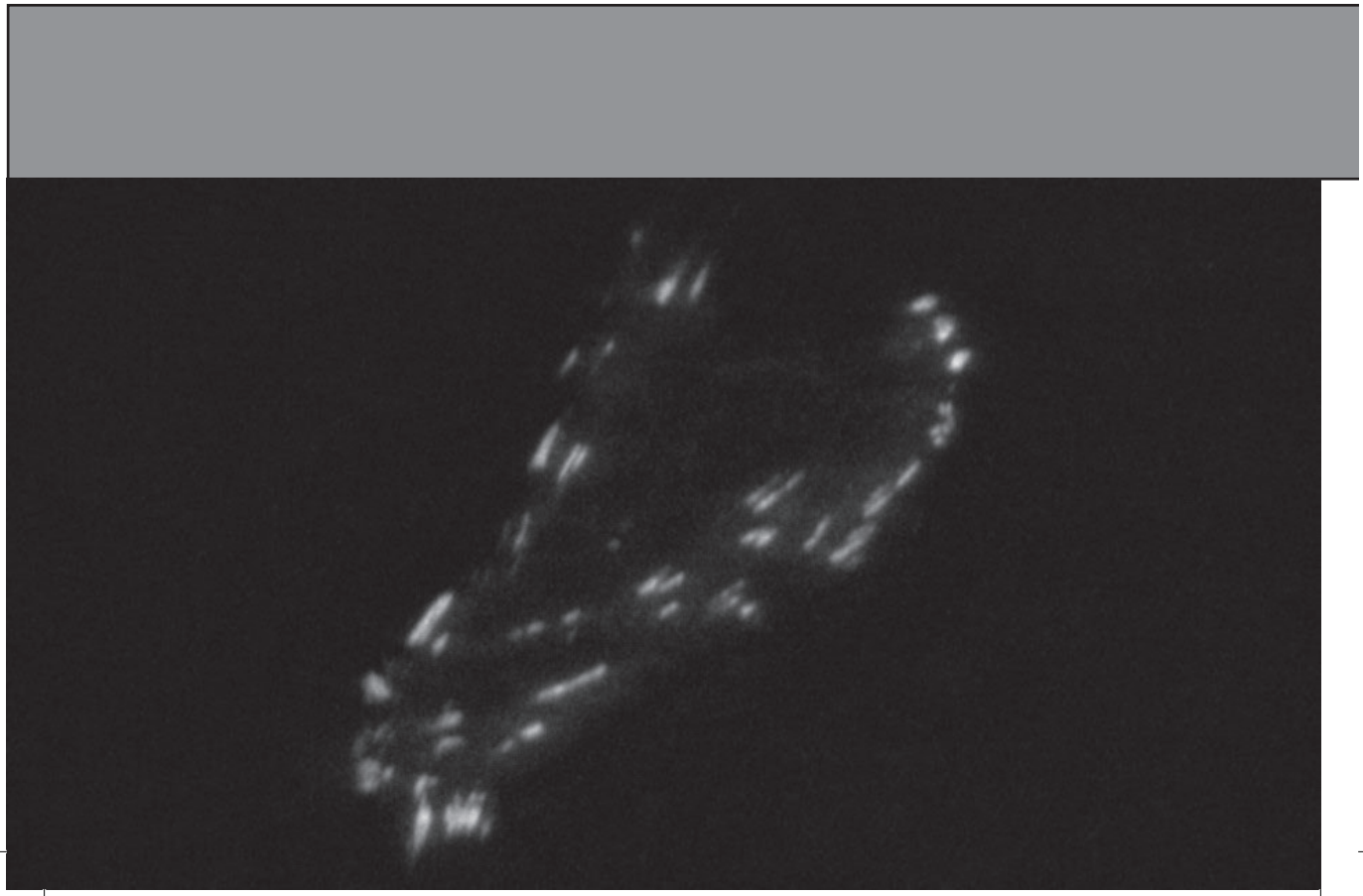

Addendum 3 &

Emma Spanjaard and Johan de Rooij

Analysis of nuclear versus cytosolic labeling: the activity of the Hippo-YAP pathway

The Hippo signaling pathway controls tissue growth and organ size. The canonical downstream transcription co-factors YAP and Taz regulate, among others, cell proliferation and apoptosis [227]. Activity of the Hippo pathway results in the phosphorylation of Yap and Taz, which drives their export out of the nucleus and thus their inactivation. The nuclear localization of YAP, and thus its activity, is also cell-density dependent and at least partially regulated by E-cadherin mediated cell-cell adhesion [228]. Whether and how the Hippo pathway and cell density cooperate in the regulation of YAP localization is under current debate[216]. The activity of the Hippo pathway can thus be visualized by staining cells for the localization of YAP where the ratio between the cytoplasmic and nuclear fractions of YAP correlates to pathway activity (and hence Yap inactivity). This assay can be used to investigate possible regulators of the Hippo-YAP pathway and that requires unbiased analysis of the nuclear versus cytosolic labeling.

In figure 1A the workflow of a method to analyze YAP localization in the nucleus versus the cytosol is depicted. For this analysis at least two types of cell labels need to be imaged: a YAP staining and a nuclear labeling (e.g. DAPI) (Figure 1B). For the analysis of densely seeded cells that is sufficient for a rough segmentation of nuclei and associated cytoplasm. For the analysis of sparse cells an additional cytosolic stain (e.g. actin) can be used for the segmentation of the cell bodies from the background (Figure1C). Alternatively, a region of interest can be drawn manually around the cells of interest, separating them from image background or different cellular environments (Figure 1D). For the detection of the nuclei, first the nuclear image is smoothed and then segmented using an iteratively determined threshold based on the bimodal intensity histogram of the image; iterations stop when convergence is reached (Figure 1B middle panel). Next, the segmented nuclei image is divided into regions containing one nucleus each with the use of a distance transform followed by a watershed. Notably, the use of this algorithm does not accurately determine cell-cell boundaries, but for the purpose of calculating a nuclear/cytoplasmic intensity ratio, this simple, computationally cheap method is efficient and not prone to artifacts. For the analysis of sparsely seeded cells, the region of interest, either drawn manually or segmented from another image, will be used as the periphery of the regions and the area outside will be excluded (Figure 1C&D, green and blue lines). Finally, in the YAP-image the average pixel intensity of each nuclear region and that of the same region outside the nucleus is measured (Figure 1B lower panel). Finally the average intensity in the cytosol is divided by the average intensity in the nucleus. The ratio will be higher when YAP is depleted from the nucleus, indicating that the Hippo pathway is active and lower if YAP is primarily localized in the nucleus. Using this method we showed that the Hippo pathway was more active in densely seeded cells than in to sparsely seeded cells, concomitant with literature (Figure 1E). This method can be used for the quantitative analysis of any protein that shown meaningful nuclear-cytoplasmic shuttling, like for instance β-catenin.

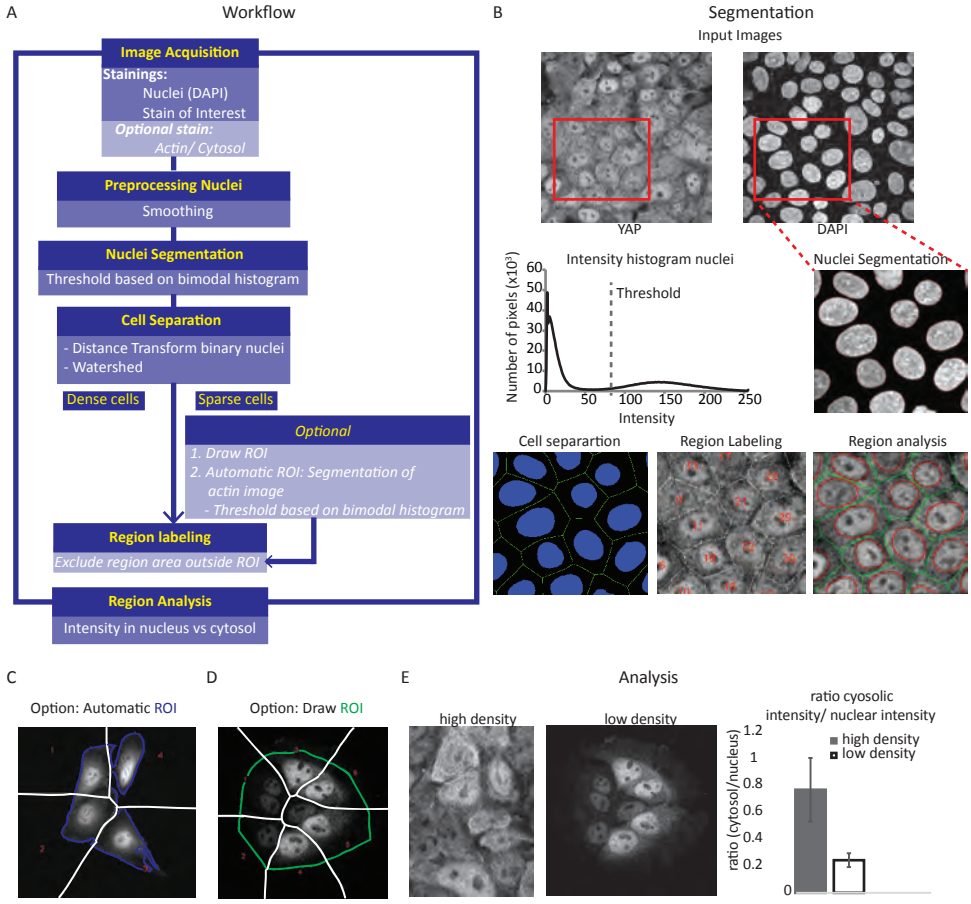

Figure 1: Workflow overview of analysis of nuclear versus cytosolic labeling

A) Workflow overview. B) Top panel: W5 cells [229] labeled by YAP (left) and DAPI (right), with red square around zoom region for explanation of method. Middle panel: Bimodal histogram of the DAPI image in which the threshold (dotted line) is determined in an iterative process (left). The DAPI image overlaid with the outline of the segmented nuclei in red (right). Bottom panel: Image of the segmented nuclei (blue) and the cell regions (green) that are determined by a distance transform and watershed on the segmented nuclei (left). Image showing the labeled cell regions in the YAP image (middle). An overlay of the resulting outline of the cell regions (green) and the nuclear region (red) on the YAP image. C) YAP image of sparsely seeded W5 cells with the labeled cellular regions outlined in white and in blue a ROI automatically defined using an actin labeled image of the cells that excludes the regions outside the ROI from the intensity analysis. D) Similar to (C) but here in green a manually drawn ROI. D) Ratio of the intensity in the cytosol over the intensity in the nucleus of an image of densely seeded cells (left image and grey bar) and sparsely seeded cell (right image and white bar).

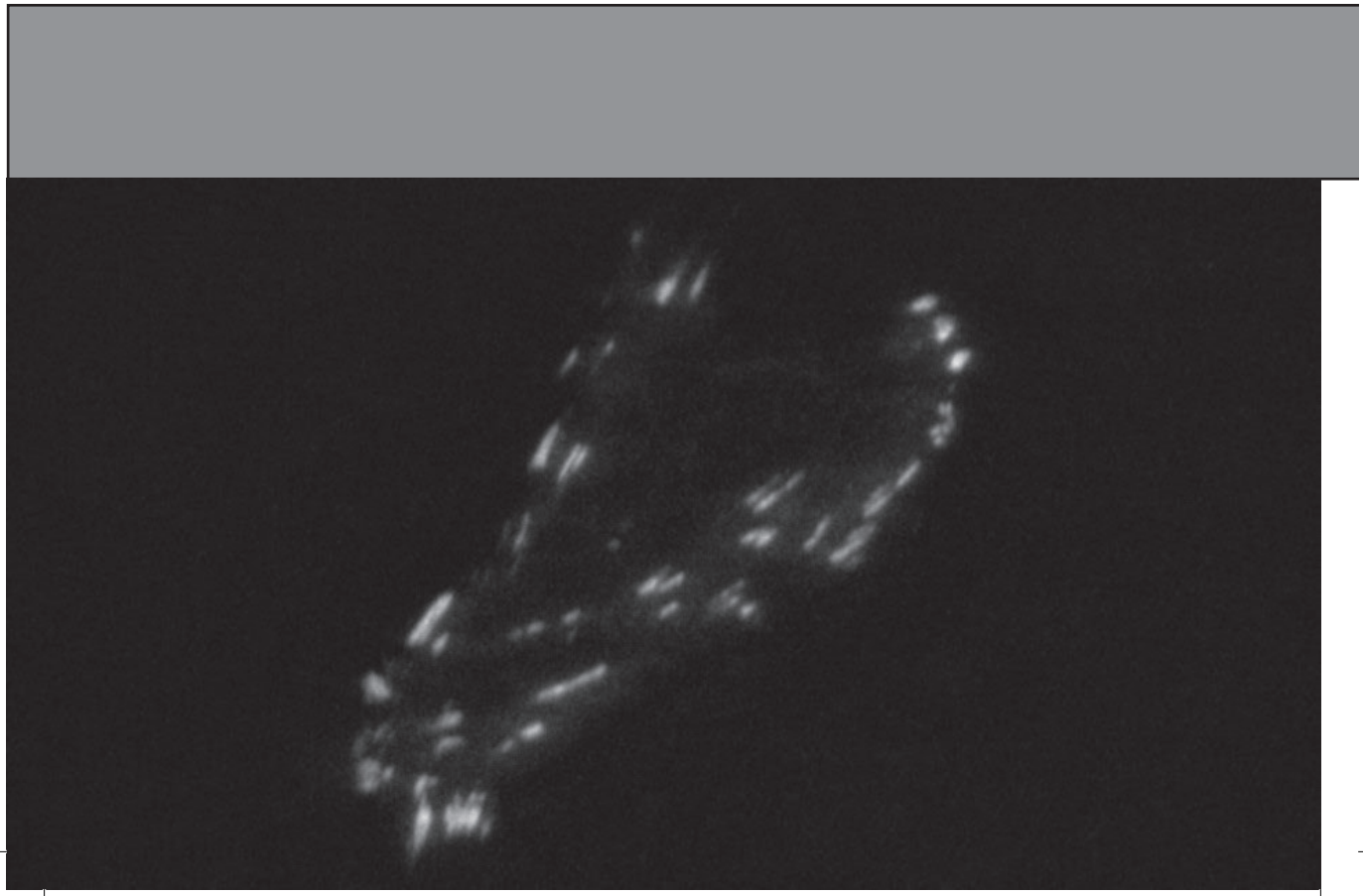

&

References
Nederlandse samenvatting
Acknowledgements
Curriculum Vitae
List of publications

References

1. Kurosaka, S. and A. Kashina, Cell biology of embryonic migration. Birth Defects Res C Embryo Today, 2008. 84(2): p. 102-22.
2. Bravo-Cordero, J.J., L. Hodgson, and J. Condeelis, Directed cell invasion and migration during metastasis. Curr Opin Cell Biol, 2012. 24(2): p. 277-83.
3. Paluch, E.K. and E. Raz, The role and regulation of blebs in cell migration. Curr Opin Cell Biol, 2013. 25(5): p. 582-90.
4. Pollard, T.D. and G.G. Borisy, Cellular motility driven by assembly and disassembly of actin filaments. Cell, 2003. 112(4): p. 453-65.
5. Parsons, J.T., A.R. Horwitz, and M.A. Schwartz, Cell adhesion: integrating cytoskeletal dynamics and cellular tension. Nat Rev Mol Cell Biol, 2010. 11(9): p. 633-43.
6. Theriot, J.A. and T.J. Mitchison, Actin microfilament dynamics in locomoting cells. Nature, 1991. 352(6331): p. 126-31.
7. Ponti, A., et al., Two distinct actin networks drive the protrusion of migrating cells. Science, 2004. 305(5691): p. 1782-6.
8. Burnette, D.T., et al., A contractile and counterbalancing adhesion system controls the 3D shape of crawling cells. J Cell Biol, 2014. 205(1): p. 83-96.
9. Choi, C.K., et al., Actin and alpha-actinin orchestrate the assembly and maturation of nascent adhesions in a myosin II motor-independent manner. Nat Cell Biol, 2008. 10(9): p. 1039-50.
10. Gardel, M.L., et al., Mechanical integration of actin and adhesion dynamics in cell migration. Annu Rev Cell Dev Biol, 2010. 26: p. 315-33.
11. Alexandrova, A.Y., et al., Comparative dynamics of retrograde actin flow and focal adhesions: formation of nascent adhesions triggers transition from fast to slow flow. PLoS One, 2008. 3(9): p. e3234.
12. Gardel, M.L., et al., Traction stress in focal adhesions correlates biphasically with actin retrograde flow speed. J Cell Biol, 2008. 183(6): p. 999-1005.
13. Giancotti, F.G. and E. Ruoslahti, Integrin signaling. Science, 1999. 285(5430): p. 1028-32.
14. Hynes, R.O., Integrins: bidirectional, allosteric signaling machines. Cell, 2002. 110(6): p. 673-87.
15. Anthis, N.J. and I.D. Campbell, The tail of integrin activation. Trends Biochem Sci, 2011. 36(4): p. 191-8.
16. Kim, C., F. Ye, and M.H. Ginsberg, Regulation of integrin activation. Annu Rev Cell Dev Biol, 2011. 27: p. 321-45.
17. Calderwood, D.A., I.D. Campbell, and D.R. Critchley, Talins and kindlins: partners in integrin-mediated adhesion. Nat Rev Mol Cell Biol, 2013. 14(8): p. 503-17.
18. Ye, F., et al., The mechanism of kindlin-mediated activation of integrin alphaIIbbeta3. Curr Biol, 2013. 23(22): p. 2288-95.
19. Ye, F., A.K. Snider, and M.H. Ginsberg, Talin and kindlin: the one-two punch in integrin activation. Front Med, 2014. 8(1): p. 6-16.
20. Ciobanasu, C., B. Faivre, and C. Le Clainche, Actomyosin-dependent formation of the mechanosensitive talin-vinculin complex reinforces actin anchoring. Nat Commun, 2014. 5: p. 3095.
21. del Rio, A., et al., Stretching single talin rod molecules activates vinculin binding. Science, 2009. 323(5914): p. 638-41.

22. Hirata, H., et al., Force-dependent vinculin binding to talin in live cells: a crucial step in anchoring the actin cytoskeleton to focal adhesions. Am J Physiol Cell Physiol, 2014. 306(6): p. C607-20.
23. Lee, H.S., et al., Two modes of integrin activation form a binary molecular switch in adhesion maturation. Mol Biol Cell, 2013. 24(9): p. 1354-62.
24. Spanjaard, E. and J. de Rooij, Mechanotransduction: vinculin provides stability when tension rises. Curr Biol, 2013. 23(4): p. R159-61.
25. Humphries, J.D., et al., Vinculin controls focal adhesion formation by direct interactions with talin and actin. J Cell Biol, 2007. 179(5): p. 1043-57.
26. Gupton, S.L. and C.M. Waterman-Storer, Spatiotemporal feedback between actomyosin and focal-adhesion systems optimizes rapid cell migration. Cell, 2006. 125(7): p. 1361-74.
27. Burnette, D.T., et al., A role for actin arcs in the leading-edge advance of migrating cells. Nat Cell Biol, 2011. 13(4): p. 371-81.
28. Vallotton, P., et al., Simultaneous mapping of filamentous actin flow and turnover in migrating cells by quantitative fluorescent speckle microscopy. Proc Natl Acad Sci U S A, 2004. 101(26): p. 9660-5.
29. Ciobanasu, C., B. Faivre, and C. Le Clainche, Actin dynamics associated with focal adhesions. Int J Cell Biol, 2012. 2012: p. 941292.
30. Small, J.V., et al., Assembling an actin cytoskeleton for cell attachment and movement. Biochim Biophys Acta, 1998. 1404(3): p. 271-81.
31. Hotulainen, P. and P. Lappalainen, Stress fibers are generated by two distinct actin assembly mechanisms in motile cells. J Cell Biol, 2006. 173(3): p. 383-94.
32. Cai, Y., et al., Nonmuscle myosin IIA-dependent force inhibits cell spreading and drives F-actin flow. Biophys J, 2006. 91(10): p. 3907-20.
33. Vicente-Manzanares, M., C.K. Choi, and A.R. Horwitz, Integrins in cell migration--the actin connection. J Cell Sci, 2009. 122(Pt 2): p. 199-206.
34. Aguilar-Cuenca, R., A. Juanes-Garcia, and M. Vicente-Manzanares, Myosin II in mechanotransduction: master and commander of cell migration, morphogenesis, and cancer. Cell Mol Life Sci, 2014. 71(3): p. 479-92.
35. Riento, K. and A.J. Ridley, Rocks: multifunctional kinases in cell behaviour. Nat Rev Mol Cell Biol, 2003. 4(6): p. 446-56.
36. Unbekandt, M. and M.F. Olson, The actin-myosin regulatory MRCK kinases: regulation, biological functions and associations with human cancer. J Mol Med (Berl), 2014. 92(3): p. 217-25.
37. Zaidel-Bar, R., et al., Functional atlas of the integrin adhesome. Nat Cell Biol, 2007. 9(8): p. 858-67.
38. Zaidel-Bar, R. and B. Geiger, The switchable integrin adhesome. J Cell Sci, 2010. 123(Pt 9): p. 1385-8.
39. Kanchanawong, P., et al., Nanoscale architecture of integrin-based cell adhesions. Nature, 2010. 468(7323): p. 580-4.
40. Pinon, P., et al., Talin-bound NPLY motif recruits integrin-signaling adapters to regulate cell spreading and mechanosensing. J Cell Biol, 2014. 205(2): p. 265-81.
41. Carisey, A., et al., Vinculin regulates the recruitment and release of core focal adhesion proteins in a force-dependent manner. Curr Biol, 2013. 23(4): p. 271-81.
42. Thievessen, I., et al., Vinculin-actin interaction couples actin retrograde flow to focal adhesions, but is dispensable for focal adhesion growth. J Cell Biol, 2013. 202(1): p.

163-77.
43. Yao, M., et al., Mechanical activation of vinculin binding to talin locks talin in an unfolded conformation. Sci Rep, 2014. 4: p. 4610.
44. Ziegler, W.H., R.C. Liddington, and D.R. Critchley, The structure and regulation of vinculin. Trends Cell Biol, 2006. 16(9): p. 453-60.
45. Xu, W., J.L. Coll, and E.D. Adamson, Rescue of the mutant phenotype by reexpression of full-length vinculin in null F9 cells; effects on cell locomotion by domain deleted vinculin. J Cell Sci, 1998. 111 (Pt 11): p. 1535-44.
46. Chen, H., et al., Spatial distribution and functional significance of activated vinculin in living cells. J Cell Biol, 2005. 169(3): p. 459-70.
47. Goksoy, E., et al., Structural basis for the autoinhibition of talin in regulating integrin activation. Mol Cell, 2008. 31(1): p. 124-33.
48. Goult, B.T., et al., Structural studies on full-length talin1 reveal a compact auto-inhibited dimer: implications for talin activation. J Struct Biol, 2013. 184(1): p. 21-32.
49. Bakolitsa, C., et al., Structural basis for vinculin activation at sites of cell adhesion. Nature, 2004. 430(6999): p. 583-6.
50. Webb, D.J., et al., FAK-Src signalling through paxillin, ERK and MLCK regulates adhesion disassembly. Nat Cell Biol, 2004. 6(2): p. 154-61.
51. Huveneers, S. and E.H. Danen, Adhesion signaling - crosstalk between integrins, Src and Rho. J Cell Sci, 2009. 122(Pt 8): p. 1059-69.
52. Mitra, S.K. and D.D. Schlaepfer, Integrin-regulated FAK-Src signaling in normal and cancer cells. Curr Opin Cell Biol, 2006. 18(5): p. 516-23.
53. Thomas, J.W., et al., The role of focal adhesion kinase binding in the regulation of tyrosine phosphorylation of paxillin. J Biol Chem, 1999. 274(51): p. 36684-92.
54. Deakin, N.O. and C.E. Turner, Paxillin comes of age. J Cell Sci, 2008. 121(Pt 15): p. 2435-44.
55. Turner, C.E., J.R. Glenney, Jr., and K. Burridge, Paxillin: a new vinculin-binding protein present in focal adhesions. J Cell Biol, 1990. 111(3): p. 1059-68.
56. Jiang, G., et al., Two-piconewton slip bond between fibronectin and the cytoskeleton depends on talin. Nature, 2003. 424(6946): p. 334-7.
57. Hu, K., et al., Differential transmission of actin motion within focal adhesions. Science, 2007. 315(5808): p. 111-5.
58. Chan, C.E. and D.J. Odde, Traction dynamics of filopodia on compliant substrates. Science, 2008. 322(5908): p. 1687-91.
59. Giannone, G., R.M. Mege, and O. Thoumine, Multi-level molecular clutches in motile cell processes. Trends Cell Biol, 2009. 19(9): p. 475-86.
60. Kuo, J.C., et al., Isolation of focal adhesion proteins for biochemical and proteomic analysis. Methods Mol Biol, 2012. 757: p. 297-323.
61. Nayal, A., et al., Paxillin phosphorylation at Ser273 localizes a GIT1-PIX-PAK complex and regulates adhesion and protrusion dynamics. J Cell Biol, 2006. 173(4): p. 587-9.
62. Subauste, M.C., et al., Vinculin modulation of paxillin-FAK interactions regulates ERK to control survival and motility. J Cell Biol, 2004. 165(3): p. 371-81.
63. Zaidel-Bar, R., et al., A paxillin tyrosine phosphorylation switch regulates the assembly and form of cell-matrix adhesions. J Cell Sci, 2007. 120(Pt 1): p. 137-48.
64. Mitra, S.K., D.A. Hanson, and D.D. Schlaepfer, Focal adhesion kinase: in command and control of cell motility. Nat Rev Mol Cell Biol, 2005. 6(1): p. 56-68.

65. Goult, B.T., et al., RIAM and vinculin binding to talin are mutually exclusive and regulate adhesion assembly and turnover. J Biol Chem, 2013. 288(12): p. 8238-49.
66. Smilenov, L.B., et al., Focal adhesion motility revealed in stationary fibroblasts. Science, 1999. 286(5442): p. 1172-4.
67. Ballestrem, C., et al., Marching at the front and dragging behind: differential alphaVbeta3-integrin turnover regulates focal adhesion behavior. J Cell Biol, 2001. 155(7): p. 1319-32.
68. Kaverina, I., O. Krylyshkina, and J.V. Small, Microtubule targeting of substrate contacts promotes their relaxation and dissociation. J Cell Biol, 1999. 146(5): p. 1033-44.
69. Stehbens, S. and T. Wittmann, Targeting and transport: how microtubules control focal adhesion dynamics. J Cell Biol, 2012. 198(4): p. 481-9.
70. Chan, K.T., D.A. Bennin, and A. Huttenlocher, Regulation of adhesion dynamics by calpain-mediated proteolysis of focal adhesion kinase (FAK). J Biol Chem, 2010. 285(15): p. 11418-26.
71. Cortesio, C.L., et al., Calpain-mediated proteolysis of paxillin negatively regulates focal adhesion dynamics and cell migration. J Biol Chem, 2011. 286(12): p. 9998-10006.
72. Franco, S.J. and A. Huttenlocher, Regulating cell migration: calpains make the cut. J Cell Sci, 2005. 118(Pt 17): p. 3829-38.
73. Winograd-Katz, S.E., et al., The integrin adhesome: from genes and proteins to human disease. Nat Rev Mol Cell Biol, 2014. 15(4): p. 273-88.
74. Heisenberg, C.P. and Y. Bellaiche, Forces in tissue morphogenesis and patterning. Cell, 2013. 153(5): p. 948-62.
75. Balaban, N.Q., et al., Force and focal adhesion assembly: a close relationship studied using elastic micropatterned substrates. Nat Cell Biol, 2001. 3(5): p. 466-72.
76. Zaidel-Bar, R., et al., Early molecular events in the assembly of matrix adhesions at the leading edge of migrating cells. J Cell Sci, 2003. 116(Pt 22): p. 4605-13.
77. Galbraith, C.G., K.M. Yamada, and M.P. Sheetz, The relationship between force and focal complex development. J Cell Biol, 2002. 159(4): p. 695-705.
78. le Duc, Q., et al., Vinculin potentiates E-cadherin mechanosensing and is recruited to actin-anchored sites within adherens junctions in a myosin II-dependent manner. J Cell Biol, 2010. 189(7): p. 1107-15.
79. Pasapera, A.M., et al., Myosin II activity regulates vinculin recruitment to focal adhesions through FAK-mediated paxillin phosphorylation. J Cell Biol, 2010. 188(6): p. 877-90.
80. Janostiak, R., et al., CAS directly interacts with vinculin to control mechanosensing and focal adhesion dynamics. Cell Mol Life Sci, 2014. 71(4): p. 727-44.
81. Sawada, Y., et al., Force sensing by mechanical extension of the Src family kinase substrate p130Cas. Cell, 2006. 127(5): p. 1015-26.
82. Kitayama, H., et al., A ras-related gene with transformation suppressor activity. Cell, 1989. 56(1): p. 77-84.
83. Boettner, B. and L. Van Aelst, Control of cell adhesion dynamics by Rap1 signaling. Curr Opin Cell Biol, 2009. 21(5): p. 684-93.
84. Kooistra, M.R., N. Dube, and J.L. Bos, Rap1: a key regulator in cell-cell junction formation. J Cell Sci, 2007. 120(Pt 1): p. 17-22.
85. Pannekoek, W.J., et al., Cell-cell junction formation: the role of Rap1 and Rap1

guanine nucleotide exchange factors. Biochim Biophys Acta, 2009. 1788(4): p. 790-6.
86. Lyle, K.S., et al., cAMP-induced Epac-Rap activation inhibits epithelial cell migration by modulating focal adhesion and leading edge dynamics. Cell Signal, 2008. 20(6): p. 1104-16.
87. Reedquist, K.A., et al., The small GTPase, Rap1, mediates CD31-induced integrin adhesion. J Cell Biol, 2000. 148(6): p. 1151-8.
88. Hattori, M. and N. Minato, Rap1 GTPase: functions, regulation, and malignancy. J Biochem, 2003. 134(4): p. 479-84.
89. Han, J., et al., Reconstructing and deconstructing agonist-induced activation of integrin alphaIIbbeta3. Curr Biol, 2006. 16(18): p. 1796-806.
90. Lafuente, E.M., et al., RIAM, an Ena/VASP and Profilin ligand, interacts with Rap1-GTP and mediates Rap1-induced adhesion. Dev Cell, 2004. 7(4): p. 585-95.
91. Post, A., et al., Rasip1 mediates Rap1 regulation of Rho in endothelial barrier function through ArhGAP29. Proc Natl Acad Sci U S A, 2013. 110(28): p. 11427-32.
92. Ando, K., et al., Rap1 potentiates endothelial cell junctions by spatially controlling myosin II activity and actin organization. J Cell Biol, 2013. 202(6): p. 901-16.
93. Bos, J.L., Linking Rap to cell adhesion. Curr Opin Cell Biol, 2005. 17(2): p. 123-8.
94. Gloerich, M. and J.L. Bos, Regulating Rap small G-proteins in time and space. Trends Cell Biol, 2011. 21(10): p. 615-23.
95. Pannekoek, W.J., et al., Epac1 and PDZ-GEF cooperate in Rap1 mediated endothelial junction control. Cell Signal, 2011. 23(12): p. 2056-64.
96. Ohba, Y., et al., Requirement for C3G-dependent Rap1 activation for cell adhesion and embryogenesis. EMBO J, 2001. 20(13): p. 3333-41.
97. Tamada, M., M.P. Sheetz, and Y. Sawada, Activation of a signaling cascade by cytoskeleton stretch. Dev Cell, 2004. 7(5): p. 709-18.
98. de Rooij, J., et al., Epac is a Rap1 guanine-nucleotide-exchange factor directly activated by cyclic AMP. Nature, 1998. 396(6710): p. 474-7.
99. Enserink, J.M., et al., A novel Epac-specific cAMP analogue demonstrates independent regulation of Rap1 and ERK. Nat Cell Biol, 2002. 4(11): p. 901-6.
100. Smal, I., et al., Multiple object tracking in molecular bioimaging by Rao-Blackwellized marginal particle filtering. Med Image Anal, 2008. 12(6): p. 764-77.
101. Vincent, L. and P. Soille, Watersheds in Digital Spaces - an Efficient Algorithm Based on Immersion Simulations. Ieee Transactions on Pattern Analysis and Machine Intelligence, 1991. 13(6): p. 583-598.
102. Frantz, C., K.M. Stewart, and V.M. Weaver, The extracellular matrix at a glance. J Cell Sci, 2010. 123(Pt 24): p. 4195-200.
103. Gumbiner, B.M., Cell adhesion: the molecular basis of tissue architecture and morphogenesis. Cell, 1996. 84(3): p. 345-57.
104. Jarvelainen, H., et al., Extracellular matrix molecules: potential targets in pharmacotherapy. Pharmacol Rev, 2009. 61(2): p. 198-223.
105. Sonnenberg, A. and R.K. Liem, Plakins in development and disease. Exp Cell Res, 2007. 313(10): p. 2189-203.
106. Carey, S., J. Charest, and C. Reinhart-King, Forces During Cell Adhesion and Spreading: Implications for Cellular Homeostasis, in Cellular and Biomolecular Mechanics and Mechanobiology, A. Gefen, Editor. 2011, Springer Berlin Heidelberg. p. 29-69.
107. Geiger, B., et al., Transmembrane crosstalk between the extracellular matrix--

cytoskeleton crosstalk. Nat Rev Mol Cell Biol, 2001. 2(11): p. 793-805.
108. Geiger, B., J.P. Spatz, and A.D. Bershadsky, Environmental sensing through focal adhesions. Nat Rev Mol Cell Biol, 2009. 10(1): p. 21-33.
109. Ginsberg, M.H., A. Partridge, and S.J. Shattil, Integrin regulation. Curr Opin Cell Biol, 2005. 17(5): p. 509-16.
110. Legate, K.R., S.A. Wickstrom, and R. Fassler, Genetic and cell biological analysis of integrin outside-in signaling. Genes Dev, 2009. 23(4): p. 397-418.
111. Luo, B.H., C.V. Carman, and T.A. Springer, Structural basis of integrin regulation and signaling. Annu Rev Immunol, 2007. 25: p. 619-47.
112. Brunton, V.G., et al., Identification of Src-specific phosphorylation site on focal adhesion kinase: dissection of the role of Src SH2 and catalytic functions and their consequences for tumor cell behavior. Cancer Res, 2005. 65(4): p. 1335-42.
113. Grashoff, C., et al., Measuring mechanical tension across vinculin reveals regulation of focal adhesion dynamics. Nature, 2010. 466(7303): p. 263-6.
114. Katsumi, A., et al., Integrins in mechanotransduction. J Biol Chem, 2004. 279(13): p. 12001-4.
115. Mierke, C.T., The role of vinculin in the regulation of the mechanical properties of cells. Cell Biochem Biophys, 2009. 53(3): p. 115-26.
116. Moore, S.W., P. Roca-Cusachs, and M.P. Sheetz, Stretchy proteins on stretchy substrates: the important elements of integrin-mediated rigidity sensing. Dev Cell, 2010. 19(2): p. 194-206.
117. Puklin-Faucher, E. and M.P. Sheetz, The mechanical integrin cycle. J Cell Sci, 2009. 122(Pt 2): p. 179-86.
118. Caron, E., Cellular functions of the Rap1 GTP-binding protein: a pattern emerges. J Cell Sci, 2003. 116(Pt 3): p. 435-40.
119. Caron, E., A.J. Self, and A. Hall, The GTPase Rap1 controls functional activation of macrophage integrin alphaMbeta2 by LPS and other inflammatory mediators. Curr Biol, 2000. 10(16): p. 974-8.
120. Katagiri, K., et al., Rap1 is a potent activation signal for leukocyte function-associated antigen 1 distinct from protein kinase C and phosphatidylinositol-3-OH kinase. Mol Cell Biol, 2000. 20(6): p. 1956-69.
121. Kinbara, K., et al., Ras GTPases: integrins' friends or foes? Nat Rev Mol Cell Biol, 2003. 4(10): p. 767-76.
122. Cullere, X., et al., Regulation of vascular endothelial barrier function by Epac, a cAMP-activated exchange factor for Rap GTPase. Blood, 2005. 105(5): p. 1950-5.
123. Fukuhara, S., et al., Cyclic AMP potentiates vascular endothelial cadherin-mediated cell-cell contact to enhance endothelial barrier function through an Epac-Rap1 signaling pathway. Mol Cell Biol, 2005. 25(1): p. 136-46.
124. Kooistra, M.R., et al., Epac1 regulates integrity of endothelial cell junctions through VE-cadherin. FEBS Lett, 2005. 579(22): p. 4966-72.
125. Jeon, C.Y., et al., p190RhoGAP and Rap-dependent RhoGAP (ARAP3) inactivate RhoA in response to nerve growth factor leading to neurite outgrowth from PC12 cells. Exp Mol Med, 2010. 42(5): p. 335-44.
126. Jeon, C.Y., et al., Neurite outgrowth from PC12 cells by basic fibroblast growth factor (bFGF) is mediated by RhoA inactivation through p190RhoGAP and ARAP3. J Cell Physiol, 2010. 224(3): p. 786-94.
127. Stockton, R.A., et al., Cerebral cavernous malformations proteins inhibit Rho kinase

to stabilize vascular integrity. J Exp Med, 2010. 207(4): p. 881-96.
128. Zieba, B.J., et al., The cAMP-responsive Rap1 guanine nucleotide exchange factor, Epac, induces smooth muscle relaxation by down-regulation of RhoA activity. J Biol Chem, 2011. 286(19): p. 16681-92.
129. Lafuente, E. and V.A. Boussiotis, Rap1 regulation of RIAM and cell adhesion. Methods Enzymol, 2006. 407: p. 345-58.
130. Lee, H.S., et al., RIAM activates integrins by linking talin to ras GTPase membrane-targeting sequences. J Biol Chem, 2009. 284(8): p. 5119-27.
131. Watanabe, N., et al., Mechanisms and consequences of agonist-induced talin recruitment to platelet integrin alphaIIbbeta3. J Cell Biol, 2008. 181(7): p. 1211-22.
132. Krugmann, S., et al., ARAP3 is a PI3K- and rap-regulated GAP for RhoA. Curr Biol, 2004. 14(15): p. 1380-4.
133. Raaijmakers, J.H., et al., The PI3K effector Arap3 interacts with the PI(3,4,5)P3 phosphatase SHIP2 in a SAM domain-dependent manner. Cell Signal, 2007. 19(6): p. 1249-57.
134. Aivatiadou, E., et al., cAMP-Epac2-mediated activation of Rap1 in developing male germ cells: RA-RhoGAP as a possible direct down-stream effector. Mol Reprod Dev, 2009. 76(4): p. 407-16.
135. Kurooka, T., et al., Dual regulation of RA-RhoGAP activity by phosphatidic acid and Rap1 during neurite outgrowth. J Biol Chem, 2011. 286(8): p. 6832-43.
136. Yamada, T., et al., RA-RhoGAP, Rap-activated Rho GTPase-activating protein implicated in neurite outgrowth through Rho. J Biol Chem, 2005. 280(38): p. 33026-34.
137. Whitehead, K.J., et al., The cerebral cavernous malformation signaling pathway promotes vascular integrity via Rho GTPases. Nat Med, 2009. 15(2): p. 177-84.
138. Arthur, W.T., L.A. Quilliam, and J.A. Cooper, Rap1 promotes cell spreading by localizing Rac guanine nucleotide exchange factors. J Cell Biol, 2004. 167(1): p. 111-22.
139. Li, L., M. Okura, and A. Imamoto, Focal adhesions require catalytic activity of Src family kinases to mediate integrin-matrix adhesion. Mol Cell Biol, 2002. 22(4): p. 1203-17.
140. Bos, J.L., et al., The role of Rap1 in integrin-mediated cell adhesion. Biochem Soc Trans, 2003. 31(Pt 1): p. 83-6.
141. Crittenden, J.R., et al., CalDAG-GEFI integrates signaling for platelet aggregation and thrombus formation. Nat Med, 2004. 10(9): p. 982-6.
142. Eto, K., et al., Megakaryocytes derived from embryonic stem cells implicate CalDAG-GEFI in integrin signaling. Proc Natl Acad Sci U S A, 2002. 99(20): p. 12819-24.
143. Springett, G.M., H. Kawasaki, and D.R. Spriggs, Non-kinase second-messenger signaling: new pathways with new promise. Bioessays, 2004. 26(7): p. 730-8.
144. Ross, S.H., et al., Ezrin is required for efficient Rap1-induced cell spreading. J Cell Sci, 2011. 124(Pt 11): p. 1808-18.
145. Patla, I., et al., Dissecting the molecular architecture of integrin adhesion sites by cryo-electron tomography. Nat Cell Biol, 2010. 12(9): p. 909-15.
146. Lock, F.E. and N.A. Hotchin, Distinct roles for ROCK1 and ROCK2 in the regulation of keratinocyte differentiation. PLoS One, 2009. 4(12): p. e8190.
147. Lock, F.E., et al., Differential regulation of adhesion complex turnover by ROCK1 and ROCK2. PLoS One, 2012. 7(2): p. e31423.

148. McBeath, R., et al., Cell shape, cytoskeletal tension, and RhoA regulate stem cell lineage commitment. Dev Cell, 2004. 6(4): p. 483-95.
149. Sun, Y., C.S. Chen, and J. Fu, Forcing stem cells to behave: a biophysical perspective of the cellular microenvironment. Annu Rev Biophys, 2012. 41: p. 519-42.
150. Thery, M., Micropatterning as a tool to decipher cell morphogenesis and functions. J Cell Sci, 2010. 123(Pt 24): p. 4201-13.
151. Giannone, G., et al., Talin1 is critical for force-dependent reinforcement of initial integrin-cytoskeleton bonds but not tyrosine kinase activation. J Cell Biol, 2003. 163(2): p. 409-19.
152. Margadant, F., et al., Mechanotransduction in vivo by repeated talin stretch-relaxation events depends upon vinculin. PLoS Biol, 2011. 9(12): p. e1001223.
153. Papagrigoriou, E., et al., Activation of a vinculin-binding site in the talin rod involves rearrangement of a five-helix bundle. EMBO J, 2004. 23(15): p. 2942-51.
154. Niola, F., et al., Id proteins synchronize stemness and anchorage to the niche of neural stem cells. Nat Cell Biol, 2012. 14(5): p. 477-87.
155. Riedl, J., et al., Lifeact: a versatile marker to visualize F-actin. Nat Methods, 2008. 5(7): p. 605-7.
156. Poulouin, L., et al., Plasma fibronectin: three steps to purification and stability. Protein Expr Purif, 1999. 17(1): p. 146-52.
157. Schwartz, M.A. and K. Denninghoff, Alpha v integrins mediate the rise in intracellular calcium in endothelial cells on fibronectin even though they play a minor role in adhesion. J Biol Chem, 1994. 269(15): p. 11133-7.
158. Franke, B., J.W. Akkerman, and J.L. Bos, Rapid Ca2+-mediated activation of Rap1 in human platelets. EMBO J, 1997. 16(2): p. 252-9.
159. Guarino, M., Src signaling in cancer invasion. J Cell Physiol, 2010. 223(1): p. 14-26.
160. Xiao, L.J., et al., Paxillin expression is closely linked to the pathogenesis, progression and prognosis of gastric carcinomas. Oncol Lett, 2014. 7(1): p. 189-194.
161. Zhang, J. and S.N. Hochwald, The role of FAK in tumor metabolism and therapy. Pharmacol Ther, 2013.
162. Kuo, J.C., et al., Analysis of the myosin-II-responsive focal adhesion proteome reveals a role for beta-Pix in negative regulation of focal adhesion maturation. Nat Cell Biol, 2011. 13(4): p. 383-93.
163. Kubow, K.E., S.K. Conrad, and A.R. Horwitz, Matrix microarchitecture and myosin II determine adhesion in 3D matrices. Curr Biol, 2013. 23(17): p. 1607-19.
164. Hynes, N.E., Tyrosine kinase signalling in breast cancer. Breast Cancer Res, 2000. 2(3): p. 154-7.
165. Nishimura, M., et al., Tyrosine phosphorylation of 100-130 kDa proteins in lung cancer correlates with poor prognosis. Br J Cancer, 1996. 74(5): p. 780-7.
166. Dunn, K.B., M. Heffler, and V.M. Golubovskaya, Evolving therapies and FAK inhibitors for the treatment of cancer. Anticancer Agents Med Chem, 2010. 10(10): p. 722-34.
167. Nunes-Xavier, C.E., et al., Protein tyrosine phosphatases as novel targets in breast cancer therapy. Biochim Biophys Acta, 2013. 1836(2): p. 211-26.
168. van Nimwegen, M.J. and B. van de Water, Focal adhesion kinase: a potential target in cancer therapy. Biochem Pharmacol, 2007. 73(5): p. 597-609.
169. Lauffenburger, D.A. and A.F. Horwitz, Cell migration: a physically integrated molecular process. Cell, 1996. 84(3): p. 359-69.

170. Sheetz, M.P., D.P. Felsenfeld, and C.G. Galbraith, Cell migration: regulation of force on extracellular-matrix-integrin complexes. Trends Cell Biol, 1998. 8(2): p. 51-4.
171. Vicente-Manzanares, M. and A.R. Horwitz, Adhesion dynamics at a glance. J Cell Sci, 2011. 124(Pt 23): p. 3923-7.
172. Webb, D.J., J.T. Parsons, and A.F. Horwitz, Adhesion assembly, disassembly and turnover in migrating cells -- over and over and over again. Nat Cell Biol, 2002. 4(4): p. E97-100.
173. Ballestrem, C., et al., Molecular mapping of tyrosine-phosphorylated proteins in focal adhesions using fluorescence resonance energy transfer. J Cell Sci, 2006. 119(Pt 5): p. 866-75.
174. Zaidel-Bar, R., et al., Hierarchical assembly of cell-matrix adhesion complexes. Biochem Soc Trans, 2004. 32(Pt3): p. 416-20.
175. Smal, I., et al., Rao-Blackwellized marginal particle filtering for multiple object tracking in molecular bioimaging. Inf Process Med Imaging, 2007. 20: p. 110-21.
176. Smal, I., et al., Quantitative comparison of spot detection methods in fluorescence microscopy. IEEE Trans Med Imaging, 2010. 29(2): p. 282-301.
177. Vincent, L., Morphological grayscale reconstruction in image analysis: applications and efficient algorithms. IEEE Trans Image Process, 1993. 2(2): p. 176-201.
178. Huttenlocher, A. and A.R. Horwitz, Integrins in cell migration. Cold Spring Harb Perspect Biol, 2011. 3(9): p. a005074.
179. Grandoch, M., et al., Epac inhibits migration and proliferation of human prostate carcinoma cells. Br J Cancer, 2009. 101(12): p. 2038-42.
180. Wehrle-Haller, B., Assembly and disassembly of cell matrix adhesions. Curr Opin Cell Biol, 2012. 24(5): p. 569-81.
181. Berginski, M.E. and S.M. Gomez, The Focal Adhesion Analysis Server: a web tool for analyzing focal adhesion dynamics. F1000Res, 2013. 2: p. 68.
182. Mohl, C., et al., Quantitative mapping of averaged focal adhesion dynamics in migrating cells by shape normalization. J Cell Sci, 2012. 125(Pt 1): p. 155-65.
183. Wurflinger, T., et al., Automated segmentation and tracking for large-scale analysis of focal adhesion dynamics. J Microsc, 2011. 241(1): p. 37-53.
184. Zamir, E., et al., Molecular diversity of cell-matrix adhesions. J Cell Sci, 1999. 112 (Pt 11): p. 1655-69.
185. Fournier, M.F., et al., Force transmission in migrating cells. J Cell Biol, 2010. 188(2): p. 287-97.
186. Laukaitis, C.M., et al., Differential dynamics of alpha 5 integrin, paxillin, and alpha-actinin during formation and disassembly of adhesions in migrating cells. J Cell Biol, 2001. 153(7): p. 1427-40.
187. Ross, S.H., et al., Rap1 can bypass the FAK-Src-Paxillin cascade to induce cell spreading and focal adhesion formation. PLoS One, 2012. 7(11): p. e50072.
188. Dull, T., et al., A third-generation lentivirus vector with a conditional packaging system. J Virol, 1998. 72(11): p. 8463-71.
189. Loerke, D., et al., Quantitative imaging of epithelial cell scattering identifies specific inhibitors of cell motility and cell-cell dissociation. Sci Signal, 2012. 5(231): p. rs5.
190. Yu, J., et al., Advances to Bayesian network inference for generating causal networks from observational biological data. Bioinformatics, 2004. 20(18): p. 3594-3603.
191. Gansner, E.R. and S.C. North, An open graph visualization system and its applications to software engineering. Software-Practice & Experience, 2000. 30(11): p. 1203-

1233.
192. Wielemaker, J., et al., Swi-Prolog. Theory and Practice of Logic Programming, 2012. 12: p. 67-96.
193. Roca-Cusachs, P., T. Iskratsch, and M.P. Sheetz, Finding the weakest link: exploring integrin-mediated mechanical molecular pathways. J Cell Sci, 2012. 125(Pt 13): p. 3025-38.
194. Plotnikov, S.V., et al., Force fluctuations within focal adhesions mediate ECM-rigidity sensing to guide directed cell migration. Cell, 2012. 151(7): p. 1513-27.
195. Oakes, P.W., et al., Tension is required but not sufficient for focal adhesion maturation without a stress fiber template. J Cell Biol, 2012. 196(3): p. 363-74.
196. Stricker, J., et al., Myosin II-mediated focal adhesion maturation is tension insensitive. PLoS One, 2013. 8(7): p. e70652.
197. Ezratty, E.J., M.A. Partridge, and G.G. Gundersen, Microtubule-induced focal adhesion disassembly is mediated by dynamin and focal adhesion kinase. Nat Cell Biol, 2005. 7(6): p. 581-90.
198. Vicente-Manzanares, M., et al., Myosin IIA/IIB restrict adhesive and protrusive signaling to generate front-back polarity in migrating cells. J Cell Biol, 2011. 193(2): p. 381-96.
199. Sheen-Chen, S.M., et al., Serum levels of hepatocyte growth factor in patients with breast cancer. Cancer Epidemiol Biomarkers Prev, 2005. 14(3): p. 715-7.
200. Siegfried, J.M., et al., The clinical significance of hepatocyte growth factor for non-small cell lung cancer. Ann Thorac Surg, 1998. 66(6): p. 1915-8.
201. Ridley, A.J., P.M. Comoglio, and A. Hall, Regulation of scatter factor/hepatocyte growth factor responses by Ras, Rac, and Rho in MDCK cells. Mol Cell Biol, 1995. 15(2): p. 1110-22.
202. Stoker, M. and M. Perryman, An epithelial scatter factor released by embryo fibroblasts. J Cell Sci, 1985. 77: p. 209-23.
203. de Rooij, J., et al., Integrin-dependent actomyosin contraction regulates epithelial cell scattering. J Cell Biol, 2005. 171(1): p. 153-64.
204. Enserink, J.M., et al., The cAMP-Epac-Rap1 pathway regulates cell spreading and cell adhesion to laminin-5 through the alpha3beta1 integrin but not the alpha6beta4 integrin. J Biol Chem, 2004. 279(43): p. 44889-96.
205. Menasche, G., et al., RIAM links the ADAP/SKAP-55 signaling module to Rap1, facilitating T-cell-receptor-mediated integrin activation. Mol Cell Biol, 2007. 27(11): p. 4070-81.
206. Altemeier, W.A., et al., Syndecan-1 controls cell migration by activating Rap1 to regulate focal adhesion disassembly. J Cell Sci, 2012. 125(Pt 21): p. 5188-95.
207. Millon-Fremillon, A., et al., Cell adaptive response to extracellular matrix density is controlled by ICAP-1-dependent beta1-integrin affinity. J Cell Biol, 2008. 180(2): p. 427-41.
208. Hirata, H., et al., Force-dependent vinculin binding to talin in live cells: a crucial step in anchoring the actin cytoskeleton to focal adhesions. Am J Physiol Cell Physiol, 2014.
209. Wong, A.S., P.C. Leung, and N. Auersperg, Hepatocyte growth factor promotes in vitro scattering and morphogenesis of human cervical carcinoma cells. Gynecol Oncol, 2000. 78(2): p. 158-65.
210. Schiller, H.B., et al., Quantitative proteomics of the integrin adhesome show a myosin

II-dependent recruitment of LIM domain proteins. EMBO Rep, 2011. 12(3): p. 259-66.
211. Franco, S.J., et al., Calpain-mediated proteolysis of talin regulates adhesion dynamics. Nat Cell Biol, 2004. 6(10): p. 977-83.
212. Stricker, J., T. Falzone, and M.L. Gardel, Mechanics of the F-actin cytoskeleton. J Biomech, 2010. 43(1): p. 9-14.
213. Aguilar-Cuenca, R., A. Juanes-Garcia, and M. Vicente-Manzanares, Myosin II in mechanotransduction: master and commander of cell migration, morphogenesis, and cancer. Cell Mol Life Sci, 2013.
214. Engler, A.J., et al., Matrix elasticity directs stem cell lineage specification. Cell, 2006. 126(4): p. 677-89.
215. Paszek, M.J., et al., Tensional homeostasis and the malignant phenotype. Cancer Cell, 2005. 8(3): p. 241-54.
216. Dupont, S., et al., Role of YAP/TAZ in mechanotransduction. Nature, 2011. 474(7350): p. 179-83.
217. Discher, D.E., P. Janmey, and Y.L. Wang, Tissue cells feel and respond to the stiffness of their substrate. Science, 2005. 310(5751): p. 1139-43.
218. Chrzanowska-Wodnicka, M. and K. Burridge, Rho-stimulated contractility drives the formation of stress fibers and focal adhesions. J Cell Biol, 1996. 133(6): p. 1403-15.
219. Riveline, D., et al., Focal contacts as mechanosensors: externally applied local mechanical force induces growth of focal contacts by an mDia1-dependent and ROCK-independent mechanism. J Cell Biol, 2001. 153(6): p. 1175-86.
220. Chang, C.W. and S. Kumar, Vinculin tension distributions of individual stress fibers within cell-matrix adhesions. J Cell Sci, 2013. 126(Pt 14): p. 3021-30.
221. Karginov, A.V., et al., Dissecting motility signaling through activation of specific Src-effector complexes. Nat Chem Biol, 2014. 10(4): p. 286-90.
222. Trusolino, L., A. Bertotti, and P.M. Comoglio, MET signalling: principles and functions in development, organ regeneration and cancer. Nat Rev Mol Cell Biol, 2010. 11(12): p. 834-48.
223. Labonte, G., A SOM neural network that reveals continuous displacement fields. Ieee World Congress on Computational Intelligence, 1998: p. 880-884.
224. Labonte, G., A new neural network for particle-tracking velocimetry. Experiments in Fluids, 1999. 26(4): p. 340-346.
225. Labonte, G., On a neural network that performs an enhanced nearest-neighbour matching. Pattern Analysis and Applications, 2000. 3(3): p. 267-278.
226. Huveneers, S., et al., Vinculin associates with endothelial VE-cadherin junctions to control force-dependent remodeling. J Cell Biol, 2012. 196(5): p. 641-52.
227. Varelas, X., The Hippo pathway effectors TAZ and YAP in development, homeostasis and disease. Development, 2014. 141(8): p. 1614-26.
228. Kim, N.G., et al., E-cadherin mediates contact inhibition of proliferation through Hippo signaling-pathway components. Proc Natl Acad Sci U S A, 2011. 108(29): p. 11930-5.
229. Baas, A.F., et al., Complete polarization of single intestinal epithelial cells upon activation of LKB1 by STRAD. Cell, 2004. 116(3): p. 457-66.

Nederlandse samenvatting

Het menselijk lichaam, en dat van alle andere dieren, bestaat uit weefsels en organen en die bestaan weer uit heel veel cellen met specifieke eigenschappen. Cellen hebben een kern met daarin het genetisch materiaal (het DNA), organellen, de organen van de cel, en verder een heleboel verschillende eiwitten. Voor de vorming van de organen en weefsels tijdens de embryonale ontwikkeling moeten cellen migreren, een proces dat later ook voor cellen uit het immuunsysteem belangrijk is. Verder moeten alle cellen goed bijeengehouden worden zodat een weefsel of orgaan functioneel is en er wel of juist niet (vloei)stoffen kunnen passeren. Celadhesie is hiervoor van groot belang omdat het zorgt voor het maken van verbindingen tussen cellen onderling en tussen cellen en bindweefsel. Fouten bij zowel celmigratie als celadhesie liggen ten grondslag aan verschillende pathologische ontwikkelingen, waaronder tumor-uitzaaiing. Het is daarom belangrijk om deze processen en de regulatie ervan te onderzoeken en te begrijpen.
Door een microscoop kunnen levende celculturen bekeken en gefilmd worden. Met de ontdekking van het groen fluorescente eiwit GFP (green fluorescent protein) en later de rode en anders gekleurde varianten is het verder mogelijk geworden om specifieke eiwitten in levende cellen een kleur te geven en onder de microscoop te kunnen bestuderen. Op die manier kunnen processen als celadhesie en celmigratie tot in het kleinste detail worden onderzocht. Het analyseren van dit soort beelden met het oog is tijdrovend en wordt soms met een vooringenomen idee gedaan waardoor de resultaten niet altijd helemaal correct zijn. Software waarmee een computer automatisch structuren in microscopiebeelden herkent, kan een oplossing hiervoor bieden.
Dit proefschrift beschrijft het met dat doel in Matlab ontwikkelde softwarepakket ‘Adquant’, waarmee automatisch cellen en adhesie-structuren herkend en gevolgd kunnen worden en vervolgens eigenschappen (zoals helderheid, grootte en snelheid) van die structuren gemeten kunnen worden. We hebben Adquant gebruikt om de effecten van verschillende stoffen en signaleringsroutes op celadhesie en celmigratie automatisch en kwantitatief te analyseren.

Met het oog lijkt het altijd vrij gemakkelijk om in een foto een object te scheiden van de achtergrond, gebaseerd op het contrast in die foto. Een computer kan niet zomaar dat soort contrasten onderscheiden, maar werkt met de getallen waaruit een digitale foto bestaat. In een zwart-witfoto staat in elke pixel een getal dat aangeeft hoe licht die pixel is. Het contrast in een foto correspondeert met de verschillen tussen lichte (hoog getal) en donkere (laag getal) pixels, en een computer kan leren daar het onderscheid tussen te maken. Op die manier kan een computer een (licht) object, bijvoorbeeld een cel, van zijn (donkere) achtergrond scheiden, een proces dat segmentatie heet. Verder geven de getallen in de pixels informatie over de eigenschappen van een object, zoals helderheid.
Adquant bevat de segmentatie- en analysemethode voor vijf verschillende onderwerpen die met celadhesie en celmigratie te maken hebben. In **hoofdstuk 2** wordt een analysemethode voor celspreiding, dat wil zeggen het plat worden en groeien van een cel die net hecht, beschreven. In de **hoofdstukken 3, 4 en 5** staat de beschrijving en het gebruik van een analysemethode voor ‘focal adhesions’; dat zijn de eiwitcomplexen waarmee een cel zich aan de ondergrond vasthecht. Tot slot staan in de addenda analysemethodes voor celmigratie, oftewel de beweging van de cel, voor de eiwitcomplexen waarmee cellen aan elkaar vastzitten, die ‘adherens junctions’ heten, en voor het aan- of uitstaan van een signaleringsroute die afhankelijk is van adhesie. De methodes hebben een vergelijkbare opbouw: elke foto wordt

eerst voorbehandeld om ruis eruit te halen. Vervolgens zijn er één of meerdere segmentatie-stappen om datgene waarin je geïnteresseerd bent, bijvoorbeeld een cel, te scheiden van de achtergrond en om informatie te krijgen over de locatie en eigenschappen zoals vorm, grootte en helderheid. Er bestaan veel verschillende segmentatie-algoritmes, maar in Adquant wordt veel gebruik gemaakt van de 'hDome' transformatie (hoofdstukken 3-5 en addendum 2) en de 'local watershed' segmentatie (hoofdstukken 2-5 en addenda 1&3). Tot slot, voor het volgen van objecten in filmpjes worden de objecten in achtereenvolgende foto's gekoppeld. Of een object gekoppeld wordt, is afhankelijk van de hoeveelheid overlap van een object in twee opeenvolgende plaatjes. Door het object op deze manier te volgen wordt er informatie verkregen over de snelheid en de richting. Aan het eind van de analyse is er per plaatje of filmpje voor elk object data verzameld die verder gebruikt kan worden.

Nu weer terug naar de celbiologie. Er bestaan verschillende vormen van celadhesie, waarbij de 'focal adhesions' (FA) voor dit proefschrift het belangrijkst zijn. Met de FAs maken de cellen de connectie met omliggend bindweefsel, of, in celculturen, met de extracellulaire matrix (ECM) waarop de cellen groeien. FAs zijn grote eiwitstructuren, met wel 150 verschillende basiseiwitten, die aan de binnenkant van de cel een complex vormen. Via integrines, eiwitten die door de membraan naar buiten steken, hechten ze aan de ECM. FAs worden gemaakt aan de voorkant van de cel en kunnen of direct worden afgebroken of groeien om dan alsnog uit elkaar te vallen. Deze continuïteit is belangrijk voor cellen om te kunnen migreren. Hoewel FAs heel dynamisch zijn in hun groei en afbraak, zijn ze verder vrij onbeweeglijk op een verplaatsing na in de richting van het centrum van de cel die 'sliding' wordt genoemd.
De betrokken eiwitten hebben allerlei verschillende, niet altijd helemaal bekende functies. Ik zal hier kort een aantal belangrijke eiwitten beschrijven. Talin is een eiwit dat direct aan de integrines bindt en kan openvouwen waardoor andere eiwitten aangetrokken worden en de FA groeit. FAK is een signaleringseiwit, een kinase, dat belangrijk is voor de groei en afbraak van de FA. Een algemeen aanwezig, structureel eiwit is paxillin, waar veel andere eiwitten aan binden. Het eiwit vinculin verstevigt de FA en komt naar de FA toe via door krachten gereguleerde processen. Vinculin kan, evenals andere FA eiwitten, aan het actinecytoskelet binden waardoor de FAs een soort anker voor de cel vormen.
Het actinecytoskelet is een flexibele structuur die groeit, krimpt en beweegt en die vormgeeft aan de cel. Het bestaat uit een netwerk van actinestrengen, oftewel filamenten, die alle weer op te delen zijn in kleine actine-eiwitten. Die filamenten kunnen door andere eiwitten tot een dikke bundel gevormd worden. Deze bundels worden langs elkaar bewogen door het motor-eiwit myosine. Dat samentrekken is belangrijk voor het voortbewegen van de cel. Een van de effecten van deze samentrekking is dat er kracht op de FAs komt te staan. FAs worden door deze kracht beïnvloed: aan de voorkant van de cel doet het ze groeien, terwijl ze er aan de achterkant van de cel door naar binnen worden getrokken, om uiteindelijk uit elkaar te vallen. De dynamiek van het cytoskelet wordt gereguleerd door de eiwitten Rho, Cdc42 en Rac die in een actieve en inactieve vorm voorkomen. Het wisselen tussen de actieve en inactieve staat wordt goed gecontroleerd. Rho regelt het samentrekken van het cytoskelet, terwijl Cdc42 en Rac zorgen voor de vertakkingen van de actinefilamenten. Deze dynamiek speelt een belangrijke rol bij celmigratie. Aan de voorkant van de cel wordt de membraan naar voren geduwd. Dat gebeurt door vertakkingen van het actinenetwerk waar Rac en Cdc42 voor zorgen. Nieuwgevormde FAs verankeren dit uitgestoken stukje membraan. Verder naar achter in de cel zorgt Rho voor samentrekking van het cytoskelet waardoor er kracht uitgeoefend wordt op de achterkant van de cel en dat trekt dat stuk van de cel naar binnen.

Zo verplaatst de cel zich.
Het signaleringseiwit Rap1 verandert, net als Rho, Rac en Cdc42, van een actieve naar inactieve vorm en omgekeerd; dit gebeurt door allerlei andere eiwitten. De activatie van Rap1 heeft een effect op celadhesie en celmigratie. Als Rap1 geactiveerd wordt in een migrerende cel, stopt deze cel met bewegen terwijl hij uitspreidt en zijn omtrek toeneemt. Bij cellen die pas kort in een petrischaaltje zijn gedaan, is heel duidelijk te zien dat activatie van Rap1 spreiding teweegbrengt. Zo'n cel die nog moet hechten, ziet er uit als een bolletje. Op het moment dat de cel hecht wordt hij platter en spreidt uit in een onregelmatig vorm. Dit gebeurt met continue uitstulpsels van de celmembraan die ook weer worden ingetrokken. Net hechtende cellen die uitspreiden terwijl Rap1 actief is, worden veel groter en ronder dan cellen waarin Rap1 niet actief is. In **hoofdstuk 2** hebben we met Adquant het effect van Rap1 op spreiding geanalyseerd. Hieruit bleek dat na Rap1-activatie cellen veel sneller spreiden en groter worden terwijl het continu intrekken en uitduwen van de celmembraan, wat spreidende cellen doen, verminderd was en dat zorgde voor het rondere uiterlijk.
Normaliter hebben cellen om te kunnen spreiden het signaleringseiwit Src nodig. De signaleringsroute van Src zorgt voor FA-formatie, zodat de cel kan hechten, en reguleert via Rho, Rac en Cdc42 het actinecytoskelet zodat de cel kan spreiden. Voor hoofdstuk 2 werd een experiment gedaan waar cellen in een petrischaaltje worden gedaan om te hechten maar dan in aanwezigheid van een remmer van het eiwit Src (PP2). Dit zorgt ervoor dat de cellen niet spreiden. Het bleek dat Rap1-activatie in die cellen het effect van de remming van Src tenietdeed: de cellen spreidden toch en FAs werden gevormd. Omdat andere eiwitten uit de Src-signaleringsroute niet waren geactiveerd door de activatie van Rap1, concludeerden we dat Rap1 onafhankelijk van de Src-signaleringsroute celspreiding en FA-formatie teweeg kan brengen. Een verklaring hiervoor zou kunnen zijn dat Rap1 via remming van Rho de dynamiek van het actine cytoskelet beïnvloedt en zo voor celspreiding zorgt. Dat Rap1 inderdaad Rho kan remmen en via welke eiwitten dat gebeurt, werd na de publicatie van dit hoofdstuk in het lab van Prof. J.L. Bos gevonden.
In het volgende hoofdstuk bestudeerden we geen spreidende cellen meer, maar de FAs in migrerende cellen. De stof HGF (Hepatocyte Growth Factor) wordt vaak in verhoogde concentratie gevonden in tumoren met een slechte prognose. Het toevoegen van HGF aan een celcultuur zorgt ervoor dat de cellen gaan migreren, als de cellen tenminste de receptor hebben voor HGF. Omdat FAs een rol spelen bij het hechten van cellen en hun dynamische opbouw en afbraak nodig is voor cellen om te kunnen bewegen, was het idee dat het uiterlijk en gedrag (grootte, helderheid, sliding) van de FAs in door HGF gestimuleerde cellen informatie kunnen geven over de eerste stappen van metastase. Het was verder bekend dat Rap1 celmigratie in door HGF gestimuleerde cellen remt en de vraag was welke eigenschappen van de FAs hierdoor allemaal veranderen. Voor **hoofdstuk 3** hebben we cellen gefilmd die door toevoeging van HGF eerst gingen migreren en dan, door activatie van Rap1, geremd werden. In deze cellen konden we de FAs zien onder de microscoop omdat ze het structurele FA-eiwit paxillin met een rood kleurenlabel tot expressie brengen. Vervolgens hebben we met Adquant de FAs herkend, gevolgd in de tijd en de eigenschappen van de FAs geanalyseerd. Die eigenschappen zijn o.a. grootte, vorm, helderheid, snelheid van sliding, oriëntatie ten opzichte van de celkern en afstand tot de celmembraan. In niet gestimuleerde cellen kwamen de gemeten eigenschappen van de FAs overeen met wat we op basis van de literatuur verwachtten, wat de goede werking van onze analysemethode bevestigde.
Rap1-activatie in de migrerende cellen remde inderdaad de migratie, cellen spreidden uit en van de FA eigenschappen veranderden de helderheid, grootte en sliding-snelheid, die

allemaal verlaagd werden. De statistische analyse, die Bayesiaans netwerkinferentie heet, liet verder zien dat de veranderingen in FA-karakteristieken meer samenhingen met de verandering in de omvang van de cel dan met celmigratie. Daaruit concludeerden we dat FA-dynamiek en celmigratie onafhankelijke processen zijn. Daarnaast, omdat HGF geen invloed bleek te hebben op de eigenschappen van de FA, concludeerden we dat de dynamiek van die eigenschappen geen goede maat is voor de eerste stappen van metastase.

In dezelfde filmpjes van cellen die door toevoeging van HGF gaan migreren om vervolgens geremd te worden door Rap1-activatie, zijn we in **hoofdstuk 4** verder gaan kijken naar de helderheid van de FAs. Elk roodgelabeld eiwit geeft een beetje signaal en als er meer eiwit aanwezig is heb je meer signaal en dus geeft de helderheid aan of er veel of juist niet zoveel eiwit aanwezig is in de FA, in dit geval meer paxillin. In cellen die niet gestimuleerd waren, zagen we dat de eerste tijd van de levensduur van de FA de helderheid toenam, om korte tijd af op het bereikte niveau te blijven en vervolgens de laatste periode weer af te nemen. Dat betekent dat wij hier een toename en afname van eiwitconcentratie observeerden en daarom noemden we dit fenomeen compactie. We zagen dat korter levende FAs minder helder werden, waaruit we concludeerden dat de gradatie van compactie afhangt van de levensduur van de FA. Deze analyse liet zien dat FAs al een tijd voordat ze niet meer zichtbaar zijn, om de een of andere reden uit elkaar beginnen te vallen. Welke signalen voor deze omslag kunnen zorgen blijft een vraag.

Stimulatie met HGF zorgde voor een verhoging en versnelling van compactie terwijl Rap1-activatie zowel de snelheid als het niveau verlaagde. Kracht op FAs zorgt ervoor dat de FAs groeien, eiwitten aangetrokken worden en dat de FAs naar binnen bewegen. Het remmen daarvan doet FAs krimpen en uiteindelijk verdwijnen. Het remmende effect van Rap1-activatie op deze eigenschappen van de FA zou, net als bij hoofdstuk 2 beschreven, misschien verklaard kunnen worden door het remmende effect van Rap1 op het samentrekken van het actine cytoskelet via Rho. Om direct te kijken of kracht van belang is voor compactie, zijn we in het volgende hoofdstuk naar effecten gaan kijken op compactie terwijl we cellen filmden in de aanwezigheid van directe remmers van het samentrekken van het cytoskelet. Daarnaast interesseerde het ons wat er gebeurt met de aanwezigheid van het eiwit vinculin in de FAs als we het samentrekken van het cytoskelet remmen. Zoals in het begin beschreven, is vinculin een eiwit dat door kracht op de FAs naar de FAs toekomt, in tegenstelling tot het algemeen aanwezige eiwit paxillin. In vergelijking met paxillin zou vinculin daarom misschien ook als eerste weer verdwijnen uit de FAs als de kracht op de FA wegvalt. Om hiernaar te kijken hebben we voor **hoofdstuk 5** cellen gefilmd, dit keer met een rood gekleurd paxillin en een groen gekleurd vinculin om de FAs te zien, en daaraan twee stoffen toegevoegd die het samentrekken van het cytoskelet remmen. Om de aanwezigheid van vinculin en paxillin goed te kunnen vergelijken, hebben we met behulp van Adquant alleen die FAs geanalyseerd waarin beide eiwitten ten minste 80% van de levensduur aanwezig zijn. Bij bestaande FAs zorgde het remmen van contractie ervoor dat de compactie stopte en de helderheid meteen begon af te nemen. Maar FAs die in de aanwezigheid van de remmers werden gevormd, lieten nog wel compactie zien: ze werden minder helder, maar de snelheid van compactie was niet anders dan toen er nog wel contractie was. Dit duidt erop dat contractie van het actinecytoskelet inderdaad van invloed is op compactie maar deze niet als enige component reguleert. Een verrassende observatie was verder dat met het remmen van contractie niet vinculin als eerste uit de FAs verdween maar paxillin, om vrij snel gevolgd te worden door vinculin. Dit is een aanwijzing dat de aanwezigheid van vinculin niet alleen maar door kracht wordt gereguleerd. Hiermee sloten we ons onderzoek naar de eigenschappen van FAs

in cellen af.
Tot slot staan in de drie addenda methodes beschreven waarmee: (**addendum 1**) celmigratie gekwantificeerd kan worden, (**addendum 2**) de aanwezigheid van eiwitten in de eiwitcomplexen waarmee cellen aan elkaar hechten gemeten kan worden en (**addendum 3**) gekeken kan worden of de hechtingsafhankelijke YAP-signaleringsroute aan of uit staat, door de intensiteit van het eiwit YAP in de kern te vergelijken met de intensiteit in de rest van de cel.

Samengevat staat in dit proefschrift een vijftal ontwikkelde methodes beschreven, onder de naam Adquant, waarmee verschillende aspecten van celmigratie en celadhesie automatisch en kwantitatief geanalyseerd kunnen worden. Deze aspecten zijn celspreiding, FA-dynamiek (tweekleurig), celmigratie en cel-celadhesie en de hechtingsafhankelijke YAP-signaleringsroute. De belangrijkste bevindingen zijn dat FA dynamiek en celmigratie onafhankelijke processen zijn en dat Rap1-activatie een bypass kan zijn voor Src signalering in celspreiding en de helderheid, snelheid en grootte van FAs vermindert in migrerende cellen. Verder beschrijven we een nieuw fenomeen: compactie van de FAs, dat deels door kracht gereguleerd wordt. Onze analyse van compactie laat zien dat afbraak van een FA al inzet lang voordat de FA ophoudt te bestaan. Zo hebben we een aantal aspecten van de celadhesie bestudeerd en kunnen met onze methode celadhesie en celmigratie verder onderzocht worden.

Dankwoord

Hier kan ik dan, aan het eind van deze zes jaar, eindelijk de mensen bedanken die de afgelopen jaren hebben bijgedragen aan de totstandkoming van dit boekje. Het zou te veel ruimte innemen om alle mensen van het Hubrecht en het UMC met wie ik koffie- of borrelpraatjes heb gevoerd apart te bedanken, ook al zijn die momenten belangrijk geweest voor het plezier waarmee ik naar het werk ging. Dus daarvoor een algemeen 'dank jullie wel'.

Johan, zonder jouw vertrouwen en enthousiasme was dit proefschrift er niet gekomen. Even bij jou binnenwandelen met een vraag, waar je altijd tijd voor vrij maakte, leidde steevast tot nieuwe ideeën en plannen. Maar niet alleen op wetenschappelijk vlak ben je een enthousiasmerend persoon, ook voor persoonlijke dingen heb je altijd tijd en met je bemoedigende en vertrouwenwekkende woorden ben je een grote steun voor me geweest.

Hans, dankje voor het vertrouwen om mij als gedeelde aio aan te nemen zonder dat we, voor zover ik weet, kennis hadden gemaakt. Je enthousiasme over en kritische blik op het project om automatisch focal adhesions te herkennen en te volgen, waren altijd nuttig en hebben het project op sommige kritieke momenten gestuurd.

Ihor Smal en Erik Meijering, thank you very much for all the help, explanations, discussions on image analysis in general and the hDome algorithm in particular. Adriaan Houtsmuller, hartelijk dank voor alle keren dat je naar Utrecht bent gekomen voor een bespreking van mijn aio-commissie waar dan, mede dankzij jou, een levendige en interessante discussie op gang kwam. Nicos Angelopoulos, a discussion with you, whether about focal adhesions or jobs, always was a pleasure. Thank you very much for the BNI analyses.

Alle De Rooijers die mij de afgelopen jaren vrijwel altijd achter de computer in onze kamer aantroffen: Stephan, jouw doelgerichtheid vond ik heel leerzaam. Verder heb ik onze dirty-minded vrijdagmiddaggesprekken vaak gemist. Quint, dat laatste geldt ook voor jou. Je was met je grootse avonturen en heerlijke kookkunsten een heel kleurrijk persoon op het lab. Ik hoop dat je plezier hebt in je bezigheden van nu. Iris, de rust op het lab. Dank je voor je attente briefjes op lastiger momenten. Floor, ik ben blij dat we samen 'opgroeiden'op het De Rooij-lab en veel hebben kunnen delen. Esteban, me gustó mucho que estabas en el labo por un año, platicando español conmigo. Sander, een dag op het lab leek nooit te lang te zijn voor jou. Je kennis en meedenken met andere projecten vond ik altijd inspirerend. Gerard, dank je voor alle, soms bijna filosofische, gesprekken en je aanstekelijk schaterlachen bij een grappige anekdote. Joppe, jouw zin om experimenten te doen maakte ook mij enthousiast, net als je muur met vrolijke stripjes. Mitchell, ik was vaak onder de indruk van je snelle begrip van projecten en vond je een gezellige kamergenoot.

Bij de Bos-groep heb ik me vanaf het begin af aan welkom gevoeld, ook voordat we op dezelfde gang zaten. Judith, met jouw verhalen en enthousiasme heb je me in het allereerste begin daarbij enorm geholpen. Willem-Jan ook: met je grappen tijdens werkbesprekingen en retraites, en de mogelijkheid om altijd even een gesprekje met je aan te knopen. Sarah, I am really happy that we went to the Gordon meeting together and shared a room. Back in Utrecht, our lunches and coffees were always interesting and a lot of fun (although other people may have found them slightly too long). Working with you has taught me a lot about Rap1 signalling and made me complete my first analysis tool. I find it really cool you want to be my paranymph. Ook dank aan alle andere (oud-) collega's voor nuttige werkbesprekingen

en de goede sfeer op de retraites; Sarah C., René, Patricia, On-Ying, Nayara, Milica, Martijn, Marlous, Marjolein, Lucas, Lars, Koen, Jantine, Hugo, Fried, Esther, Carla, Anouk en Anneke. Ingrid , dank je voor het maken van allerlei Epac-lijnen. Holger, thank you for your input on the analysis in chapter 4.
Dank aan de mensen van de Burgering-groep voor de gezelligheid op de retraites. David en Astrid, practicum begeleiden was leuk met jullie. Marten, ik hoop dat je nog eens cellen kan tracken bij de groep-De Rooij. Harm-Jan, dankje voor alle keren dat je even binnen kwam wandelen om te vragen hoe het stond met de afronding van mijn proefschrift.
Marianne, hartelijk dank voor het soepel laten verlopen van alle administratieve onderdelen van het promoveren. Heren van de IT van het UMCU, Marc, Erik en Wim, hartelijk dank voor het installeren van Matlab voor onze groep en voor het feit dat ik altijd even met een vraag kon binnenwandelen.

De Van Rheenen-groep wil ik bedanken voor de nuttige discussies en input tijdens de werkbesprekingen en retraites die we de eerste paar jaar samen hebben gehad. Jacco, dank je voor al je kritische vragen in mijn aio-commissie. Laila, Evelyne, Anoek, Nynke en Saskia, dank jullie voor de gezellige praat, o.a. als ik met een van jullie tegelijkertijd bij de microscopen zat.

Ook wil ik mensen bedanken van buiten het lab die hebben meegeleefd en de nodige ontspanning hebben geboden. Ten eerste, omdat dit in zekere zin nog lab-gerelateerd is, de hispanohablantes; aan die etentjes denk ik met veel plezier terug. Bas, je fascinatie voor de gekke facetten van de Nederlandse taal vind ik tof. Coert, het is fijn dat ik met jou over allerlei bijzaken van het werk kan kletsen.
Dan mensen met wie ik de laatste jaren muziek heb gemaakt. Sophie, ik vond de repetities van ons Hubrecht-duo altijd gezellig en hoop dat we nog eens samen zullen spelen. Josien, dank je dat je me voor het trio hebt gevraagd toen je me muziek zag kopieren op het Hubrecht en voor het fijne samenspelen. Job, doen we weer eens een Bach-duetje? Ook enorm bedankt voor alle toffe concerten die ik van je heb gehoord. Marloes, ons kwartet heeft dan wel niet zo lang bestaan, ik hoop dat wij nog vaak samen dwarsfluit zullen spelen.

Ivonne, onze uitjes en afspraken zijn een onmisbare afleiding geweest. Trijsje, van simpele woordgrap tot promotie-onderzoek, we kunnen het delen en dat biedt soelaas.
Valérie, Marc, Clémentine et Cécile, merci beaucoup pour le bienvenu que vous m'avez donné en votre famille.
Bastiaan, onze fietstochtjes van en naar Utrecht CS het laatste jaar maakten de reis gewoonweg leuk. Dank je voor je luisterend oor, je andere blik en je suggesties. Ik vind het tof dat je nu op het Hubrecht werkt en dat je mijn paranimf wil zijn. Friede, dank je voor alle etentjes die je voor me kookte in de laatste drukke periode.
Rosa, dank je voor al de heel gezellige uurtjes die wij samen, en ook met Mirjam, hebben doorgebracht en je heldere kijk op de dingen. Jeroen, dank je voor af en toe een advies over planning en andere lastige situaties.
Lo en Marleen, bij jullie kan ik met alles aankomen; jullie zijn altijd geïnteresseerd. Dank voor nog zoveel meer dan de steun in de afgelopen jaren.
Thanks to this thesis I happened to be in Barcelona in the same weekend as you, Nicolas. It is easy: ma vie est plus belle avec toi et j' ai hâte de commencer une nouvelle chapitre avec toi après la défense de ce thèse.

&

Curriculum Vitae

Emma Spanjaard werd geboren op 28 augustus 1983. In 2001 behaalde zij haar diploma aan het Barlaeus gymnasium te Amsterdam. Na een jaar muziek te hebben gestudeerd aan het Canterbury Christ Church University College in Engeland, begon zij in september 2002 aan de bachelor opleiding Medische Biologie aan de Universiteit van Amsterdam. In 2005 sloot ze die af en in 2007 behaalde ze cum laude het master diploma van Medische Biologie aan de UvA. Tijdens deze master heeft ze eerst stage gelopen bij dr. Johan de Rooij op het NKI waar ze cel-celadhesie onderzocht. Tijdens een tweede stage heeft ze in het lab van prof. dr. Geert Kops aan het UMCU, onder supervisie van dr. Nannette Jelluma, de functie van Bub3 in het mitotic checkpoint bestudeerd. In 2008 begon ze aan haar promotieonderzoek bij dr. Johan de Rooij en prof. dr. Hans Bos waarvan de resultaten in dit proefschrift staan beschreven.

List of publications

Spanjaard E, Smal I, Angelopoulos N, Verlaan I, Meijering E, Wessels L, Bos J.L, de Rooij J. Quantitative imaging uncouples Focal Adhesion dynamics from the regulation of cell migration.
Submitted for publication

Spanjaard E, de Rooij J. Mechanotransduction: vinculin provides stability when tension rises.
Current Biology 2013, vol. 23 (pp159-161)

Magliozzi R, Low TY, Weijts BG, Cheng T, **Spanjaard E**, Mohammed S, van Veen A, Ovaa H, de Rooij J, Zwartkruis FJ, Bos JL, de Bruin A., Heck AJ, Guardavaccaro D. Control of epithelial cell migration and invasion by the IKKbeta- and C1Kalpha- mediated degradation of RAPGEF2.
Developmental Cell 2013, vol.27 (pp574-585)

Ross S*, **Spanjaard E***, Post A, Vliem, MJ, Kristyanto H, Bos JL, de Rooij J. Rap1 can bypass the FAK-Src-Paxillin cascade to induce cell spreading and focal adhesion formation.
PloSOne 2012, vol. 7 (e50072)
* these authors contributed equally to this work

Huveneers S, Oldenburg J*, **Spanjaard E***, van der Krogt G, Grigoriev I, Akhmanova A, Rehmann H, de Rooij J. Vinculin associates with endothelial VE-cadherin junctions to control force-dependent remodeling.
J Cell Biol. 2012, vol. 196 (pp 641-652)
* these authors contributed equally to this work

Loerke D, le Duc Q, Blonk I, Kerstens A, **Spanjaard E**, Machacek M, Danuser G, de Rooij J. Quantitative imaging of epithelial cell scattering identifies specific inhibitors of cell motility and cell-cell dissociation.
Sci Signal. 2012, vol. 5 (rs5)

Consonni SV, Gloerich M, **Spanjaard E**, Bos JL. cAMP regulates DEP domain-mediated binding of the guanine nucleotide exchange factor Epac1 to phosphatidic acid at the plasma membrane.
Proc Natl Acad Sci U S A. 2012, vol.109 (pp 3814-3819)

Pannekoek WJ, van Dijk JJ, Chan OY, Huveneers S, Linnemann JR, **Spanjaard E**, Brouwer PM, van der Meer AJ, Zwartkruis FJ, Rehmann H, de Rooij J, Bos JL. Epac1 and PDZ-GEF cooperate in Rap1 mediated endothelial junction control.
Cell Signal. 2011, vol. 23 (pp 2056-2064)

&